Title

Flavor symmetric sectors and collider physics

Journal

Journal of High Energy Physics, 2011(10)

ISSN

1126-6708

Authors

Grinstein, Benjamín
Kagan, Alexander L
Trott, Michael
et al.

Publication Date

2011-10-01

DOI

10.1007/jhep10(2011)072

Peer reviewed

Flavor Symmetric Sectors and Collider Physics

Benjamín Grinstein*

Department of Physics, University of California at San Diego, La Jolla, CA 92093

Alexander L. Kagan† and Jure Zupan‡§

Department of Physics, University of Cincinnati, Cincinnati, Ohio 45221,USA

Michael Trott¶

Perimeter Institute for Theoretical Physics, Waterloo, ON N2J-2W9, Canada

(Dated: August 22, 2011)

We discuss the phenomenology of effective field theories with new scalar or vector representations of the Standard Model quark flavor symmetry group, allowing for large flavor breaking involving the third generation. Such field content can have a relatively low mass scale $\lesssim \mathrm{TeV}$ and $O(1)$ couplings to quarks, while being naturally consistent with both flavor violating and flavor diagonal constraints. These theories therefore have the potential for early discovery at LHC, and provide a flavor safe "tool box" for addressing anomalies at colliders and low energy experiments. We catalogue the possible flavor symmetric representations, and consider applications to the anomalous Tevatron $t\,\bar{t}$ forward backward asymmetry and B_s mixing measurements, individually or concurrently. Collider signatures and constraints on flavor symmetric models are also studied more generally. In our examination of the $t\,\bar{t}$ forward backward asymmetry we determine model independent acceptance corrections appropriate for comparing against CDF data that can be applied to any model seeking to explain the $t\,\bar{t}$ forward backward asymmetry.

‡ On leave of absence from University of Ljubljana, Depart. of Mathematics and Physics, Jadranska 19, 1000 Ljubljana, Slovenia and Josef Stefan Institute, Jamova 39, 1000 Ljubljana, Slovenia.

*Electronic address:bgrinstein@ucsd.edu

†Electronic address:kaganalexander@gmail.com

§Electronic address:jure.zupan@cern.ch

¶Electronic address:mtrott@perimeterinstitute.ca

Contents

I. INTRODUCTION

In recent years, the study of New Physics (NP) that lies close to the electroweak (EW) energy scale has been motivated primarily by the hierarchy problem. However, it is possible that the correct solution to this problem or the detailed nature of EW symmetry breaking remain to be proposed. Experimental input, as expected from the LHC, is crucial. Furthermore, hints for new physics (NP) may have already emerged from the Tevatron. In this paper we are motivated by recent experimental anomalies at the Tevatron and the strong discovery potential at LHC to explore collider signatures of new physics (NP) sectors that are flavor symmetric. They will be taken to be invariant under the global flavor symmetry group $\mathrm{G_F} = \mathrm{U(3)_{U_R}} \times \mathrm{U(3)_{D_R}} \times \mathrm{U(3)_{Q_L}}$, or its subgroup $\mathrm{H_F} = \mathrm{U(2)_{U_R}} \times \mathrm{U(2)_{D_R}} \times \mathrm{U(2)_{Q_L}} \times \mathrm{U(1)_3}$ (where the quarks of the first two families are in doublets of the corresponding $\mathrm{SU(2)}$ factors). The group $\mathrm{G_F}$ is the global symmetry of the Standard Model (SM) in the limit where one can neglect the Yukawa interactions

$$\mathcal{L}_Y = Y_U \, \bar{u}_R \, H^T \, i\sigma_2 \, Q_L - Y_D \, \bar{d}_R \, H^\dagger \, Q_L + \mathrm{h.c.}\,, \tag{1}$$

where Y_U and Y_D are the up and down quark Yukawa matrices, respectively.

The NP sectors will contain scalar or vector fields that have masses $\lesssim$ TeV and $\mathcal{O}(1)$ couplings to quarks. At the same time they will be consistent with flavor changing neutral current (FCNC) constraints precisely because of their flavor structure, as long as the breaking of the flavor symmetries is sufficiently small. In the SM the top and bottom Yukawa couplings break the flavor group $\mathrm{G_F}$ to its $\mathrm{H_F}$ subgroup. We

take this breaking into account in our analysis of NP sectors that are initially $\mathrm{G_F}$ symmetric. The existence of the $\mathrm{H_F}$ symmetry at low energies protects these theories against dangerously large FCNC's, e.g., in neutral meson mixing. This protection satisfies the naturalness criteria of Glashow and Weinberg [1] and is not the result of simply tuning parameters. Note that NP models that have an approximate $\mathrm{H_F}$ symmetry are sometimes referred to as models of next to minimal flavor violation [2]. The breaking of $\mathrm{H_F}$ in the SM is due to the other quark masses and the CKM mixing angles, and is thus small. The precise mechanism by which $\mathrm{H_F}$ is broken in the NP sector will not be important when we explore flavor diagonal collider signatures. However, the nature of $\mathrm{H_F}$ breaking will be relevant to our discussion of low energy FCNC's, see below.

Scalar and vector fields with dimension four $\mathrm{G_F}$ invariant direct couplings to quarks are limited in their allowed charge assignments by flavor and the SM gauge symmetry. There are only 14 different nontrivial flavor representations allowed in each case. In the case of $\mathrm{H_F}$ symmetric models the possible NP fields are conveniently classified in terms of these representations, with the understanding that they need not come in complete $\mathrm{G_F}$ multiplets. A systematic exploration of new flavor symmetric sectors is therefore feasible, either in general, or with the aim of explaining a particular anomaly.[1]

New flavor symmetric sectors that are perturbatively coupled to quarks are particularly interesting to consider as candidate explanations for Tevatron anomalies. In the first part of this paper, we focus our attention on two $> 3\sigma$ anomalies: (i) the CDF measurement of the $t\bar{t}$ forward backward asymmetry, $A_{FB}^{t\bar{t}}$, for $m_{\bar{t}t} \geq 450\,\mathrm{GeV}$ [6] is 3.4σ away from the NLO SM prediction. (A recent DØ analysis [7] does not observe a significant $m_{t\bar{t}}$ dependence in the "folded" detector level asymmetries, but it appears to be consistent with the CDF detector level measurements within errors.) The inclusive $t\bar{t}$ forward backward asymmetry, averaged over the CDF semileptonic [6] and hadronic [8] $t\bar{t}$ decay samples and the recent DØ measurement [7], is $\approx 3\sigma$ from the NLO SM prediction; (ii) the like sign dimuon asymmetry measured by DØ is 3.9σ away from the SM expectation [9, 10]. Each of these anomalies, if confirmed, points to a relatively low scale of NP with a significant coupling to quarks. We identify flavor symmetric models that have the potential to explain them either individually or simultaneously, and study related constraints. In the case of $\mathrm{G_F}$ symmetric models, under the assumption that the NP only couples to quarks, some hierarchies among these couplings would be required in order to consistently explain the $A_{FB}^{t\bar{t}}$ anomaly, e.g., due to the absence of dijet or $t\bar{t}$ resonances at the Tevatron and LHC. Thus, breaking of the $\mathrm{G_F}$ symmetry to $\mathrm{H_F}$ would be necessary. Alternatively, one could consider $\mathrm{H_F}$ symmetric models where the more constrained

[1] Color symmetric fermion content that mixes with the SM fermion fields is not as constrained in its allowed representations. Initial studies of vector-like fermions have also been undertaken in Refs. [4, 5]. Of the models studied only two were natural in the Glashow-Weinberg sense [5].

quark couplings would simply be absent.

It is possible that the above anomalies could be due to statistical fluctuations or underestimates of theoretical or experimental errors. Even if this turns out to be the case, the models we explore in this paper are interesting in their own right, as they have strong discovery prospects at LHC. Again, this is because their flavor symmetric structures allow for sub-TeV NP mass scales. In the second part of this paper, we address the phenomenology of flavor symmetric sectors more generally. The global flavor symmetries we consider could be accidental, or they could be a remnant of the underlying mechanism generating the SM flavor structure (such as non-Abelian horizontal symmetries). We do not concern ourselves with the UV origin of these symmetries, but instead focus on the collider and low energy phenomenology of the new sectors. This approach is inspired by effective field theories (EFT), where one generally constructs all possible interactions consistent with the symmetries of interest. The analysis of flavor diagonal collider constraints and signatures can then be kept quite general, i.e., independent of the way $\mathrm{H_F}$ is broken, as already mentioned. For simplicity, in attempts to explain a measured deviation from the SM we will only consider the phenomenology of single $\mathrm{G_F}$ multiplets (or the corresponding $\mathrm{H_F}$ multiplets), effectively assuming that there is a significant mass gap with other possible representations. Moreover, we will only consider their couplings to quarks. Note that more generally, these fields could couple to additional states transforming under $\mathrm{G_F}$ or $\mathrm{H_F}$, possibly providing them with additional decay channels.

The determination of low energy flavor physics constraints on flavor symmetric models generally requires the breaking of $\mathrm{H_F}$ to be specified. When determining these constraints we assume the Minimal Flavor Violation (MFV) hypothesis [11, 12], i.e., that *all* breaking of $\mathrm{H_F}$ is due to the SM Yukawas. This enforces maximal consistency with FCNC constraints through a symmetry principle, and allows us to explore how low the NP mass scale can be. In all the models we consider, the new states can have EW scale masses. In MFV models that lead to class-2 operators (those that involve right handed fields) in the language of [13], the breaking of $\mathrm{H_F}$ can actually be orders of magnitude larger then assumed in MFV, while still obeying the FCNC bounds.

The paper is organized as follows. In Section II we list all vector and scalar representations of the form we have motivated, and write down in detail the vector field Lagrangians for two examples. In Section III we systematically discuss the potential of models of this form to explain the $A_{FB}^{t\bar{t}}$ anomaly, the DØ dimuon anomaly, and related phenomenology. In Section IV we explore existing bounds on these models from LEP, electroweak precision data (EWPD), FCNCs and dijet studies at the LHC and Tevatron. In Section V we discuss additional LHC phenomenology. Finally, in Section VI we give our conclusions. Many details have been relegated to the Appendices. In Appendix A we list the details of flavor symmetric vector Lagrangians, in Appendix B we gives the details of $2 \to 2$ scattering calculations and phenomenology, and in Appendix

Case	$SU(3)_c$	$SU(2)_L$	$U(1)_Y$	$U(3)_{U_R} \times U(3)_{D_R} \times U(3)_{Q_L}$	Couples to
$I_{s,o}$	1,8	1	0	(1,1,1)	$\bar{d}_R \gamma^\mu d_R$
$II_{s,o}$	1,8	1	0	(1,1,1)	$\bar{u}_R \gamma^\mu u_R$
$III_{s,o}$	1,8	1	0	(1,1,1)	$\bar{Q}_L \gamma^\mu Q_L$
$IV_{s,o}$	1,8	3	0	(1,1,1)	$\bar{Q}_L \gamma^\mu Q_L$
$V_{s,o}$	1,8	1	0	(1,8,1)	$\bar{d}_R \gamma^\mu d_R$
$VI_{s,o}$	1,8	1	0	(8,1,1)	$\bar{u}_R \gamma^\mu u_R$
$VII_{s,o}$	1,8	1	-1	($\bar{3}$,3,1)	$\bar{d}_R \gamma^\mu u_R$
$VIII_{s,o}$	1,8	1	0	(1,1,8)	$\bar{Q}_L \gamma^\mu Q_L$
$IX_{s,o}$	1,8	3	0	(1,1,8)	$\bar{Q}_L \gamma^\mu Q_L$
$X_{\bar{3},6}$	$\bar{3}$,6	2	-1/6	(1,3,3)	$\bar{d}_R \gamma^\mu Q_L^c$
$XI_{\bar{3},6}$	$\bar{3}$,6	2	5/6	(3,1,3)	$\bar{u}_R \gamma^\mu Q_L^c$

TABLE I: The flavor and gauge representations for vector fields that can couple directly to quarks through G_F symmetric dimension four interactions without the insertion of a Yukawa matrix. Q_L^c denotes the right handed conjugate representation of the left handed SM doublet.

C we give a detailed discussion of constraints from meson mixing amplitudes.

II. G_F SYMMETRIC REPRESENTATIONS

We are interested in scalars and vectors that couple directly to quarks through dimension four interactions. The scalar fields of this form are renormalizable models, while the vector fields are nonrenormalizable. In this section we list all the possible representations of G_F and the SM gauge group that such fields can have when G_F is unbroken. The vector field representations are listed in Table I and the scalar field representations are listed in Table II (the latter have been studied and classified in [3, 14]). This completes the program initiated in [3]. The complete set of H_F symmetric representations which can couple directly to quarks through dimension four interactions appear in these tables as submultiplets of the G_F representations. For example, in model $VI_{s(o)}$, the corresponding H_F symmetric vector representations would consist of a triplet, a complex doublet and a singlet of $SU(2)_{U_R}$, which are color singlets (octets), or a subset of these.

Several remarks are in order before we construct the Lagrangians.

- $I_{s,o}$, $II_{s,o}$ and $III_{s,o}$ carry the same quantum numbers and are thus a sub-classification of interactions of a single field. For instance, in the case of a color singlet vector with the same couplings to

Case	$SU(3)_c$	$SU(2)_L$	$U(1)_Y$	$U(3)_{U_R} \times U(3)_{D_R} \times U(3)_{Q_L}$	Couples to
S_I	1	2	1/2	(3,1,$\bar{3}$)	$\bar{u}_R \; Q_L$
S_{II}	8	2	1/2	(3,1,$\bar{3}$)	$\bar{u}_R \; Q_L$
S_{III}	1	2	-1/2	(1,3,$\bar{3}$)	$\bar{d}_R \; Q_L$
S_{IV}	8	2	-1/2	(1,3,$\bar{3}$)	$\bar{d}_R \; Q_L$
S_V	3	1	-4/3	(3,1,1)	$u_R \; u_R$
S_{VI}	$\bar{6}$	1	-4/3	($\bar{6}$,1,1)	$u_R \; u_R$
S_{VII}	3	1	2/3	(1,3,1)	$d_R \; d_R$
S_{VIII}	$\bar{6}$	1	2/3	(1,$\bar{6}$,1)	$d_R \; d_R$
S_{IX}	3	1	-1/3	($\bar{3}$,$\bar{3}$,1)	$d_R \; u_R$
S_X	$\bar{6}$	1	-1/3	($\bar{3}$,$\bar{3}$,1)	$d_R \; u_R$
S_{XI}	3	1	-1/3	(1,1,$\bar{6}$)	$Q_L \; Q_L$
S_{XII}	$\bar{6}$	1	-1/3	(1,1,3)	$Q_L \; Q_L$
S_{XIII}	3	3	-1/3	(1,1,3)	$Q_L \; Q_L$
S_{XIV}	$\bar{6}$	3	-1/3	(1,1,$\bar{6}$)	$Q_L \; Q_L$
$S_{H,8}$	$1, 8$	2	1/2	(1,1,1)	$\bar{Q}_L u_R, \; \bar{Q}_L d_R$

TABLE II: Different scalar representations that are not singlets under the flavor group that are G_F symmetric [3] (the upper rows). The two flavor singlet representations are in the last row and were discussed in [14].

Q_L, u_R, d_R this is just the baryonic Z'. We found it useful to split the interactions into three subgroups. At colliders there is no interference among these interactions up to effects suppressed by light quark masses (but if there are relations between their couplings this can have important consequences for the predicted cross section; for example, for a purely axial gluon the NP interference with the SM amplitude does not contribute to the top pair production cross section [15–17]). In the treatment of FCNCs the interference effects are trivial to include in the analysis.

- Many of the scalar and vector fields do not lead to proton decay at any order in perturbation theory due to the SM gauge symmetry and G_F. The vectors X–XI and scalars S_V–S_{XIV} carry baryon number $\pm 2/3$ and may lead to proton decay if they also couple to lepto-quark bilinears, *e.g.,* $\bar{L}_L^c \gamma^\mu u_R$ and $\bar{L}_L^c \gamma^\mu d_R$ for fields X and XI, respectively. This type of coupling is not possible for scalars or vectors in the color **6** representation and can be forbidden for the **3** color representation fields by extending the flavor group to the lepton sector of the SM [3] .

- We assume that the new quanta have weak scale masses and that the cut-off of the theory is well above the weak scale so that we only need to focus on dimension four interactions for most of our

discussion. Other dimension four couplings such as $B_{\mu\nu}\mathrm{Tr}(V^\mu V^\nu)$, with $B_{\mu\nu}$ the hypercharge field strength and V_μ the vector fields, are not directly relevant to the phenomenology of interest in this paper. We leave the exploration of these interactions to a future publication.

- The kinetic terms (with flavor breaking insertions) can always be made universal through field redefinitions. Below, we only write down the interaction terms.

- Tree-level exchanges of fields in a single representation of $\mathrm{G_F}$ cannot explain *both* of the Tevatron anomalies simultaneously for any of the models considered. Models $\mathrm{VII_{s,o}}$ and $\mathrm{S_I}$ do, however, lead to enhanced $A_{FB}^{t\bar{t}}$, while not modifying the $t\bar{t}$ differential spectrum. At the same time they give new CP violating contributions to B_s and B_d mixing of the right order of magnitude to yield the observed like-sign dimuon asymmetry.

The interaction Lagrangians for the color triplet and sextet scalar fields are given in [3]. For vector fields the $\mathrm{G_F}$ symmetric interactions are given by $\bar{q}\gamma^\mu T^a q' V_\mu^a$, where T^a represents a product of generators of color, flavor, and weak SU(2), or some subset thereof, while $q^{(\prime)}$ are the u_R, d_R or Q_L family triplets, as appropriate [2]. To write down the $\mathrm{G_F}$ breaking interactions it is useful to (initially) adopt some of the formalism of MFV and promote $Y_{U,D}$ to spurions that formally transform as bi-fundamentals of $\mathrm{G_F}$

$$Y_U \to V_U\, Y_U\, V_Q^\dagger, \qquad Y_D \to V_D\, Y_D\, V_Q^\dagger. \tag{2}$$

Here $V_{U,D,Q}$ are elements of $\mathrm{SU(3)_{U,D,Q}}$, respectively. Assuming full MFV breaking of $\mathrm{G_F}$, all interactions are then formally invariant under $\mathrm{G_F}$ even for nonzero Yukawa couplings. We will mostly work to the first nontrivial order in top Yukawa insertions (the resummation to all orders can be done using a nonlinear representation of $\mathrm{G_F}$, see [13, 19–21]). The explicit forms of the interactions for all the vector models are given in Appendix A. Here we show two examples, models $\mathrm{VI_{s,o}}$ and $\mathrm{X_{\bar{3},6}}$.

Fields $\underline{\mathrm{VI_{s(o)}}}$ are $\mathrm{SU(3)_R}$ flavor octets, color singlets (octets). The individual field components are V_μ^B ($V_\mu^{A,B}$), where the color label A and flavor label B both run over $1..8$. To compress the expressions we introduce

$$V_\mu^s = T^B V_\mu^B, \qquad V_\mu^o = \mathcal{T}^A T^B V_\mu^{A,B}. \tag{3}$$

with flavor (color) Gell-Mann matrices $T^B(\mathcal{T}^A)$ normalized to $\mathrm{Tr}[T^A T^B] = \delta^{AB}/2$. The renormalizable interactions between quarks and fields $\mathrm{VI_{s,o}}$ are

$$\mathcal{L}_{\mathrm{VI_{s,o}}} = \eta_1^{s,o}\, \bar{u}_R \not{V}^{s,o} u_R. \tag{4}$$

[2] In $\mathrm{H_F}$ symmetric models the Lagrangians are trivially obtained from the corresponding $\mathrm{G_F}$ symmetric Lagrangians, allowing for the possibility that only particular submultiplets of the $\mathrm{G_F}$ symmetric representations are present.

There are also terms that break $\mathrm{G_F} \to \mathrm{H_F}$,

$$\Delta\mathcal{L}_{\mathrm{VI_{s,o}}} = [\eta_2^{s,o}\,\bar{u}_R(\not{V}^{s,o}\Delta_U)u_R + h.c.] + \tilde{\eta}_3^{s,o}\,\bar{u}_R(\Delta_U\not{V}^{s,o}\Delta_U)u_R + \dots . \tag{5}$$

We kept only the breaking due to $\Delta_U \equiv Y_U\,Y_U^\dagger$ insertions. These are diagonal in the up-quark basis and change the coupling of third generation quarks to the vector fields (explicitly written out in Appendix A, Eqs. (A5), (A6)). Note that $\eta_2^{s,o}$ can be complex and possibly a source of beyond the SM CP violation, of interest when considering B_s mixing, while $\tilde{\eta}_3^o$ is real. Insertions of $Y_U Y_D^\dagger Y_D Y_U^\dagger$ are also possible to break the symmetry further and are almost diagonal in the up quark basis, while the off-diagonal elements lead to FCNC's. We postpone the discussion of these until Section IV D.

The $\mathrm{G_F} \to \mathrm{H_F}$ breaking also splits the vector mass spectrum. The flavor invariant mass terms are

$$\mathcal{L}_{VI_a}^{mass} = (1+\delta_{a,o})\left\{m_{V_a}^2\,\mathrm{Tr}\left[\tilde{V}_\mu^a\,\tilde{V}^{\mu a}\right] + \lambda\,(H^\dagger\,H)\,\mathrm{Tr}\left[\tilde{V}_\mu^a\,\tilde{V}^{\mu a}\right]\right\}, \qquad a = o, s, \tag{6}$$

where the color and $\mathrm{SU}(3)$ indices are suppressed, and there is no summation over $a = o, s$ (the Kronecker delta $\delta_{a,o}$ insures the proper normalization for the color octet fields). Note that $\tilde{V}$ is defined when rotating to the mass eigenstate basis; see Appendix A. Adding the $\mathrm{G_F} \to \mathrm{H_F}$ breaking terms $(1+\delta_{a,o})\zeta_1 m_V^2 \mathrm{Tr}\big[\tilde{V}_\mu\,\Delta_U\,\tilde{V}^\mu\big]$ and $(1+\delta_{a,o})\zeta_2 m_V^2 \mathrm{Tr}\big[\Delta_U\,\tilde{V}_\mu\,\Delta_U\tilde{V}^\mu\big]$, the mass spectrum of the vector states is (suppressing the o, s labels)

$$m_{1,2,3}^2 = m_V^2 + \frac{\lambda}{2}v^2, \qquad m_{4,5,6,7}^2 = m_1^2 + m_V^2\,\frac{\zeta_1}{2}\,y_t^2, \qquad m_8^2 = m_4^2 + m_V^2\,\frac{2\zeta_2}{3}\,y_t^4. \tag{7}$$

Note that $\lambda, \zeta_{1,2}$ are all real. The vectors $V_{1,2,3}$ and $V_{4,5,6,7}$ are degenerate since $\mathrm{SU}(2)_\mathrm{U}$ is only broken by light quark Yukawas, not by y_t.

Fields $\mathrm{X}_{\bar{3},6}$ are weak doublets in the bi-fundamental representation $(1,3,3)$ of the flavor group. The color anti-triplets have field components $(V_\mu)_{i,j}^{r\gamma}$, and color sextets the field components $(V_\mu)_{i,j,\alpha,\beta}^r = (V_\mu)_{i,j,\beta,\alpha}^r$, with r the weak $\mathrm{SU}(2)_\mathrm{L}$ index, α, β, γ the color indices, while i and j are the indices of the $(1,3,1)$ and $(1,1,3)$ representations respectively. The tree level quark coupling Lagrangian terms are (suppressing all the indices apart from color, see also Eqs. (A30), (A31))

$$\mathcal{L}_{X_{\bar{3}}} = \eta_1\,\epsilon_{\alpha\beta\gamma}\,\bar{d}_R^\alpha \not{V}^\gamma\,Q_L^{c\beta} + h.c., \qquad \mathcal{L}_{X_6} = \eta_1\,\bar{d}_R^\alpha(\not{V})_{\alpha,\beta}\,Q_L^{c\beta} + h.c. \tag{8}$$

Note that the V_μ fields transform as $V_\mu \to V_D V_\mu V_Q^T$, where $d_R \to V_D d_R$ and $Q_L^c \to V_Q^* Q_L^c$. The mass terms are

$$\mathcal{L}_{X_{o,s}}^{\mathrm{mass}} = m_V^2\mathrm{Tr}(V_\mu V^{\mu\dagger}) + \lambda\,(H^\dagger\,H)\mathrm{Tr}(V_\mu V^{\mu\dagger}) + \lambda'\mathrm{Tr}(H_r V_\mu^r H^{s\dagger} V_s^{\mu\dagger}) + \lambda'\mathrm{Tr}(H_r^C V_\mu^r H^{Cs\dagger} V_s^{\mu\dagger}), \tag{9}$$

where we have suppressed all the traced over flavor, color and weak indices (except in the last two terms where we show explicitly the weak contractions). We use $[(V_\mu)_{i,j}^{r\gamma}]^* = (V_\mu^\dagger)_{r\gamma}^{j,i}$, and similarly for the sextet.

Note that the last two terms break the mass degeneracy between charge $1/3$ and charge $-2/3$ components of V_μ weak doublets. The flavor is broken through Yukawa insertions

$$\Delta\mathcal{L}^{\rm mass}_{X_{o,s}}/m_V^2 = \zeta_1 {\rm Tr}(V_\mu Y_D^\dagger Y_D V^{\mu\dagger}) + \zeta_2 {\rm Tr}(Y_D Y_D^\dagger V_\mu V^{\mu\dagger}) + \zeta_3 {\rm Tr}(V_\mu Y_U Y_U^\dagger V^{\mu\dagger}) + \cdots , \qquad (10)$$

where we do not write down the terms with more than two Yukawa insertions or the similar terms with Higgs fields. The resulting $\mathrm{H_F}$ symmetric spectrum for charge $2/3$ vectors is

$$m^2_{11,12,21,22} = m_V^2 + \frac{1}{2}(\lambda+\lambda')\,v^2, \qquad m^2_{13,23,32,31,33} = m^2_{11} + \zeta_3 m_V^2 y_t^2. \qquad (11)$$

The interactions of mass eigenstates $\tilde{V}_{kl}$ with mass eigenstate quarks (denoted with primes) are given by (showing explicitly only color contractions, see also Eqs. (A32), (A32))

$$\begin{aligned}
\mathcal{L}_{X_{\bar{3}}} &= \eta_1\, \epsilon_{\alpha\beta\gamma}\, (\bar{d'_R})^\alpha \tilde{\not{V}}_1^\gamma\, (u'_L)^{c\beta} + \eta_1\, \epsilon_{\alpha\beta\gamma}\, (\bar{d'_R})^\alpha \tilde{\not{V}}_2^\gamma V_{\rm CKM}\, (d'^c_L)^\beta + h.c.,\\
\mathcal{L}_{X_6} &= \eta_1\, (\bar{d'_R})^\alpha (\not{V})_{\alpha,\beta}\, (u'_L)^{c\beta} + \eta_1\, (\bar{d'_R})^\alpha (\not{V})_{\alpha,\beta} V_{\rm CKM}\, (u'_L)^{c\beta} + h.c.,
\end{aligned} \qquad (12)$$

where $\tilde{V}_1$ and $\tilde{V}_2$ are the mass eigenstate vector fields of the $\mathrm{SU}(2)$ doublet. The residual $\mathrm{H_F}$ flavor universality of these interactions can be broken by insertions of the spurions $Y_U^\dagger Y_U$ and $Y_D^\dagger Y_D$. In MFV this is the only form of further flavor breaking. The rest of the Lagrangian constructions are collected in the Appendix A.

III. PHENOMENOLOGY OF TEVATRON ANOMALIES

We now discuss two recent experimental anomalies observed at the Tevatron: the large forward-backward asymmetry $A_{FB}^{t\bar{t}}$, and the like-sign dimuon anomaly in B_s decays. In this section, we systematically address the following questions:

- Is it possible to explain either of the two anomalies assuming $\mathrm{H_F}$ symmetric models? By which charge and flavor assignments?
- Are closely related experimental constraints simultaneously obeyed?
- Is it possible to explain both anomalies using just a single $\mathrm{H_F}$ symmetric field?

A common feature of models put forward to explain the $A_{FB}^{t\bar{t}}$ anomaly [3, 15–18, 22–83] is that they have $O(1)$ NP couplings to the up quark. They fall roughly into two classes, those with s-channel exchange above a TeV[3] [25, 26, 75], in which case the axial vector NP couplings to the top quarks and up quarks must

[3] For a recent exception with a sub-TeV axigluon, see [17].

be of opposite sign [25, 26], and those with sub-TeV t-channel exchange [18, 22, 23, 26–28, 57], in which case large inter-generational couplings are required (for additional possibilities, see [29]). The couplings in either class could arise from large flavor violation in the underlying theory, which may lead to violations of FCNC constraints in $K^0 - \bar{K}^0, B_d^0 - \bar{B}_d^0, D^0 - \bar{D}^0$ mixing, $B \to K\pi$, or $b \to s\gamma$, unless the couplings are carefully aligned (see, e.g., [30, 31, 34]). Moreover, the t-channel models can lead to excessive (flavor violating) single top or same sign top pair production at the Tevatron and LHC [22].

However, flavor violation is not necessary for large $A_{FB}^{t\bar{t}}$ [35]. Note that in $t\bar{t}$ production no net top quark flavor charge is generated. Furthermore, models with an unbroken $\mathrm{H_F}$ subgroup do not generate FCNCs in processes with light quarks. The exact size of FCNCs then depends on the size of $\mathrm{H_F}$ breaking. If this breaking is MFV-like the FCNCs are generically suppressed below present bounds. The flavor symmetries also eliminate single top and same sign top production.

Many new models have also been put forward to explain the D$\emptyset$ dimuon anomaly [84–91]. Together with possible indications for deviations from the SM in $B_s \to J/\psi\,\phi$ decays and $B^- \to \tau^-\,\nu$ decays, it may point to a NP phase in $B_{s,d}$ mixing. Intriguingly, MFV suffices to explain the dimuon anomaly [92]. After discussing flavor symmetric fields and the $A_{FB}^{t\bar{t}}$ anomaly, we will examine whether these fields can also give large enough contributions to B_s mixing, under the assumption of MFV breaking of $\mathrm{H_F}$.

A. General analysis of the $t\,\bar{t}$ forward backward asymmetry

We entertain the possibility that $A_{FB}^{t\bar{t}}$ is enhanced above SM levels via tree level exchanges of flavor symmetric scalars or vectors. The experimental evidence for such enhancement is as follows. Using $5.3\mathrm{fb}^{-1}$ of data CDF measured an inclusive asymmetry $A_{FB}^{t\bar{t}} = 0.158 \pm 0.072 \pm 0.017$ in the $t\,\bar{t}$ rest frame (fixing $m_t = 172.5\,\mathrm{GeV}$) [6]. In a channel with both t and $\bar{t}$ decaying semileptonically an even larger asymmetry was found, $A_{FB}^{t\bar{t}} = 0.42 \pm 0.15 \pm 0.05$ [8]. Similarly, a recent DØ analysis finds $A_{FB}^{t\bar{t}} = 0.196 \pm 0.060^{+0.018}_{-0.026}$ using $5.4\mathrm{fb}^{-1}$ of data [7]. Combining in quadrature the statistical and systematic errors of the three measurements gives $A_{FB}^{t\bar{t}} = 0.200 \pm 0.047$. This is to be compared to the SM prediction $A_{FB}^{t\bar{t},SM} = 0.072^{+0.011}_{-0.007}$ from an approximate NNLO QCD calculation [93] with $m_t = 173.1\,\mathrm{GeV}$ and using the MSTW2008 set of PDFs [94]. Inclusion of electroweak corrections leads to an enhancement of the asymmetry, with $A_{FB}^{t\bar{t},SM} = 0.09 \pm 0.01$ recently obtained in Ref. [95]. In the $p\bar{p}$ frame, a recent approximate NNLO calculation [96] gives $A_{FB}^{t\bar{t}\,SM} = 0.052^{+0.000}_{-0.006}$ with $m_t = 173\,\mathrm{GeV}$, to be compared with the CDF value of $A_{FB}^{t\bar{t}} = 0.150 \pm 0.058 \pm 0.024$ [6]. The approximate NNLO SM predictions use the known NLO results [97–99] and build on recent progress in NNLO calculations [100–105]. DØ also reports a leptonic asymmetry $A_{FB}^{l} = 0.152 \pm 0.038^{+0.010}_{-0.013}$ to be compared to the MC@NLO prediction of

Observable	Measurement	SM predict.
$A_{FB}^{t\bar{t}}$	$\left.\begin{array}{l} 0.158 \pm 0.072 \pm 0.017\,[6] \\ 0.42 \pm 0.15 \pm 0.05\,[8] \\ 0.196 \pm 0.060^{+0.018}_{-0.026}\,[7] \end{array}\right\} \simeq 0.200 \pm 0.047$	$(7.24^{+1.04+0.20}_{-0.67-0.27}) \cdot 10^{-2}$[93]
$A_{FB}^{t\bar{t}}(M_{t\bar{t}} > 450\text{GeV})$	$0.475 \pm 0.101 \pm 0.049$ [6]	$(11.1^{+1.7}_{-0.9}) \cdot 10^{-2}$[93]
$A_{FB}^{t\bar{t}}(M_{t\bar{t}} < 450\text{GeV})$	$-0.116 \pm 0.146 \pm 0.047$ [6]	$(5.2^{+0.9}_{-0.6}) \cdot 10^{-2}$ [93]
$A_{FB}^{t\bar{t}}(\lvert\Delta y\rvert < 1.0)$	$0.026 \pm 0.104 \pm 0.056$ [6]	$(4.77^{+0.39}_{-0.35}) \cdot 10^{-2}$ [93]
$A_{FB}^{t\bar{t}}(\lvert\Delta y\rvert > 1.0)$	$0.611 \pm 0.210 \pm 0.147$ [6]	$(14.59^{+2.16}_{-1.30}) \cdot 10^{-2}$ [93]
$\sigma_{t\bar{t}}$	(6.9 ± 1.0)pb [108]	$\left\{\begin{array}{l} (6.63^{+0.00}_{-0.27})\text{pb [106]} \\ (7.08^{+0.00+0.36}_{-0.24-0.27})\text{pb [107]} \end{array}\right.$

TABLE III: Measurements and predictions for observables in $t\bar{t}$ production at the Tevatron. We quote the approximate NNLO QCD prediction of $A_{FB}^{t\bar{t}}$ from [93] using MSTW2008 PDFs [94]. The two other choices for PDFs give results in agreement with these [93]. Among the cross section predictions obtained in [106] we quote the 1PI_{SCET} one.

$A_{FB}^{l,\text{SM}} = 0.021 \pm 0.001$ [7].

CDF reported evidence that the anomalously large asymmetry rises with the invariant mass of the $t\,\bar{t}$ system, with $A_{FB}^{t\bar{t}}(M_{t\bar{t}} > 450\,\text{GeV}) = 0.475 \pm 0.114$, while $A_{FB}^{t\bar{t}}(M_{t\bar{t}} < 450\,\text{GeV}) = -0.116 \pm 0.153$ [6]. A similar rise of the asymmetry with respect to the absolute top vs. anti-top rapidity difference $|\Delta y| = |y_t - y_{\bar{t}}|$ was also reported by CDF with $A_{FB}^{t\bar{t}}(|\Delta y| < 1.0) = 0.026 \pm 0.104 \pm 0.056$ and $A_{FB}^{t\bar{t}}(|\Delta y| > 1.0) = 0.611 \pm 0.210 \pm 0.147$ [6]. The recent DØ analysis [7] does not observe a significant rise of the "folded" detector level asymmetry with respect to $M_{t\bar{t}}$ and $|\Delta y|$. However, until these results are unfolded they can not be directly compared to the CDF measurements, although at the detector level they appear to be consistent within errors. We collect the above results in Table III.

Any NP enhancement of $A_{FB}^{t\bar{t}}$ must not spoil the agreement between the measured production cross section, $\hat{\sigma}_{t\,\bar{t}}$, and the SM predictions. At NLO with NNLL summation of threshold logarithms, the SM prediction is $\sigma_{t\bar{t}} = (6.63^{+0.00}_{-0.27})$pb [106] (using MSTW2008 pdf sets and 1PI_{SCET} choice of kinematic variables and resummations – the other choices give consistent results but with larger error bars). This is somewhat smaller than the approximate NNLO result (for $m_t = 173$ GeV), $\sigma_{t\bar{t}} = 7.08^{+0.00+0.36}_{-0.24-0.27}$ pb [107] (see also [100, 104, 105]). Both of these results agree well, within errors, with the measured CDF result based on $4.6 fb^{-1}$ of data [108] $\sigma_{t\,\bar{t}}(m_t = 173.1\,\text{GeV}) = 6.9 \pm 1.0\text{pb}$. Thus the NP contribution to the $t\bar{t}$ cross section, $\sigma_{t\bar{t}}^{\text{NP}}$, is tightly constrained.

Good agreement between experiment and SM predictions is also seen in the differential cross section $d\sigma/dM_{t\bar{t}}$. This has important implications for the viability of different NP models. For instance, comparing the measured and predicted cross sections together with the measured and predicted $A_{FB}^{t\bar{t}}$, for $M_{t\bar{t}} > 450$

GeV, one finds that the NP contributions need to reduce the backward $t\bar{t}$-scattering cross section (a statement valid at 2σ). This can only happen if NP interferes with the SM [35]. NP in the s-channel which interferes with the single gluon exchange amplitude must therefore be due to color octet fields. In general s-channel resonances lead to significant effects in $d\sigma/dM_{t\,\bar{t}}$. However, this may be avoided for a purely axial gluon that is broad [17], in particular regions of parameter space. There are no such clear requirements on the charge assignments of possible t-channel NP contributions. However, a characteristic high mass tail in the spectrum could lead to tension with the Tevatron and future LHC cross section measurements at large $M_{t\bar{t}}$.

We collect expressions to be used in our analysis below. The total cross section $\sigma_{t\,\bar{t}}$, forward-backward asymmetry $A_{FB}^{t\bar{t}}$, and the cross sections for forward and backward scattering $\sigma_{F,B}$ are defined as

$$\sigma_{t\,\bar{t}} = \sigma_F + \sigma_B, \qquad A_{FB}^{t\bar{t}} = \frac{\sigma_F - \sigma_B}{\sigma_F + \sigma_B}, \qquad \sigma_{F(B)} = \int_{0(-1)}^{1(0)} d\cos\theta \, \frac{d\sigma}{d\cos\theta}, \tag{13}$$

where θ is the angle between incoming proton and outgoing top quark. We use NLO SM predictions for $\sigma_{t\,\bar{t}}$ and $d\sigma_{t\,\bar{t}}/dM_{t\bar{t}}$, and LO predictions for the NP corrections (including interference with the SM). To obtain $A_{FB}^{t\bar{t}}$ we define a partonic level asymmetry,

$$A_{FB}^{NP+SM} = \frac{\sigma_F^{NP} - \sigma_B^{NP}}{(\sigma_F^{\rm NP+SM})_{LO} + (\sigma_B^{\rm NP+SM})_{LO}} + A_{FB}^{SM}\left(\frac{\sigma^{SM}}{\sigma^{SM}+\sigma^{NP}}\right), \tag{14}$$

which is to be compared against the binned unfolded partonic level results of [6]. We use the NLO + NNLL SM predictions for the forward, backward and total cross sections [109], the $t\bar{t}$ spectrum [109] and $A_{FB}^{t\bar{t},SM}$ [93]. For concreteness, for $M_{t\,\bar{t}} < 450$ GeV we take the central values $\sigma^{SM} = 4.23$ pb and $A_{FB}^{t\bar{t},SM} = 0.052$, while for $M_{t\,\bar{t}} > 450$ GeV we take $\sigma^{SM} = 2.40$ pb and $A_{FB}^{t\bar{t},SM} = 0.111$ (MSTW08 pdfs); for the inclusive asymmetry (in the $t\bar{t}$ rest frame) we take $A_{FB}^{t\bar{t}} = 0.0724$.

1. Acceptance effects

As pointed out in [30, 110], care is needed when comparing NP predictions to the experimental parton level $A_{FB}^{t\bar{t}}$ and $M_{t\bar{t}}$ differential spectrum deduced by CDF [6, 108], since the deconvolution was done assuming the SM. The acceptance corrections are especially important if NP enhances top production in the very forward region This is because the SM $t\bar{t}$ event distribution is more central. We take into account the CDF experimental cuts using correction factors ϵ_i. For the $i-$th bin in $M_{t\bar{t}}$ one needs to multiply the calculated partonic $t\bar{t}$ cross section $d\sigma^{\rm NP}/dM_{t\bar{t}}$ by ϵ_i in order to compare with the CDF measured partonic cross section $(d\sigma^{\rm NP}/dM_{t\bar{t}})^{\rm CDF}$

$$\left(\frac{d\sigma^{\rm NP}}{dM_{t\bar{t}}}\right)_i^{\rm CDF} = \epsilon_i \times \left(\frac{d\sigma^{\rm NP}}{dM_{t\bar{t}}}\right)_i. \tag{15}$$

$M_{t\bar{t}}$ (GeV): $/\Delta y$:	$0-0.6$	$0.6-1.2$	$1.2-1.8$	$1.8-2.4$	$2.4-3.0$
$350-400$	2.42	2.23	–	–	–
$400-450$	3.44	2.74	1.95	–	–
$450-500$	4.29	3.32	1.75	–	–
$500-550$	5.25	3.50	2.34	1.18	–
$550-600$	5.61	4.39	2.67	1.15	–
$600-700$	6.59	4.81	3.01	1.09	0.42
$700-800$	7.38	6.06	3.49	1.34	0.45
$800-1400$	6.68	6.26	4.30	1.83	0.42

TABLE IV: Acceptances ϵ_{ij} (in %) to be used for emulating the CDF deconvolution to parton level measurements (cf. eqs. (15) - (17)). Note that the ϵ_{ij} do not depend on the NP model and are symmetric in $\Delta y \leftrightarrow -\Delta y$.

There is no summation over i in this equation. Since CDF is using SM acceptances and no bins in Δy in the deconvolution of the $d\sigma/dM_{t\bar{t}}$ measurement in [6], the ϵ_i are given by the ratio of acceptances for the NP model and the SM

$$\epsilon_i = \frac{\epsilon_i^{\rm NP}}{\epsilon_i^{\rm SM}}, \tag{16}$$

where $\epsilon_i^{\rm NP(SM)}$ are calculated by splitting each i-th $M_{t\bar{t}}$ bin into j bins in $\Delta y = y_t - y_{\bar{t}}$

$$\epsilon_i^{\rm NP(SM)} = \frac{\sum_j \epsilon_{ij}\sigma_{ij}^{\rm NP(SM)}}{\sum_j \sigma_{ij}^{\rm NP(SM)}}, \tag{17}$$

and the sum is over the bins in Δy. Here ϵ_{ij} is the acceptance for each $(M_{t\bar{t}}, \Delta y)$ bin, and $\sigma_{ij}^{\rm NP(SM)}$ is the corresponding cross section integrated over the bin. The above expressions are approximate in so far as the bins have finite sizes, and the spill-over of events between different bins is not taken into account. The acceptances are calculated by simulating the partonic $t-\bar{t}$ cross section using `MadGraph4.4.30` [111], decaying the top quarks in `Pythia6.4` [112], which also simulates the LO showering and hadronization, and using `PGS` for detector simulation. The events were read into `Mathematica`, where the cuts from [6, 113] were implemented. The resulting values for the acceptances ϵ_{ij} are collected in Table IV.

In Fig. 1 the correction factors ϵ_i are shown as a function of the $M_{t\bar{t}}$ bin for two benchmarks points (corresponding to illustrative couplings and mass valuers) in models $\mathrm{VI_{s,o}}$ which exhibit substantial departures from the SM acceptances. Results for $d\sigma/dM_{t\bar{t}}$ and $A_{FB}^{t\bar{t}}$ for the two model $\mathrm{VI_o}$ benchmark points in Fig. 1 were shown previously without acceptance corrections [35]. The differential distributions with acceptance corrections are compared to those in [35] in Fig. 2. We see that the corrections bring the predicted spectrum for the light vector example into good agreement with experiment. For the remaining $\mathrm{G_F}$ representations

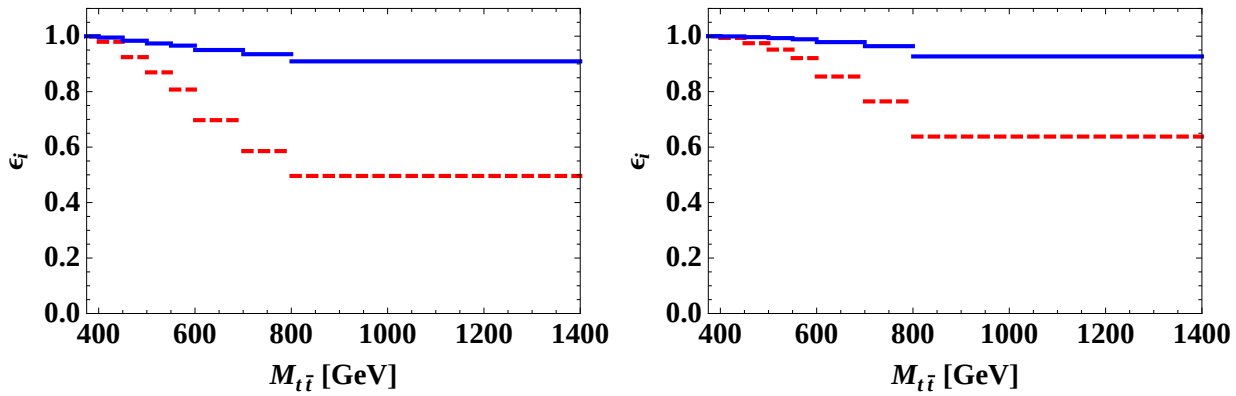

FIG. 1: The correction factors ϵ_i for t-channel dominated vector models $\mathrm{VI_s}$ (left) and $\mathrm{VI_o}$ (right), where $(m_V, \sqrt{\eta_{ij}\eta_{33}}, \eta_{i3}, \Gamma_V/m_V)$=(300 GeV, 1, 1.33, 0.08)[dashed red]; (1200 GeV, 2.2, 4.88, 0.5)[solid blue].

discussed below, the correction factors are not as important. For models $\mathrm{S_V}$, $\mathrm{VIII_s}$ and $\mathrm{IX_s}$ the ϵ_i are below 15%, and for the others they are below 5%, for all $M_{t\bar{t}}$ bins and all benchmarks points considered.

The pattern of acceptance corrections ϵ_i can be understood from the angular dependence of the NP contribution to the differential cross section in each model. For instance, the t-channel exchange of a vector with mass m_V leads to a Rutherford scattering peak in the forward direction for $m^2_{t\bar{t}} >> m^2_V$. Specifically, the expressions for the NP cross sections contain characteristic t-channel $(1-\cos\theta)^{2,4}$ factors in the denominators, whose angular dependence is reinforced by $(1+\cos\theta)^2$ factors in the numerators, where θ is the top quark scattering angle in the $t\bar{t}$ center of mass frame. Thus, models $\mathrm{VI_{s,o}}$ with light vector masses favor forward top-quark production at large $M_{t\bar{t}}$, yielding ϵ_i that are substantially less than 1 in the high $M_{t\bar{t}}$ bins. In models $\mathrm{S_I}$ (t-channel) and $\mathrm{S_V}$, $\mathrm{S_{VI}}$ (u-channel), the angular dependence introduced by the characteristic $(1\mp\cos\theta)^{2,4}$ factors in the denominators is offset by $(1\mp\cos\theta)^2$ factors in the numerators, which leads to central NP top-quark production, as in the SM. The result is that the ϵ_i in these models are actually slightly larger than 1.

To apply the acceptance corrections to $A^{t\bar{t}}_{FB}$ we follow CDF, where $A^{t\bar{t}}_{FB}$ was obtained using four bins in $M_{t\bar{t}}$ and Δy: $M_{t\bar{t}}$ above or below 450 GeV and Δy positive or negative. The correction factor for each of the four bins is given as in Eqs. (15)-(17), except that the sum in (17) now runs over all j with either $\Delta y > 0$ or $\Delta y < 0$, and over the appropriate values of i with either $M_{t\bar{t}} > 450$ GeV or $M_{t\bar{t}} < 450$ GeV. We find that the corrections are small for all of the models we consider. For instance, for the light vector color octet example in Fig. 1 the shift is from an uncorrected $A^{t\bar{t}}_{FB} = (0.10949, 0.357)$ to a corrected $A^{t\bar{t}}_{FB} = (0.10953, 0.339)$, where the first and second numbers are the low and high mass bins in $A^{t\bar{t}}_{FB}$. The small shifts in $A^{t\bar{t}}_{FB}$ are due to the coarse binning in $M_{t\bar{t}}$ [110]. In particular, the high mass bin is dominated

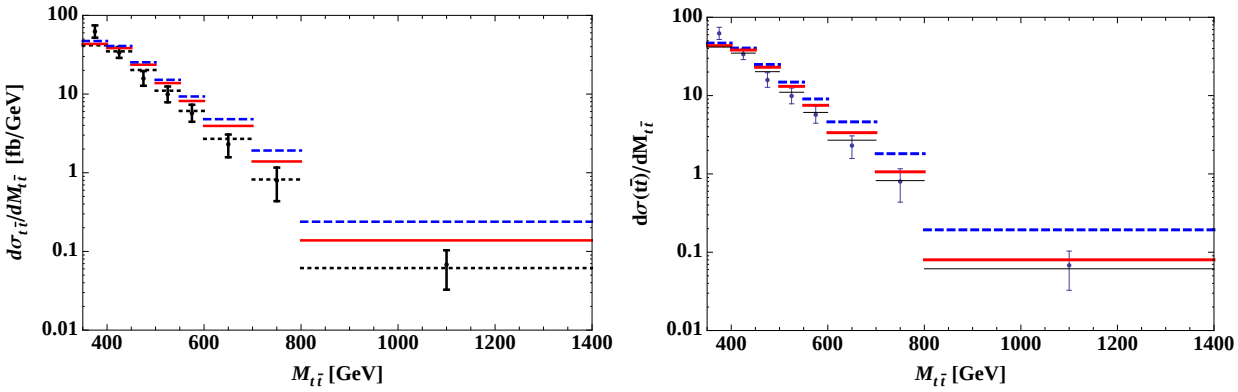

FIG. 2: The effect of acceptance corrections on the vector model discussed in [35]. Before acceptance corrections (left), after corrections applied (right). For the parameters $(m_V, \sqrt{\eta_{ij}\eta_{33}}, \eta_{i3}, \Gamma_V/m_V)$: solid red $(300\,\mathrm{GeV}, 1, 1.33, 0.08)$; dashed blue $(1200\,\mathrm{GeV}, 2.2, 4.88, 0.5)$.

by events with $M_{t\bar{t}}$ near 450 GeV, which are more central, as in the SM.

2. *The $t\,\bar{t}$ phenomenology of $\mathrm{H_F}$ symmetric scalar fields*

The flavor symmetric models introduced in Section II and collected in Tables I, II can couple to light and heavy quark bilinears with unsuppressed couplings. They are thus interesting candidates to explain the $A_{FB}^{t\bar{t}}$ anomaly, as noted in [3, 35, 36]. In the case of scalars, $\mathrm{SU(2)_L}$ singlet color triplets or color sextets and $\mathrm{SU(2)_L}$ doublet color singlets have previously been identified as being promising for explaining the $A_{FB}^{t\bar{t}}$ anomaly [18, 32, 33, 35–37, 114]. Here, we will focus on some of the flavored versions listed in Table II. Our results overlap with past studies, but we also include color triplet and sextet scalars that couple to initial state down quarks, that have not been studied as extensively. We find that these models may also be viable, although they generically require a coupling that is a factor of ~ 2 larger than if the up quark is in the initial state. This rule of thumb also holds for the vector models that we will study in next subsection.

We show results below for models $\mathrm{S_{V,VI}}$ that couple to initial state up quarks, for models $\mathrm{S_{IX,X}}$ that couple to initial state down quarks, and model $\mathrm{S_I}$ that couples to initial state up and down quarks. (Flavored color sextets and color triplets were considered previously in [35, 36]). We expect models $\mathrm{S_{XI}} - \mathrm{S_{XIV}}$ to yield results similar to those for $\mathrm{S_{IX}}, \mathrm{S_X}$. The scalar models $\mathrm{S_{III}}$ and $\mathrm{S_{IV}}$ are in the $\mathbf{1}$ and $\mathbf{8}$ color representations respectively. These models are known to generically suppress $A_{FB}^{t\bar{t}}$ when interfering with the SM [18] and we do not consider them further.

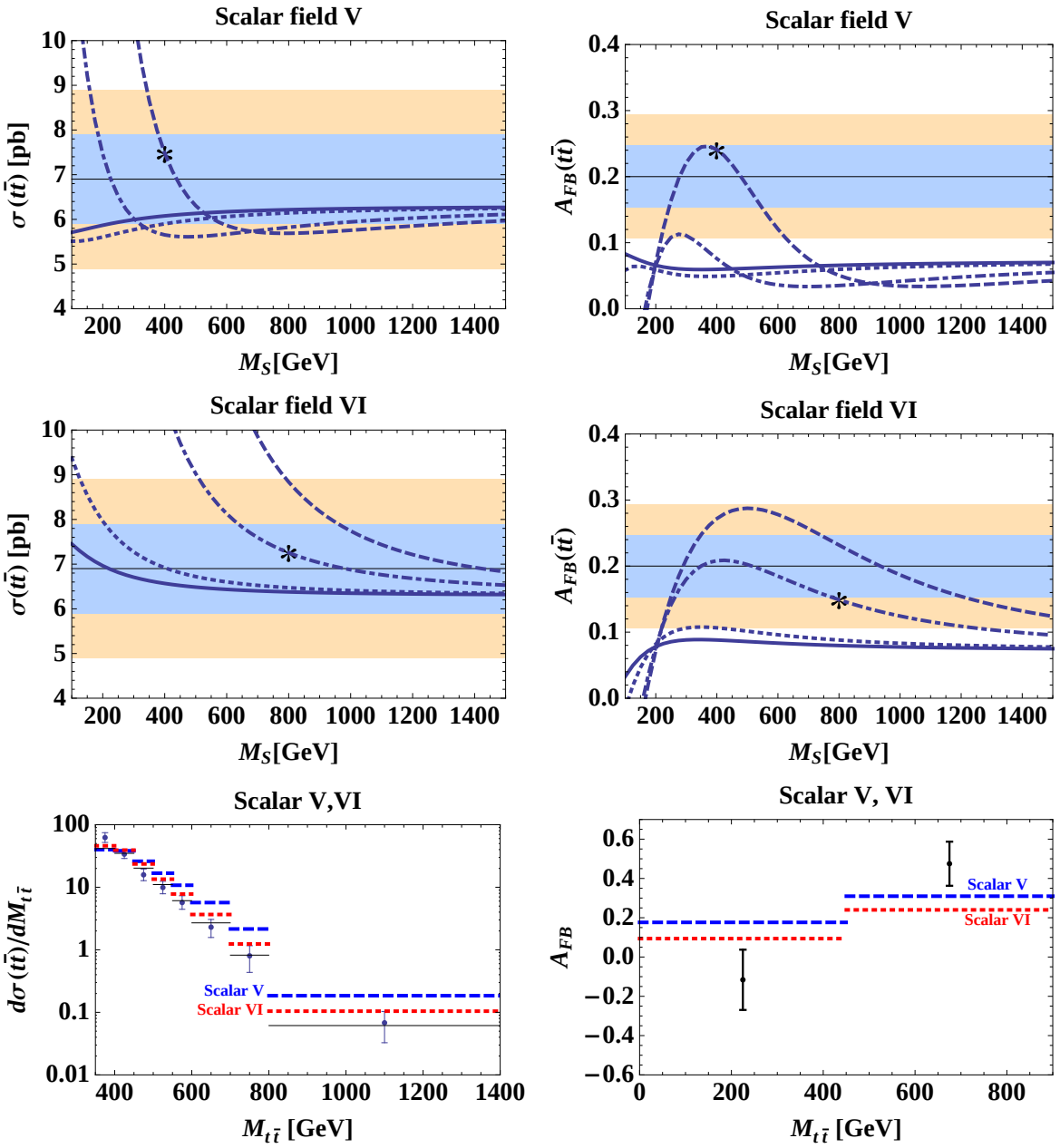

FIG. 3: Upper two rows: predictions for the inclusive cross sections $\sigma(t\bar{t})$ and inclusive forward-backward asymmetry $A_{FB}(t\bar{t})$ as a function of scalar mass m_S for models $\mathrm{S_V}, \mathrm{S_{VI}}$ and couplings $\eta = 1/4$ (solid line), $1/2\sqrt{2}$ (dotted), $1/\sqrt{2}$ (dot-dashed), 1 (dashed) compared to 1σ and 2σ experimental (shaded) bands. Predictions for $A_{FB}^{t\bar{t}}$ with $M_{t\bar{t}}$ below and above 450 GeV and for $d\sigma_{t\,\bar{t}}/dM_{t\,\bar{t}}$ are compared to the experimental data from [6, 108] in the last row for benchmark points labeled with a $\star$ in the inclusive predictions ($m_S = 400$ GeV for $\mathrm{S_V}$ and 800 GeV for $\mathrm{S_{VI}}$).

The interaction Lagrangians for scalar models $\mathrm{S_I}$ and $\mathrm{S_{IX}}$ are

$$\mathcal{L}_{\mathrm{I}} = \eta\,(\,S^0_{ij}\bar{u}_{i\,L}u_{j\,R} + S^-_{ij}\bar{d}_{i\,L}u_{j\,R}) + h.c., \tag{18}$$

$$\mathcal{L}_{\mathrm{IX}} = \eta\,\epsilon_{\alpha\beta\gamma}S^{\alpha}_{ij}d_R^{i\,\beta}\,u_R^{j\,\gamma} \;+\; h.c., \tag{19}$$

where i, j and α, β, γ denote flavor and color indices, respectively. Explicit forms of the interaction Lagrangians for the remaining scalar models under discussion, $\mathrm{S_{V,VI,X}}$ are collected in Appendix A. In the $\mathrm{G_F}$ symmetric limit the decay widths of the scalars are $\kappa\,\eta^2\,m_S/16\pi$, where η is the coupling of the scalar field to the SM quarks, and $\kappa = 1,\ 8,\ 8,\ 2,\ 2$ in models $\mathrm{S_I}, \mathrm{S_V}$, $\mathrm{S_{VI}}$, $\mathrm{S_{IX}}$, $\mathrm{S_X}$, respectively (assuming all quark decay channels are open and ignoring phase space effects). The interaction Lagrangians explicitly defining η are collected in Appendix A, while the relevant NP cross section formulae for top quark pair production can be found in Appendix B.

In Figs. 3 and 4 we collect predictions for the inclusive $A_{FB}^{t\bar{t}}$ and $\sigma_{t\,\bar{t}}$ as functions of the scalar masses in models $\mathrm{S_V}$, $\mathrm{S_{VI}}$, $\mathrm{S_{IX}}$, and $\mathrm{S_X}$, for several values of the couplings η to quarks. These results do not depend on whether one is considering the $\mathrm{G_F}$ symmetric limits in Eqs. (19), (A37), and (A38)), or the $\mathrm{H_F}$ symmetric limits (with the couplings of the light quarks to the top identified with the chosen values of η). Large effects on $A_{FB}^{t\bar{t}}$ are possible, while remaining within the 2σ bounds for $\sigma_{t\,\bar{t}}$. In general $\mathcal{O}(1)$ couplings η are required. Therefore, some $\mathrm{G_F} \to \mathrm{H_F}$ flavor breaking will be necessary in order to satisfy the dijet constraints on the couplings to light quark pairs, particularly in models $\mathrm{S_{VI}}$ and $\mathrm{S_X}$ (we comment on this further below). For example, recent LHC dijet measurements imply that in model $\mathrm{S_{VI}}$ the couplings of light quarks to ~ 1 TeV mass scalars should be $\lesssim 0.1$, see Section IV C.

A strong constraint on these models is consistency with the measured $d\sigma(t\,\bar{t})/dM_{t\bar{t}}$ distribution. To demonstrate the potential of these models to explain the $A_{FB}^{t\bar{t}}$ anomaly and their impact on this spectrum we pick particular benchmark values for the scalar masses and couplings, denoted by a $\star$ in Figs. 3, 4. The resulting $d\sigma(t\,\bar{t})/dM_{t\bar{t}}$ spectra and $A_{FB}^{t\bar{t}}$ in the low and high $M_{t\bar{t}}$ bins are shown in the last rows of Figs. 3, 4. We do not apply K-factors to the NP cross sections in any of the models we consider. A genuine NLO calculation for these models is beyond the scope of this work, but is clearly required before precise conclusions can be drawn regarding the effects of the various models on the $d\sigma/dM_{t\bar{t}}$ distributions. All chosen points predict a significantly enhanced $A_{FB}^{t\bar{t}}$ in the high invariant mass bin. In general, these models reduce the good agreement between the SM and measured $d\sigma(t\,\bar{t})/dM_{t\bar{t}}$ spectrum, while improving the agreement in $A_{FB}^{t\bar{t}}$. Clearly, there is significant tension between satisfying the constraints on the $M_{t\bar{t}}$ distribution while simultaneously creating a large $A_{FB}^{t\bar{t}}$ enhancement, as has recently been emphasized in [37, 44]. Recent DØ data [7] shows a preference for a smaller $A_{FB}^{t\bar{t}}$ in the high $M_{t\bar{t}}$ bin. While the $M_{t\bar{t}}$ dependence of $A_{FB}^{t\bar{t}}$ has not been unfolded by DØ , and thus cannot be directly compared to the results in Figs. 3 and 4, some of the tension may be alleviated with the new data.

The flavor breaking naturally present in this framework can reduce the remaining tension with measurements associated with the light quark sector, e.g., from the dijet bounds mentioned above. For instance, keeping the leading insertions in y_t^2 that break $\mathrm{G_F} \to \mathrm{H_F}$, the Lagrangian for scalar model $\mathrm{S_{IX}}$ in the mass

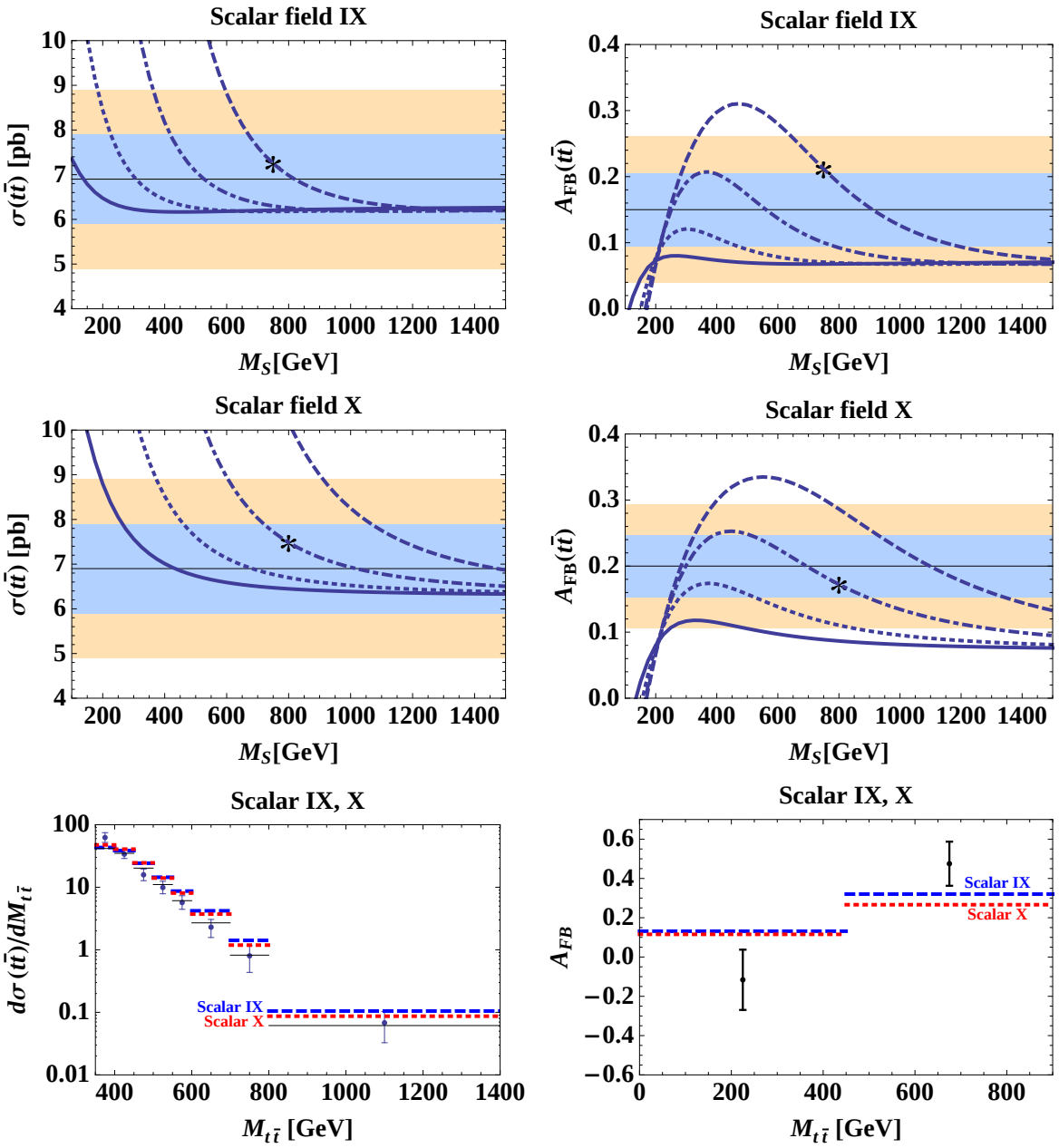

FIG. 4: The same as Fig. 3, but for models $S_{X,IX}$ and couplings $\eta = 1/\sqrt{2}$ (solid line), 1 (dotted), $\sqrt{2}$ (dot-dashed), 2 (dashed). Benchmark masses are $m_S = 750$ GeV (S_{IX}) and $m_S = 800$ GeV (S_X).

eigenstate basis becomes,

$$\mathcal{L}_{IX} = \eta_1 \, (d'_R)_{\alpha i} \, (u'_R)_{\beta j} \, S'^{i,j}_{\gamma} \, \epsilon^{\alpha\beta\gamma} + \left(\eta_1 + 2\,\eta_2\, y_t^2\right) (d'_R)_{\alpha i} \, (t'_R)_{\beta} \, S'^{i,3}_{\gamma} \, \epsilon^{\alpha\beta\gamma}, \tag{20}$$

with $j = \{1, 2\}$ and $i = \{1, 2, 3\}$. The mass spectrum is split, with $m^2_{i3} = m^2_{ij} + \tilde{\zeta}_1 m^2_S$. Depending on the signs of $\eta_{1,2}$ and $\tilde{\zeta}_1$ one can have an enhanced coupling to top quarks (compared to couplings to light quarks) with a suppressed mass scale of the m^2_{i3} components of the scalar. This can naturally lead to larger effects

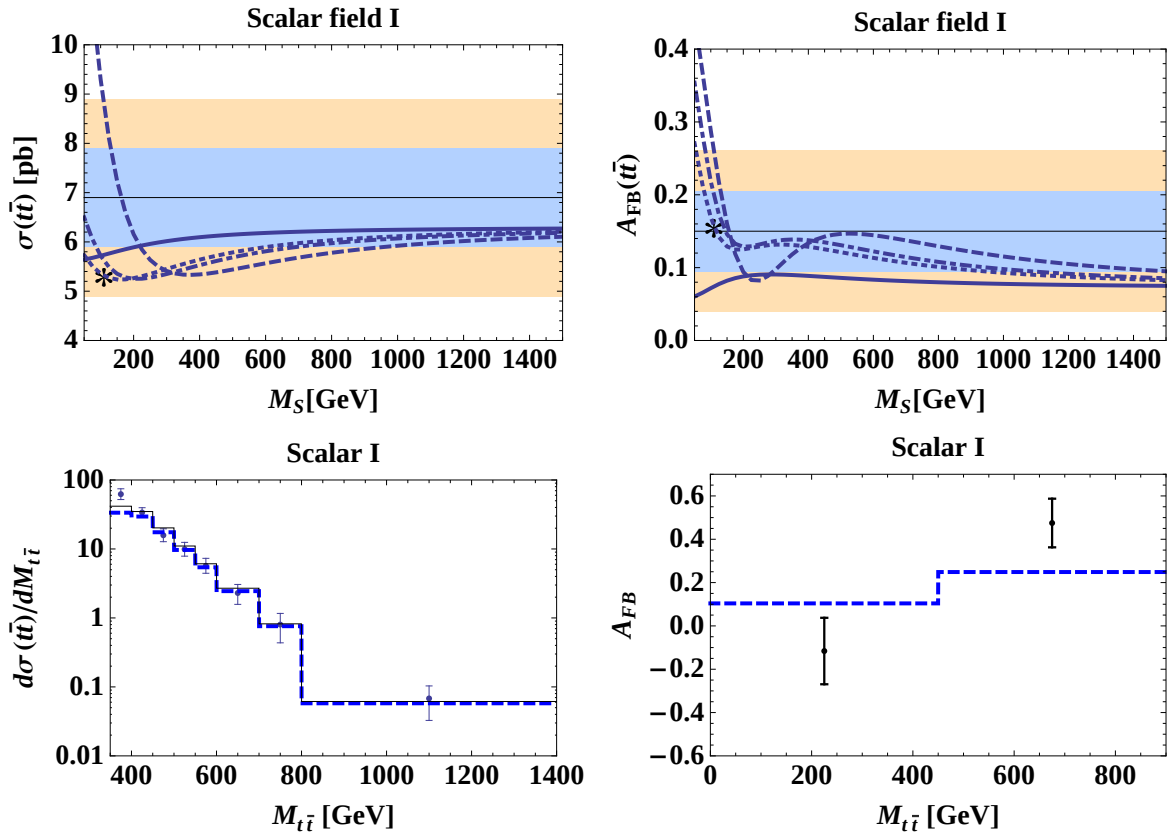

FIG. 5: Upper row: predictions for the cross section $\sigma(t\bar{t})$ and inclusive forward-backward asymmetry $A_{FB}(t\bar{t})$ as a function of scalar mass m_S for model $\mathrm{S_I}$ and coupling $\eta = 1/3$ (solid curve), $2/3$ (dotted), $3/4$ (dot-dashed), 1 (dashed). Predictions for $A_{FB}^{t\bar{t}}$ with $M_{t\bar{t}}$ below and above 450 GeV and for $d\sigma_{t\,\bar{t}}/dM_{t\,\bar{t}}$ are shown in the last row for the benchmark point labeled with a $\star$ in the inclusive predictions ($m_S = 110$ GeV).

on top phenomenology, such as $A_{FB}^{t\bar{t}}$ and $\sigma_{t\,\bar{t}}$, while at the same time weakening the impact of the dijet constraints (see Section IV C). This situation is similarly realized in the other scalar models. Alternatively, one could consider minimal $\mathrm{H_F}$ symmetric versions of models $\mathrm{S_{IX}}$ and $\mathrm{S_X}$, which only contain the scalar $\mathrm{G_F}$ submultiplets transforming as $(1, 2, 1)$ under $\mathrm{H_F}$ (they only couple the light quarks directly to the top quark), while in the minimal $\mathrm{H_F}$ symmetric versions of models $\mathrm{S_V}$ and $\mathrm{S_{VI}}$ one would consider the $(2, 1, 1)$ representations of $\mathrm{H_F}$.

Finally, we discuss model $\mathrm{S_I}$.[4] (Models with flavored scalar doublets have previously been considered in [32, 33]). For illustration, we can define the left-handed (LH) quark fields in Eq. (18) in either the up or down quark mass eigenstate basis (with the right-handed (RH) up quarks in their mass eigenstate basis). In both cases, the recent DØ upper bounds [116] on anomalous resonant dijet production in W +

[4] Note that two studies have recently concluded [37, 114] that a (color singlet) $SU(2)_L$ doublet would be the most promising, among the possible scalar representations, for explaining the $t\bar{t}$ asymmetry with minimal distortion of the Tevatron and LHC $M_{t\bar{t}}$ spectra.

jets imply that the couplings of the scalars to light quarks should satisfy $\eta_{ij} \lesssim 0.2$, $i,j = \{1,2\}$, given the light scalar doublet masses favored by the $A_{FB}^{t\bar{t}}$ anomaly (see below and Section IV C). Significant breaking of $\mathrm{G_F} \to \mathrm{H_F}$ would, therefore, be necessary in order to accommodate $O(1)$ scalar-top quark-light quark couplings. However, we reiterate that $\mathrm{H_F}$ symmetry protects against NP contributions to $K-\bar{K}$ and $D-\bar{D}$ mixing, as well as to single top and same sign top production.

If the LH quarks in Eq. 18 are defined in the up mass basis, then the $B \to K\pi$ branching ratio constraints [37, 115] would also impose the bound $\eta_{3i} \lesssim 0.2$, $i = \{1,2\}$, see Section IV D. Therefore, in this case top phenomenology would be well approximated by a minimal $\mathrm{H_F}$ symmetric model consisting of scalar $\mathrm{SU(2)_L}$ doublets which transforms as $(1,1,2,a)$ under $\mathrm{H_F}$, where the $U(1)_3$ charge a is opposite to that of the top and bottom quarks ($\mathrm{U(2)_{Q_L}}$ is defined with respect to the LH up quark mass eigenstate basis). We can write the corresponding interaction Lagrangian, in the quark mass eigenstate bases, as

$$\mathcal{L}^{\rm min}_{\rm I(a)} = \eta\,(S^0_{i\,3}\,\bar{u}'_{i\,L}\,t'_R + S^-_{i\,3}\,(V^\dagger_{\rm CKM})_{j\,i}\,\bar{d}'_{j\,L}\,t'_R) + h.c., \tag{21}$$

where $i = \{1,2\}$, $j = \{1,2,3\}$ and $V_{\rm CKM}$ is the Cabbibo-Kobayashi-Maskawa (CKM) matrix. If the LH quarks in Eq. (18) are defined in the down quark mass eigenstate basis, there are two minimal $\mathrm{H_F}$ symmetric and flavor safe alternatives for $A_{FB}^{t\bar{t}}$ enhancement: exchange of scalar $\mathrm{SU(2)_L}$ doublets which transform as $(2,1,1,a)$, or as $(1,1,2,a)$ ($\mathrm{U(2)_{Q_L}}$ is now defined with respect to the LH down quark mass eigenstate basis). The relevant interaction Lagrangians would be

$$\mathcal{L}^{\rm min}_{\rm I(b)} = \eta\,(S^0_{3\,i}\,\bar{u}'_{j\,L}\,(V_{\rm CKM})_{j\,3}\,u'_{i\,R} + S^-_{3\,i}\,\bar{b}'_L\,u'_{i\,R}) + h.c., \tag{22}$$

or

$$\mathcal{L}^{\rm min}_{\rm I(c)} = \eta\,(S^0_{i\,3}\,\bar{u}'_{j\,L}\,(V_{\rm CKM})_{j\,i}\,t'_R + S^-_{i\,3}\,\bar{d}'_{i\,L}\,t'_R) + h.c., \tag{23}$$

respectively, where $i = \{1,2\}$, $j = \{1,2,3\}$. For the light scalar masses ($\lesssim 130$ GeV) and $O(1)$ couplings η favored by $A_{FB}^{t\bar{t}}$, options I(a) and I(c) above (Eqs. (21), (23)) are disfavored at the 4σ level by constraints on non-oblique corrections to the Z couplings to quarks, whereas option I(b) (Eq. (22)) is consistent at 2σ, see Section IV B. In a generalization of option I(b) to complete $\mathrm{G_F}$ multiplets, non-oblique correctons would dictate that the couplings η_{i3} need to be roughly a factor of 2 smaller than η_{3i} for $i = \{1,2\}$, while Wjj constraints would dictate the bounds $\eta_{ij} \lesssim 0.2$ for $i,j = \{1,2\}$.

In Fig. 5 we show predictions for $A_{FB}^{t\bar{t}}$ (inclusive and $M_{t\bar{t}}$ bins) and $d\sigma/dM_{t\bar{t}}$ corresponding to Eq. (22). Our results confirm the findings in [37] for $A_{FB}^{t\bar{t}}$ enhancement with scalar doublets: given CDF data the preferred scalar mass is small, below 130 GeV, while the coupling η is $O(1)$. Also, the difference between the asymmetries in the low and high mass bins is not large when the latter is enhanced (which could be

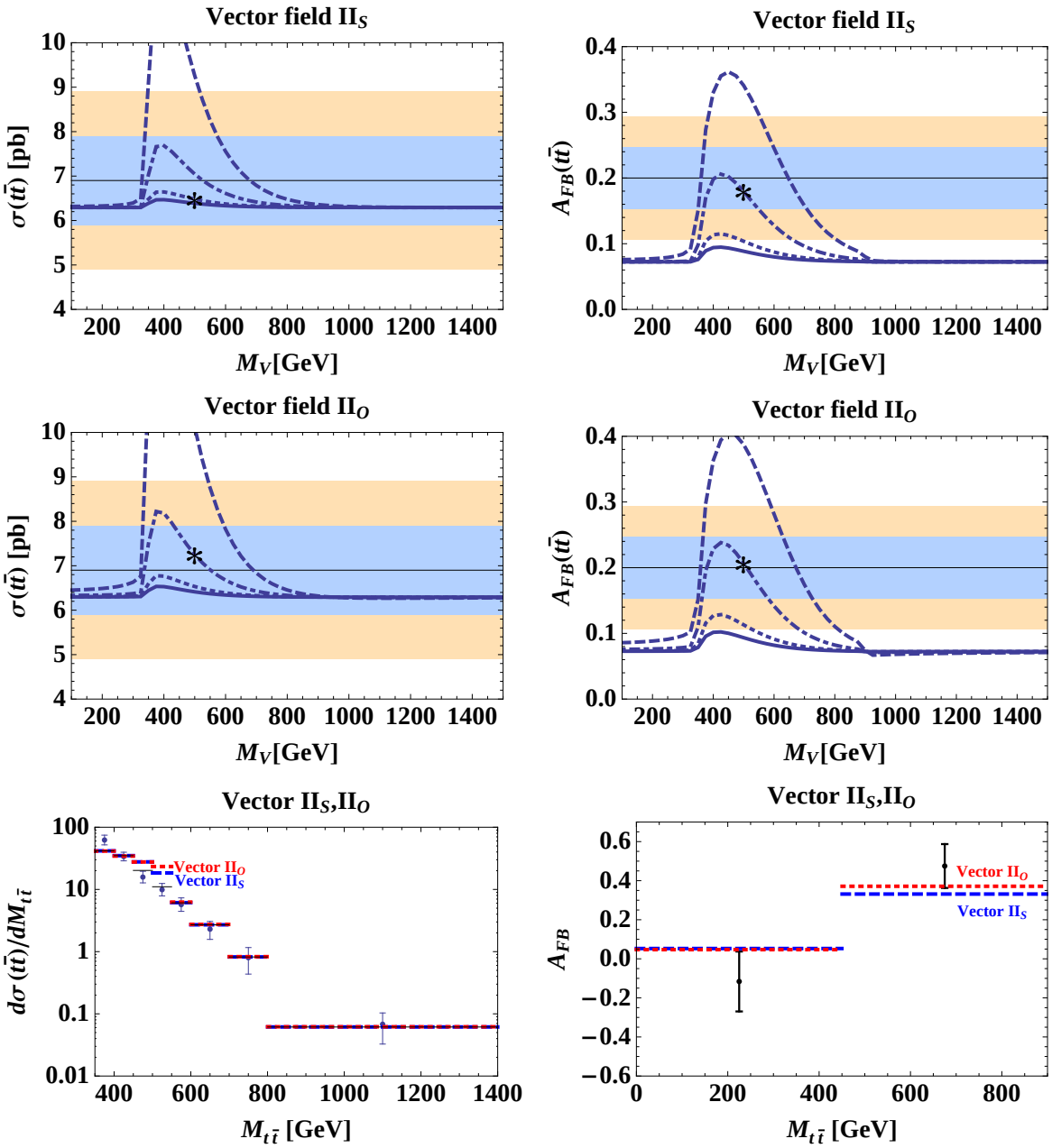

FIG. 6: Upper two rows: predictions for total cross sections $\sigma(t\bar{t})$ and inclusive forward-backward asymmetry $A_{FB}(t\bar{t})$ as a function of vector mass m_V for models II$_{s,o}$ and couplings $f_q f_t = 1/256$ (solid curve), $1/128$ (dotted), $1/32$ (dot-dashed), $1/8$ (dashed). The bands are the one and two σ measurements of $A_{FB}^{t\bar{t}}$ and $\sigma_{t\,\bar{t}}$. The predictions for A_{FB} with $M_{t\bar{t}}$ below and above 450 GeV and for $d\sigma_{t\,\bar{t}}/dM_{t\,\bar{t}}$ are shown in the last row for benchmark points labeled with a $\star$ in the inclusive predictions ($M_V = 500$ GeV). The data are summarized in Table III.

welcome in view of the recent DØ $A_{FB}^{t\bar{t}}$ measurements), and there is minimal impact on the $M_{t\bar{t}}$ spectrum. Finally, we note that for our benchmark points the bounds on the top quark decay width are not violated by new top quark decays to a scalar and a light quark (even though there are 2 times as many such modes in I(b) than previously considered in [37]).

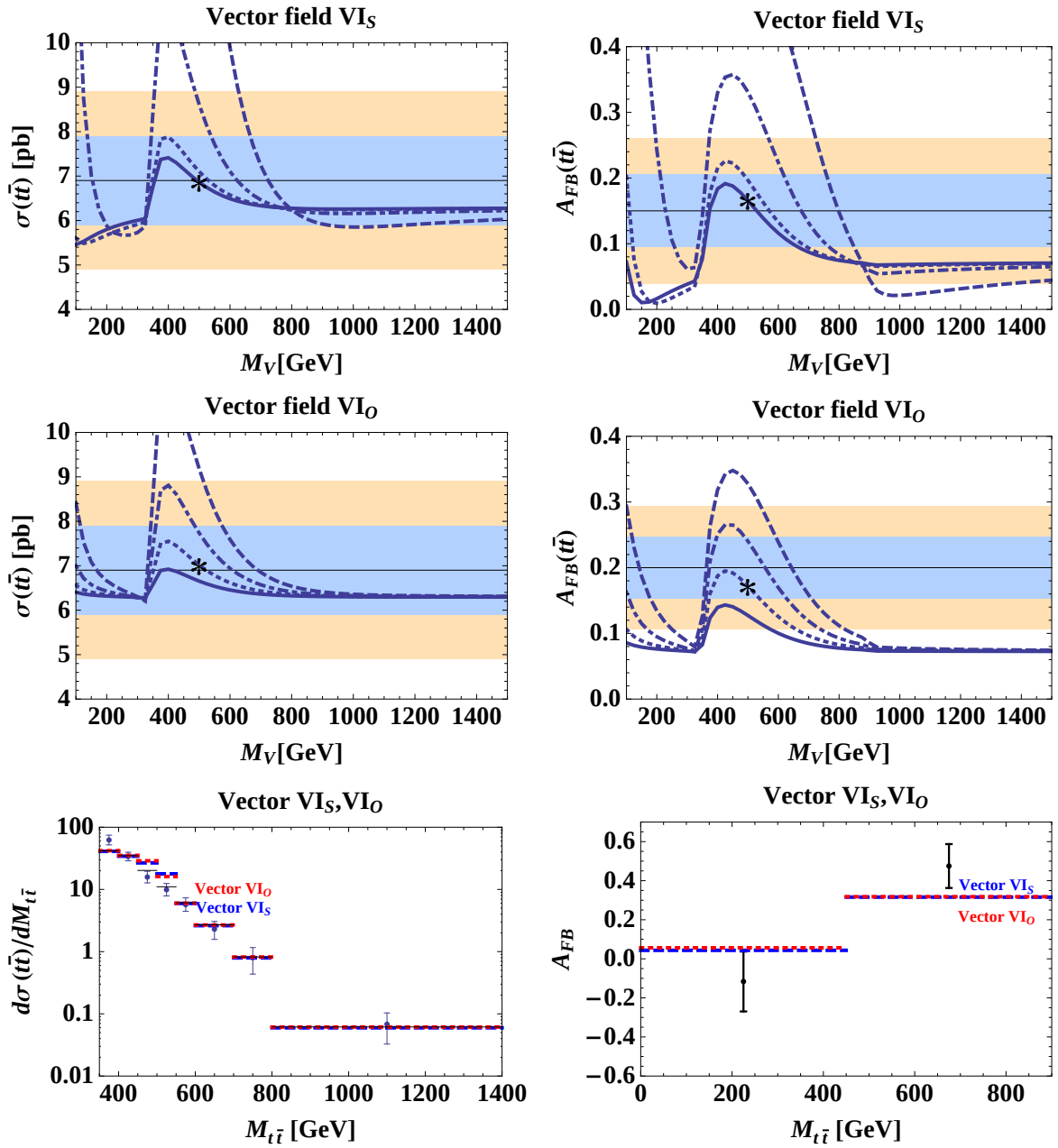

FIG. 7: Same as Fig. 6 but for vector models $\mathrm{VI_{s,o}}$ and couplings $f_q f_t = f_{qt}^2 = 1/4\sqrt{2}$ (solid curve), $1/4$ (dotted), $1/\sqrt{2}$ (dot-dashed), $2\sqrt{2}$ (dashed) for model $\mathrm{V_s}$ and couplings $f_q f_t = f_{qt}^2 = 1/16$ (solid curve), $1/8$ (dotted), $1/4$ (dot-dashed), $1/2$ (dashed) for model $\mathrm{V_o}$. For the benchmark points, $m_V = 500$ GeV.

3. *The $t\bar{t}$ phenomenology of $\mathrm{H_F}$ symmetric vector fields*

In flavor symmetric scalar models, $t\bar{t}$ production can only proceed via the u or t channels. Flavor symmetric vector models differ in this respect, as $t\bar{t}$ production can also proceed in the s channel or both in s and t channels simultaneously. Top phenomenology in these models is dictated to a large extent by which channel dominates. The sizes of the couplings required in order to explain the top asymmetry are roughly

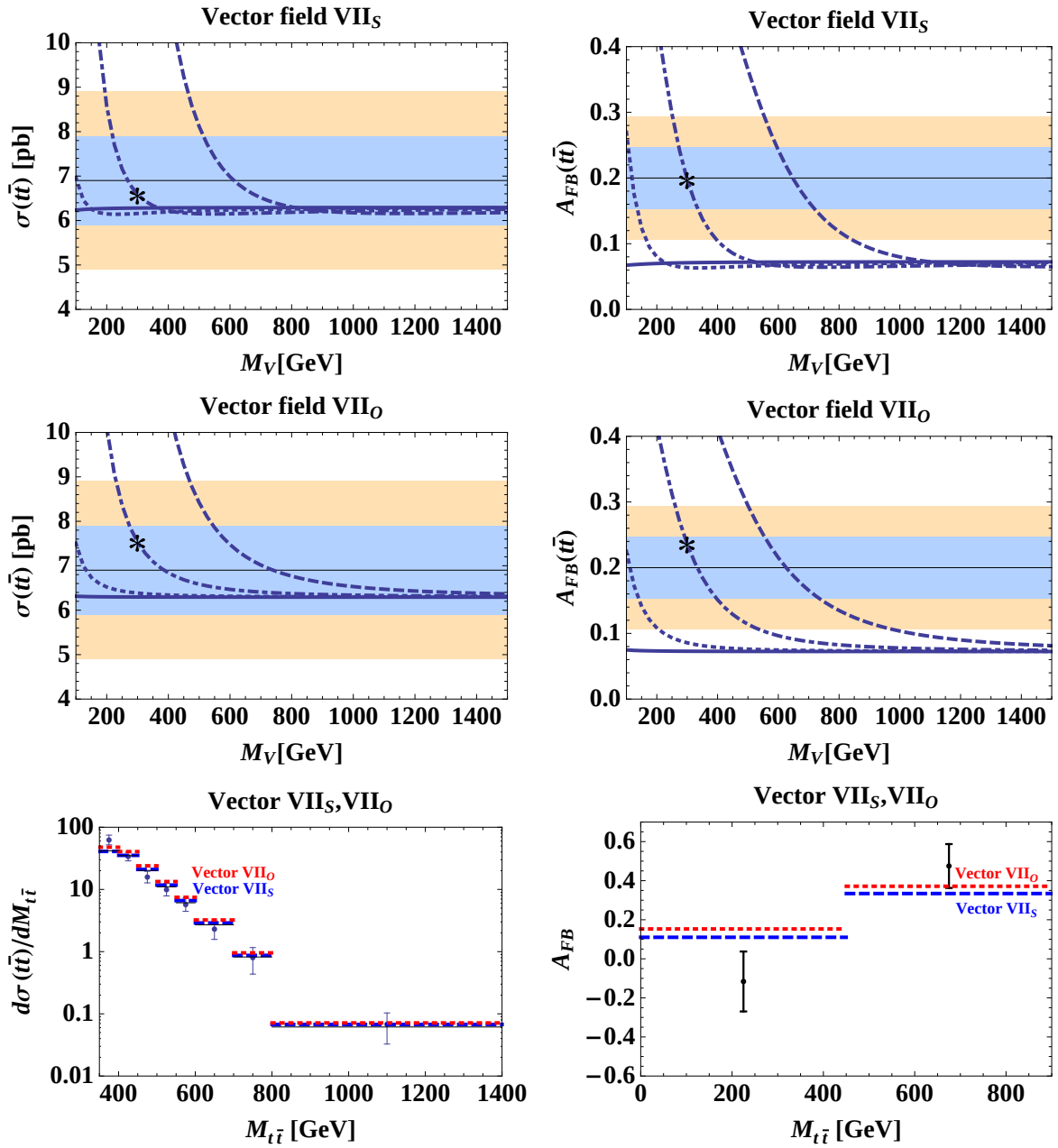

FIG. 8: Same as Fig. 6 but for pure t channel vector models $\mathrm{VII_{s,o}}$ and coupling $f_{qt} = 1/5$ (solid curve), $4/5$ (dotted), $8/5$ (dot-dashed), $16/5$ (dashed) for model $\mathrm{V_s}$ and couplings $f_{qt} = 1/4$ (solid curve), 1 (dotted), $9/4$ (dot-dashed), 4 (dashed) for model $\mathrm{V_o}$. For the benchmark points, $m_V = 300$ GeV.

fixed by whether the vectors couple to up or down quarks in the initial states, as in the scalar models. The Lagrangians for the vector models are given in Section II and Appendix A. Expressions for the $q\,\bar{q} \to t\,\bar{t}$ cross sections for models $\mathrm{I}-\mathrm{XI}$ are collected in Appendix B. They are given in terms of effective couplings of the vectors to light quarks (f_q), to top quarks (f_t), and to top and light quarks (f_{qt}), defined in terms of $\eta_{1,2}$ etc, see Table VII. In this section we use these couplings as numerical inputs. In the $\mathrm{G_F}$ symmetric limit ($y_t = 0$), one has $f_q = f_t = f_{qt}$. Among the vector models, $\mathrm{I_s}$ and $\mathrm{V_{s,o}}$ do not contribute to top

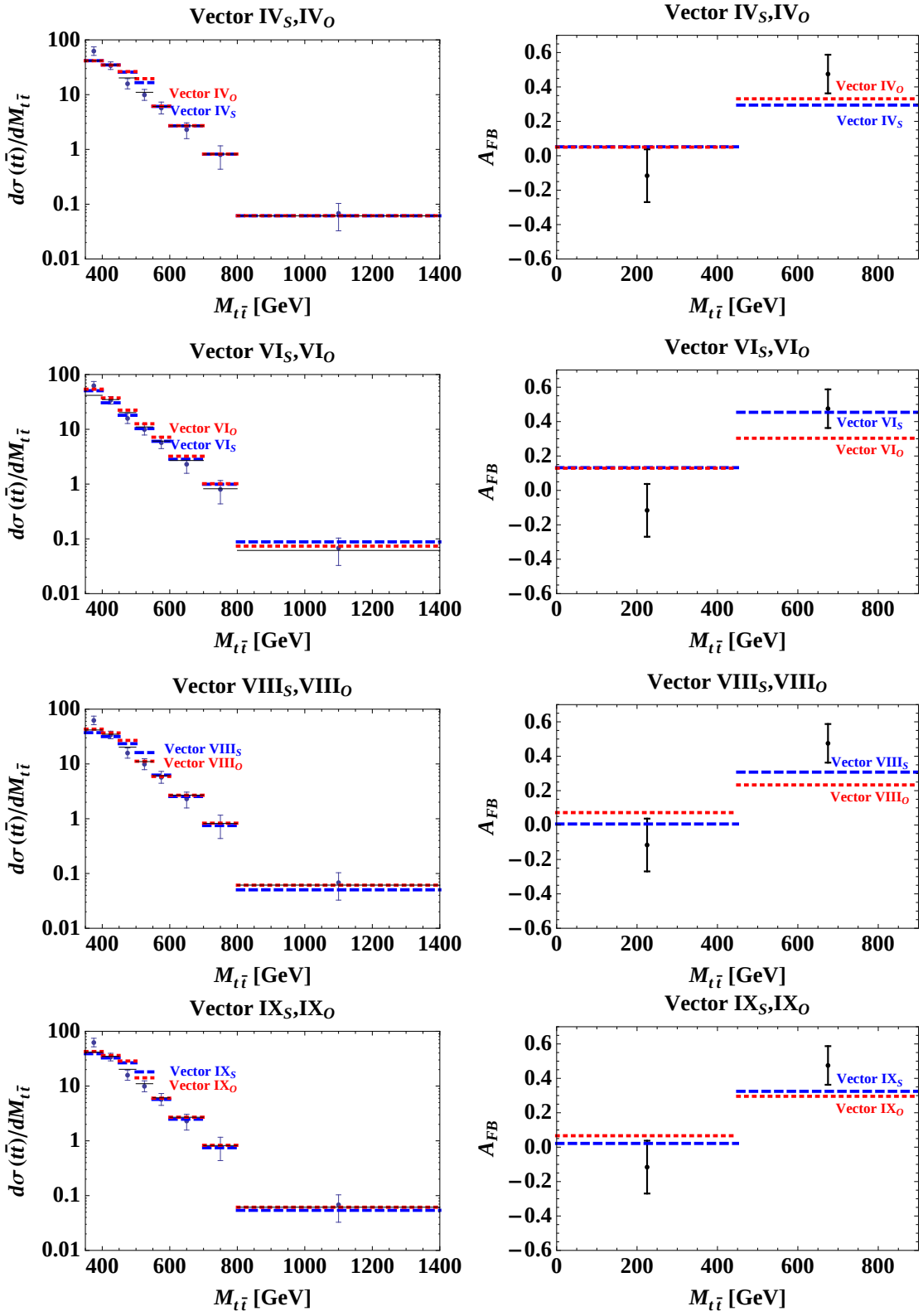

FIG. 9: Predictions for $d\sigma/dM_{t\bar{t}}$ and A_{FB} for a set of vector models, $\mathrm{IV_{s,o}}, \mathrm{VI_{s,o}}, \mathrm{VIII_{s,o}}, IX_{s,o}$ fixing m_V =500 GeV (except for $\mathrm{VI_{s,o}}$ where m_V =350 GeV, and using flavor breaking choices for couplings to quarks; $(\sqrt{f_q f_t}, f_{qt}) = (0.1, 0.3)\mathrm{IV_s}$; $(0.1, 0.3)\mathrm{IV_o}$; $(0.55, 1.3)\mathrm{VI_s}$; $(0.55, 1.3)\mathrm{VI_o}$ and $(\eta_1, \eta_2) = (1.4, -0.4)\mathrm{VIII_s}$; $(1.3, -0.5)\mathrm{VIII_o}$; $(1.1, -0.4)\mathrm{IX_s}$; $(1.1, -0.4)\mathrm{IX_o}$.

production, and $\mathrm{I_s}$, $\mathrm{II_s}$ and $\mathrm{III_s}$ do not interfere with the SM amplitude at tree-level.

We begin with an examination of the representative models $\mathrm{II_{s,o}}$, which only contribute in the s-channel. The vector decay widths are given by $m_V\,(2f_q^2+f_t^2)/8\pi$ ($\mathrm{II_s}$) and $m_V\,(2f_q^2+f_t^2)/48\pi$ ($\mathrm{II_o}$), neglecting phase space suppression due to top quarks in the final state. In the first two rows of Fig. 6 we collect predictions for the inclusive $A_{FB}^{t\bar{t}}$ and $\sigma_{t\,\bar{t}}$ as functions of the vector masses, for several values of the product $f_q f_t$. We have taken vector decay widths appropriate for the $\mathrm{G_F}$ symmetric limit: $m_V 3 f_q f_t/8\pi$ ($\mathrm{II_s}$) and $m_V f_q f_t/16\pi$ ($\mathrm{II_o}$). In the last row, predictions for $d\sigma/dM_{t\bar{t}}$ and $A_{FB}^{t\bar{t}}$ in the low and high $M_{t\bar{t}}$ bins are shown for the benchmark points (denoted by a $\star$). Good fits to the inclusive cross section and the top asymmetries can be obtained. However, agreement with $d\sigma/dM_{t\bar{t}}$ is much harder to achieve, as the effect of the s-channel resonance is clear. The bounds from the Tevatron can be avoided if $m_V \gtrsim 1\,\mathrm{TeV}$. Unfortunately, for $m_V \gtrsim 1\,\mathrm{TeV}$ and $O(1)$ couplings the effect on $A_{FB}^{t\bar{t}}$ is strongly reduced. The LHC $d\sigma/dM_{t\bar{t}}$ spectrum would also be problematic. It is possible, though, to hide a light s channel resonance via an increase of its decay width due to additional non-$q\bar{q}$ final states, as has recently been discussed in the context of pure s-channel axial-vector models [17]. Another possibility for increasing the vector decay widths may be to consider the $\mathrm{G_F}$ breaking hierarchy $f_q^2 << f_t^2$, keeping the product $f_q f_t$ fixed.

The flavor octet models $\mathrm{VI_s}$ and $\mathrm{VI_o}$ contain admixtures of s and t channel contributions, while the flavor $(3,\bar{3},1)$ models $\mathrm{VII_s}$ and $\mathrm{VII_o}$ are purely t channel. The s channel contributions in $\mathrm{VI_{s,o}}$ are due to the vectors associated with the generator T^8 of $\mathrm{SU(3)_{U_R}}$ and the coupling product $f_q f_t$. The t channel contributions are due to the vectors associated with the generators $T^{4,..,7}$ and the coupling product f_{qt}^2. While the generic problem of s channel resonances persists, it is mitigated by their relative suppression compared to the t channel contributions (the coefficients $C_{1,2}$ are significantly smaller than C_3 for these models, see Table VII), by possible cancelations between the two channels, and by the absence of interference between the SM and NP s channel contribution in $\mathrm{VI_s}$ ($C_5 = 0$). The s channel effects can be further diminished, if the vector decay widths are enhanced by additional non-$q\bar{q}$ final states.[5] This assumption was implicit in the model $\mathrm{VI_o}$ examples presented in [35] and Fig. 1. In the following, we only consider vector decays to quark bilinears. In the $\mathrm{G_F}$ symmetric limit ($f_q = f_t = f_{qt}$) the decay widths can be written as $f_{qt}^2 m_V/16\pi$ ($\mathrm{VI_s}$ and $\mathrm{VII_s}$) and $f_{qt}^2 m_V/96\pi$ ($\mathrm{VI_o}$ and $\mathrm{VII_o}$). Finally, s channel effects in $\mathrm{VI_{s,o}}$ would be suppressed in the $\mathrm{G_F}$ breaking limit $f_q f_t << f_{qt}^2$ (this breaking is natural due to the large top yukawa), and would be absent entirely in the minimal $\mathrm{H_F}$ symmetric realizations which only contain the complex $\mathrm{SU(2)_{U_R}}$ doublets associated with the $SU(3)_{U_R}$ flavor generators $T^{4,..,7}$.

[5] Given that these models are by themselves non-renormalizable, it is reasonable to expect that renormalizable UV completions could contain additional vector decay modes.

We show the effect of the models $\mathrm{VI_{s,o}}$ and $\mathrm{VII_{s,o}}$ on $A_{FB}^{t\bar{t}}$ and $\sigma_{t\,\bar{t}}$ in the $\mathrm{G_F}$ symmetric limit in Figs. 7 and 8, respectively. In the purely t-channel models $\mathrm{VII_{s,o}}$, we see that it is possible to enhance $A_{FB}^{t\bar{t}}$, while at the same time not introducing any visible deviations in the $d\sigma/dm_{t\bar{t}}$ differential spectrum. For models $\mathrm{VI_{s,o}}$, on the other hand, we see that it is difficult to enhance $A_{FB}^{t\bar{t}}$ sufficiently, without obtaining excessive s channel peaks in the $d\sigma/dM_{t\bar{t}}$ spectra, as in the model $\mathrm{II_{s,o}}$ examples above. However, as already noted, much better agreement with the measured spectrum can be achieved in this case, if $\mathrm{G_F}$ is broken down to its subgroup $\mathrm{H_F}$[6]. In Fig. 9 we show such examples, with $f_q f_t << f_{qt}^2$, for various vector models. The decay widths of the different vectors in a $\mathrm{G_F}$ multiplet will not be equal in this limit. For simplicity, we have identified all the widths in each multiplet with the quantities $m_V f_q f_t/16\pi\times$ $(3, 1/2, 1, 1/6, 2, 1/3, 1/2, 1/12)$ in models $\mathrm{IV_s}$, $\mathrm{IV_o}$, $\mathrm{VI_s}$, $\mathrm{VI_o}$, $\mathrm{VIII_s}$, $\mathrm{VIII_o}$, $\mathrm{IX_s}$, $\mathrm{IX_o}$, respectively (which would hold in the $\mathrm{G_F}$ symmetric limit, neglecting phase space differences). The rationale for this approximation is that the s channel resonance widths are associated with the coupling products f_q^2 and f_t^2, whereas the widths of the t channel resonances, controlled by the product f_{qt}^2, have minimal impact on the $M_{t\bar{t}}$ spectrum. In addition, as we will see in Section IV C (see Table VI), dijet constraints on the light quark vector couplings f_q are relatively mild, so that the relation $f_q^2 = f_t^2 = f_q f_t$ would be phenomenologically viable in the light vector examples of Fig. 9.

4. Limits from LHC measurements of the $t\,\bar{t}$ invariant mass spectrum.

Recently, the first measurements of the $t\bar{t}$ invariant mass spectrum at the LHC have been presented by the ATLAS and CMS collaborations. With up to 0.7 pb^{-1} the ATLAS collaboration obtains $\sigma_{t\bar{t}} = 176 \pm 5(\mathrm{stat})^{+13}_{-10}(\mathrm{syst.}) \pm 7(\mathrm{lumi.})$ pb, while using $36\mathrm{pb}^{-1}$ the CMS collaboration obtains a combined cross section $\sigma_{t\bar{t}} = 158 \pm 10(\mathrm{uncor.}) \pm 15(\mathrm{cor.}) \pm 6(\mathrm{lumi.})$ pb [120]. This is to be compared with the NLO+NNLL predictions or the approximate NNLO predictions for the inclusive cross section that are listed in Ref. [106], and range between $\sigma_{t\bar{t}} = 157 \pm 13$ pb and $\sigma_{t\bar{t}} = 145 \pm 11$ pb, depending on the approximation used. ATLAS and CMS have also presented promising first measurements of the differential cross section at 200 pb^{-1} and 886 pb^{-1} [121], respectively.

In the near future the differential cross section measurements will place meaningful constraints on the models we have considered. We therefore present below some representative examples of their impact on

[6] Whereas in models $\mathrm{VII_{s,o}}$ the $\mathrm{G_F} \to \mathrm{H_F}$ breaking is not needed in order to obtain good agreement with the $d\sigma/dm_{t\bar{t}}$ spectrum, it may be required to evade dijet and $B \to K\pi$ constraints.

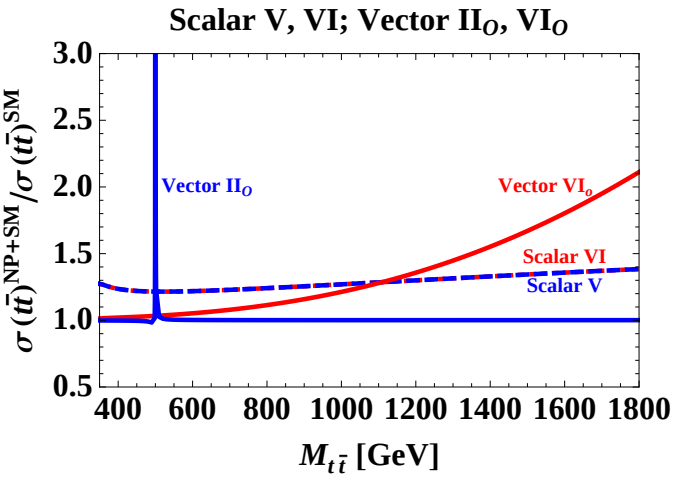

FIG. 10: Predictions for the ratio $(d\sigma(t\,\bar{t})_{NP+SM}/dM_{t\bar{t}})/(d\sigma(t\,\bar{t})_{SM}/dM_{t\bar{t}})$ for scalar and vector models. The scalar model examples are for model $\mathrm{S_V}$ with $(\eta, m_S) = (1, 400\,\mathrm{GeV})$ dashed blue, and for model $\mathrm{S_{VI}}$ with $(\eta, m_S) = (1/\sqrt{2}, 800\,\mathrm{GeV})$ dotted red. The vector model examples are for $\mathrm{II_o}$ with $(f_q = f_t, M_V) = (1/\sqrt{32}, 500\,\mathrm{GeV})$ solid blue, and for with $(f_q\, f_t, f_{qt}, M_V) = (0.5, 2, 500\,\mathrm{GeV})$ solid red.

the differential spectrum. In Fig. 10 we show the ratio

$$R_\sigma = \frac{d\sigma(t\,\bar{t})_{NP+SM}/dM_{t\bar{t}}}{d\sigma(t\,\bar{t})_{SM}/dM_{t\bar{t}}}. \tag{24}$$

in models $\mathrm{II_o}, \mathrm{VI_o}, \mathrm{S_V}$, and $\mathrm{S_{VI}}$ for the benchmark points shown in Figs. 6, 7, and 9. In the ratio we use SM NLO+NNLL prediction from Ref. [109], while NP contribution including interference with the SM is calculated at LO, mirroring our procedure for Tevatron predictions used in previous sections. In Fig. 10 a sharp resonant peak is clearly visible for the disfavored pure s-channel model $\mathrm{II_o}$. Once convoluted with the experimental resolution the peak will be less prominent. For instance assuming 10 GeV resolution the peak leads to an $\mathcal{O}(30\%)$ enhancement of the cross section in the bin containing the peak. The model $\mathrm{VI_o}$ example contains a rise in the tail region associated with the Rutherford scattering peak that is characteristic of t-channel models with $\mathcal{O}(1)$ couplings. The scalar models $\mathrm{S_V}$ and $\mathrm{S_{VI}}$, being u-channel models, display a relative enhancement throughout the entire differential spectrum [44], similarly to the case at Tevatron (see Fig. 3). Model $\mathrm{S_I}$ displays virtually no deviation from the SM spectrum, as pointed out in Refs. [37, 68].

B. Contributions to $B_s - \bar{B}_s$ mixing

There is some evidence for NP contributions to the measurement of the B_s mixing phase. A 3.9σ deviation from the negligible SM prediction has been measured in the like-sign dimuon charge asymmetry by the DØ collaboration [9, 10]. This result is in agreement [92, 122] with a hint for a nonzero weak phase

in B_s mixing (measured through flavor tagged decays [123, 124]). The hints for NP in B_s mixing have two preferred solutions [92], with

$$h_s \sim 0.5, \sigma_s \sim 130^\circ \text{ and } h_s \sim 2, \sigma_s \sim 100^\circ. \tag{25}$$

Here, $h_{s,d}$ and $2\sigma_{s,d}$ denote the magnitude and phase, respectively, of the NP contribution to the $B_{s,d}$ mixing amplitude, normalized to the SM one (see also (C3)). Note that the above results have been obtained using the older measurement of the dimuon asymmetry [9]. Since the two measurements are consistent, we do not expect a significant change in the position of the two minima. There is also a slight preference for $h_d \sim 0.2$, $\sigma_d \sim 100^\circ$, but at slightly more than 1σ h_d is consistent with zero. At 3σ one finds $h_d < 0.5$ for all σ_d [92].

The flavor symmetric models can be grouped by whether or not they can give contributions to $B_s - \bar{B}_s$ mixing. The models in which the new fields only couple to u_R fall into the latter category These are models $\mathrm{II}_{s,o}$, $\mathrm{VI}_{\mathrm{s,o}}$ and $\mathrm{S}_{\mathrm{V,VI}}$. Then there are models in which the NP contributions first arise at loop level: $\mathrm{VII}_{\mathrm{s,o}}$ and $\mathrm{S}_{\mathrm{IX,X}}$, which couple to d_R and u_R, , $\mathrm{XI}_{\bar{3},6}$ and $\mathrm{S}_{\mathrm{I,II}}$ that couple to u_R and Q_L. For the remaining models tree level contributions to B_s mixing are possible.

For a quantitative analysis one needs to specify the $\mathrm{H_F}$ breaking. We will adopt the MFV hypothesis, assuming that the breaking in the NP sector is only due to the SM Yukawa couplings. (for an example with maximal breaking of H_F see [31]). This hypothesis ensures that the FCNCs generated from the exchange of NP fields have SM CKM suppression, making the FCNC constraints easier to satisfy. MFV scalar fields that can lead to the dimuon anomaly have been discussed in the literature previously [88–91]. We begin by classifying the flavor symmetric vector and scalar fields that can contribute to B_s mixing at tree level. Most of the details are relegated to Appendix C.

The MFV models fall in two categories:"universal models" leading to class 1 $\Delta B = 2$ mixing operators in the terminology of [13], and "yukawa suppressed" models that give rise to class 2 operators and are additionally suppressed by light quark yukawa couplings, $y_{s,d}$. In universal models the NP contributions (normalized to the SM) are equal in the B_s and B_d mixing amplitudes. This is in some tension with experiment, where there are indications for large effects in B_s mixing, i.e., $50\% - 200\%$ of the SM amplitude. Measurements in the B_d system, on the other hand, can accommodate a NP contribution of up to $\sim 20\%$. Universal models can thus explain the dimuon anomaly only if the real effect is on the lower end of the experimentally preferred range for B_s mixing and on the upper range for B_d mixing.

The simplest examples of universal MFV models that can explain the dimuon anomaly are the two scalar doublet model, where in our notation the higgs linear combination without a vev is $\mathrm{S_H}$ [89–91], and the color-octet, weak-doublet scalar model S_8 [14]. Effects are large even for $m_S = 1$ TeV, if the couplings of the flavor breaking terms η_i and the bottom Yukawa coupling y_b are $\mathcal{O}(1)$. For the SM value

$y_b \sim 0.02$ the mass scale for the new uncharged scalars would have to be quite low. Such a low mass scale, surprisingly, is consistent with present phenomenology for S_8 [125]. Similar comments apply to the other universal models, $\mathrm{III}_{\mathrm{s,o}}, \mathrm{IV}_{\mathrm{s,o}}, \mathrm{VIII}_{\mathrm{s,o}}, \mathrm{IX}_{\mathrm{s,o}}$ and $\mathrm{S}_{\mathrm{XIV}}$. In order to obtain the right size of h_s for the dimuon anomaly one needs $\eta_i \sim 0.1$, if $m_{S,V} = 1$ TeV.

The yukawa suppressed models can have mixing amplitudes suppressed either by one power or two powers of light yukawas. For y_s^2 suppressed models, $\mathrm{I}_{\mathrm{s,o}}, \mathrm{V}_{\mathrm{s,o}}$ and $\mathrm{S}_{\mathrm{VIII}}$, the B_s mixing anomaly can be potentially explained only if $y_b, \eta_i \sim \mathcal{O}(1)$ and the masses of NP fields are no more that a few 100 GeV. The NP contributions to B_d are predicted to be too small to be observed in this case, since they are additionally suppressed by y_d^2/y_s^2. The singly y_s suppressed models, $\mathrm{X}_{\bar{3},6}$ and $\mathrm{S}_{\mathrm{I}}, \mathrm{S}_{\mathrm{III}}$, give contributions to h_s of the right order of magnitude for $\eta_i \sim \mathcal{O}(1)$ and $m_{S,V} \sim 1$ TeV. There is also an effect predicted for B_d mixing with size $h_d \sim 0.1$.

A number of flavor symmetric models can potentially explain both the B_s mixing and $A_{FB}^{t\bar{t}}$ anomalies simultaneously. If enhanced B_s mixing is due to tree level exchange, the NP fields need to couple to left-handed doublets if they are to also contribute to $t\bar{t}$ production. The relevant models are $\mathrm{III}_{\mathrm{s,o}}, \mathrm{IV}_{\mathrm{s,o}}, \mathrm{VIII}_{\mathrm{s,o}}$ and $\mathrm{IX}_{s,o}$, where for TeV masses, the flavor breaking couplings need to be $\eta_i \sim \mathcal{O}(0.1)$. However, none of these models seem to fit the observed data in top pair production particularly well (See Fig. 9 for models $\mathrm{IV}_{\mathrm{s,o}}, \mathrm{VIII}_{\mathrm{s,o}}$ and $\mathrm{IX}_{s,o}$. The models $\mathrm{III}_{\mathrm{s,o}}$ are pure s-channel and thus lead to large deviations in the $t\bar{t}$ differential cross section.).

There are also four models of interest that exhibit linear Yukawa suppression and can in principle contribute to B_s mixing and to the $A_{FB}^{t\bar{t}}$ anomaly simultaneously. These are models $\mathrm{X}_{\bar{3},6}$ and models $\mathrm{S}_{\mathrm{III}}$, S_{IV}. However, due to their color representation $\mathrm{S}_{\mathrm{III}}$, S_{IV}, have limited potential to explain $A_{FB}^{t\bar{t}}$, while $\mathrm{X}_{\bar{3},6}$ reduce rather than increase $A_{FB}^{t\bar{t}}$.

This leaves us with models where the contributions to B_s mixing are loop suppressed. These are the vector models $\mathrm{VII}_{\mathrm{s,o}}$, $\mathrm{XI}_{\bar{3},6}$ and the scalar models $\mathrm{S}_{\mathrm{I}}, \mathrm{S}_{\mathrm{II}}, \mathrm{S}_{\mathrm{IX,X}}$. They lead to contributions to B_s and B_d mixing which are universal, if one assumes MFV. Among these, models $\mathrm{VII}_{\mathrm{s,o}}$ and S_{I} can also explain the present top data. The contributions to B_s mixing can also carry a new weak phase, as required by the dimouon charge asymmetry.

For instance, model S_{I}, see Eq. (21), contains contributions that are proportional to the product of the generally complex quantity $4\eta_0^2\eta_3^2$ (where these coefficients are defined in Table X in Appendix C) with a loop function that is of the same order of magnitude as the SM one, with its precise value depending on the size of m_S. The $B \to K\pi$ branching ratios require $\sqrt{\eta_0\eta_3} \lesssim 1/4$ (see Section IV D), while $A_{FB}^{t\bar{t}}$ favors $\eta_0 \sim 1$. Thus, CPV contributions to B_s mixing of $\mathcal{O}(20\%)$ are readily attainable for S_{I} scalar masses of order 100 GeV. Similar considerations apply to models $\mathrm{VII}_{\mathrm{s,o}}$.

IV. EXISTING EXPERIMENTAL CONSTRAINTS ON A FLAVOR SYMMETRIC SECTOR

We now determine some of the existing experimental constraints on flavor symmetric extensions of the SM. We examine bounds on direct production at LEP, from electroweak precision data (EWPD) and from collider searches at the Tevatron and LHC. We also determine the (residual) FCNC constraints.

Our aim is characterize the general phenomenological bounds whenever possible and to check if some of the models that we have identified as promising candidates are consistent with other phenomenology in some detail. Our results are not completely comprehensive, as at times we have to focus on particular sample models. However, we believe our results are valuable to gain some intuition as to the current phenomenological constraints on a flavor symmetric sector.

A. LEP Constraints

The LEP constraints depend on how the new states couple to electrons and to the pair of final state fermions. In this section we will discuss the constraints on the vector models from LEP in some detail. The constraints for scalar models are very similar, see [3] for some details. Limits on anomalous four jet events at LEP give a kinematic lower bound for pair production of the scalar models of $105\,\mathrm{GeV}$ [3]. For the vector and scalar models signals that involve couplings to quarks and leptons are the most problematic at LEP. For a Z' vector boson that couples to quarks (electrons) with couplings $g_z z_{fB}$ ($g_z z_{eA}$), the bound is [126]

$$M_{Z'}^2 \geq \frac{g_z^2}{4\,\pi}\,|z_{eA}\,z_{fB}|\,(\Lambda_{AB}^f)^2\,. \tag{26}$$

with $A, B = \{L, R\}$ the chirality of the fermions. Typically $\Lambda_{AB}^f \sim 10$ TeV, leading to mass bounds on the order of $M_{Z'} \gtrsim 1$ TeV.

The vectors in nontrivial color or flavor representations ($\mathrm{I_o} - \mathrm{IV_o}$ or $\mathrm{V} - \mathrm{XI}$) are protected from having tree level exchanges of this form. For models protected by flavor symmetry one is forced to have the insertion of Yukawa matrices. The final operating energy of LEP was $\sqrt{s} = 209 < 2m_t$ so the flavor symmetry is sufficient to remove this bound for models $\mathrm{V} - \mathrm{XI}$. These bounds do apply to $\mathrm{I_s} - \mathrm{IV_s}$ unless the couplings to electrons are somehow suppressed, *e.g.*, by extending flavor symmetry to the lepton sector.

For the models where the bound (26) does not hold, there are constraints from covariant derivative couplings to Z and γ in the kinetic terms of the vectors (the factor N is set by requiring canonical normalization),

$$\mathcal{L}_K = N\mathrm{Tr}\left(D_\mu V_\nu^\dagger\, D^\mu V^\nu - D_\mu V_\nu^\dagger\, D^\nu V^\mu\right)\,. \tag{27}$$

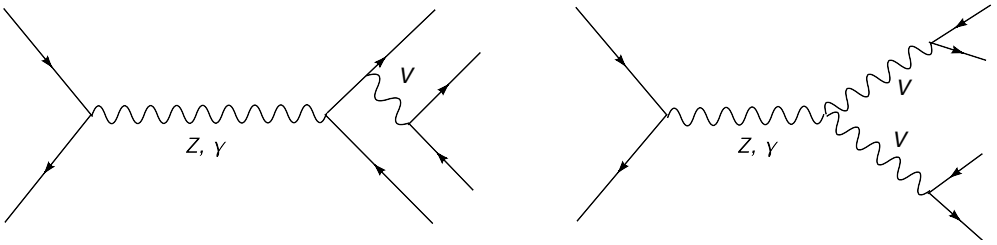

FIG. 11: Tree level generation of multi-jet events at LEP due to flavor symmetric vectors. Similar diagrams (and bounds) exist for scalars and the first diagram is representative of the emissions of the vectors and scalars off the final state fermions.

Some tree level processes that would lead to anomalous four jet events at LEP are shown in Fig. 11. These processes do proceed even in the absence of flavor violation. Furthermore, for vector pair production (the second diagram) the couplings of the Z or γ to the vectors are fixed by gauge invariance. This implies a kinematic bound of $M_V \gtrsim 105\,\mathrm{GeV}$ on the flavor symmetric vectors. The analogous diagram for the scalar models is the origin of the kinematic bound on the scalar masses discussed in [3].

The first diagram(s) can lead to a stronger bound for a vector or a scalar model as the vector or scalar is singly produced and has an order one branching ratio to anomalous multi-jet final states due to the flavor quantum numbers it carries. We find that this production process gives a cross section of $0.20|\eta|^2$ pb^{-1} for $M_V = 120\,\mathrm{GeV}$, or, with an integrated luminosity of 500 pb above this mass scale, a total of $100|\eta|^2$ events. The number of expected events falls rapidly with increasing M_V and is below $12|\eta|^2$ for $M_V \geq 140\,\mathrm{GeV}$. Assuming an order one branching ratio to anomalous multi-jet final states, this implies that the mass bound on the vectors from LEP is $M_V \gtrsim 150\,\mathrm{GeV}$ for $\mathcal{O}(1)$ couplings. Colored vectors will have similar mass bounds from LEP from anomalous multijet events. The calculation for the scalar models is very similar, resulting in the same approximate bounds.

In summary, we consider the minimum LEP lower bound for all vector and scalar models to be $\gtrsim 150\,\mathrm{GeV}$ when order one couplings exist for the fields to quarks. A dedicated study would be required for each model to obtain more precise bounds. However, we note that while scalar (doublet) masses below 150 GeV were only considered in model $\mathrm{S_I}$, see Eq. 22, for enhancing $A_{FB}^{t\bar{t}}$, this bound could easily be evaded by making the charged components of the scalar doublets heavier. Single exchange of the neutral components (the ones involved in $t\bar{t}$ production), as in the scalar analog of the first diagram of Fig. 11, would lead to kinematically suppressed virtual $t\bar{t}$ pair production. The LEP bound can be generically stronger for a color singlet that does not transform under the flavor group: for vectors $\mathrm{I_s} - \mathrm{IV_s}$ the lower mass bound is $\gtrsim 1\,\mathrm{TeV}$ for order one couplings to leptons and quarks.

B. Electroweak precision tests

We consider the models for massive $\mathrm{H_F}$ symmetric vector and scalar fields to be effective field theories. Up to this point we have assumed that the cut-off of the theory, Λ, is high enough that we can neglect operators suppressed by powers of Λ. For the scalar models, in principle, we do not have to consider effects of higher dimensional operators. In this case, for scalar models that are $\mathrm{SU_L}(2)$ singlets, the results of [3] show that the generic lower bound from fitting to EWPD is $m_s \gtrsim 100\ \mathrm{GeV}$. The LEP bounds we have just derived are stronger than these bounds for scalar models that do not break custodial symmetry.

Below, we summarize our findings for model $\mathrm{S_I}$, for which particularly light scalar doublets were considered in the context of $\mathrm{A_{FB}^{\bar{t}t}}$. We find that it is easily consistent with S parameter bounds, even in the presence of nine light doublets, as in the $\mathrm{G_F}$ symmetric realization, rather than only two, as in the minimal $\mathrm{H_F}$ symmetric versions I(a) - I(c) (Eqs. (21) – (23)) considered in the previous section (we have generalized the analysis of [37] for a single scalar doublet). The T parameter bounds are easily satisfied in the minimal versions, with neutral scalar doublet component masses as low as 110 GeV and heavier charged component masses of 150 GeV, a mass splitting that may be required in order to simultaneously evade the LEP bounds discussed above and enhance $A_{FB}^{t\bar{t}}$ to observed levels. Mass splitting between the charged and neutral scalar doublet components can be obtained via $\mathrm{G_F}$ symmetric couplings to the SM Higgs vacuum expectation value. We have also checked the sizes of non-oblique corrections in the minimal versions of $\mathrm{S_I}$. In options I(a) and I(c), loop graphs containing the top quark lead to problematic shifts in the LH down and strange quark couplings to the Z. For instance, taking charged scalar masses of 150 GeV, neutral scalar masses of 110 GeV, and couplings $\eta \approx 2/3$ yields $\delta g_{s_L}/g_{s_L}$, $\delta g_{d_L}/g_{d_L} \approx -0.0046$, roughly 2σ in excess of the 2 σ upper bound obtained, for equal shifts in the two couplings, from the Z hadronic width. In option I(b), loop graphs containing the charm and up quarks lead to a shift in the LH bottom quark coupling to the Z. For the same parameter choices (see Fig. 5) the shift is $\delta g_{b_L}/g_{b_L} \approx -0.0028$, which is consistent with R_b at 2σ. We therefore conclude that whereas I(b) is a viable option for enhancing $A_{FB}^{t\bar{t}}$, this is unlikely for cases I(a) and I(c).

For the massive vector fields we do have to consider the effects of higher dimensional operators suppressed by the cut off scale as the theory is nonrenormalizable. This is particularly the case when considering electroweak precision data (EWPD) for vectors. To the effective fields we have considered at the scale $\mu \sim M_V$ we should add dimension six operators. These arise from integrating out heavier modes of the UV complete theory. At the electroweak scale $\mu \sim m_Z$ we integrate out also the vectors and can match onto an effective field theory constructed from only the SM fields, appropriate for examining EWPD. The dimension six operators then receive contributions from vectors and from heavier fields from the UV

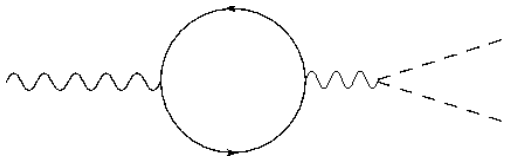

FIG. 12: Contribution to the operator $\mathcal{O}_1$ generated by the SM through mixing with the SM B field.

completion.

For cases $\mathrm{I_s}-\mathrm{IV_s}$, the EFT will in general have a dangerous dimension 4 operator $\mathcal{O}_1 = V^\mu\,(H^\dagger\,D_\mu\,H)$. Integrating out the vectors gives the dimension six operator $\mathcal{O}_T = |H^\dagger\,D_\mu\,H|^2/M_V^2$, well constrained by EWPD. For positive (negative) Wilson coefficient C_T the bound on the vector mass is $M_V \geq 5.6\,(4.6)\,\mathrm{TeV}\times\sqrt{|C_T|}$ (adding only this operator to the SM EWPD fit, and taking $m_h = 115\,\mathrm{GeV}$) [127].

The operator $\mathcal{O}_1$ could be suppressed by the unknown dynamics in the UV theory. However, it is also generated via the quarks that the vectors couple to and SM interactions, see Fig. 12. Due to mixing with the SM B field (with coupling g) as shown an effective wilson coefficient of $\mathrm{C}_1 \simeq \Sigma_i\,y_i^2\,\eta^2\,g^3\,v^4/(16\pi^2\,M_V^2)^2$ is generated, where y_i is the quark Yukawa coupling and the sum is over all the allowed flavors (we neglect small $\mathrm{G_F}$ breaking). The bound is very weak as this is effectively a two loop effect due to mass mixing with the B field. This gives a bound $M_V/\eta^{2/5} \gtrsim 50\,\mathrm{GeV}$ for models $\mathrm{II_s}, \mathrm{III_s}, \mathrm{IV_s}$ generated through SM interactions, weaker than the LEP bound discussed. The bound is even weaker if the vector only couples to down quarks and y_b is not enhanced from its SM value. Models that transform under flavor can still generate this operator through SM interactions but require the insertion of the appropriate number of Yukawas in $\mathcal{O}_1$. If the vector transforms under $\mathrm{SU}(3)_\mathrm{c}$ the operator $\mathcal{O}_1$ is forbidden. In general, if this operator is not present due to matching onto the underlying theory, the bound through custodial symmetry violating loop effects is weaker than the direct production LEP bound.

Note that a key assumption of this analysis — fitting to EWPD with the SM supplemented with a single operator such as $\mathcal{O}_T$ — is not well justified. We leave a more complete analysis of EWPD to a future publication but note that non oblique observables, such as R_b and the decay width of the SM Z boson potentially can place stronger bounds on the $\mathrm{H_F}$ symmetric fields with a large number of degrees of freedom. This is particularly the case when flavor off diagonal couplings are present and the top quark mass scale is present in large numbers of loop corrections to R_b and Γ_Z.

C. Tevatron and LHC dijet Constraints

At the LHC and the Tevatron the most relevant constraints on flavor universal couplings come from dijet resonance searches and dijet angular distribution studies. These constraints limit the couplings of the $\mathrm{H_F}$

symmetric fields to the light quarks. In this section we give a brief account of these dijet bounds on scalar models $\mathrm{S_V}, \mathrm{S_{VI}}$ and vector models $\mathrm{II_o}$, $\mathrm{VI_o}$, and $\mathrm{VI_s}$, relegating details of the calculations to Appendix B. These models are of interest for the tevatron's top quark forward-backward asymmetry, $A_{FB}^{t\bar{t}}$. The vector examples contain prominent dijet contributions in both the s and t-channels at the tevatron and LHC. Scalar model $\mathrm{S_V}$ is u-channel dominated, due to the flavor antisymmetry of its quark couplings (s-channel effects are present in the $uc \to uc$, $\bar{u}c \to \bar{u}c$ channels); model $\mathrm{S_{VI}}$ contains s-channel ($uu \to uu$) and u-channel contributions. Related bounds on some of these models were also discussed recently in [35, 36, 128].

The relevant scalar interaction Lagrangians in the $\mathrm{G_F}$ symmetric limit are given in Eq. (A37). The relevant vector Lagrangians are listed in Eqs. (4)–(12) in Section II, and in Appendix A (with $\mathrm{G_F}$ breaking corrections also discussed). Expressions for the dijet cross sections in these models are given in Appendix B. The new scalar or vector fields can have $\mathcal{O}(1)$ couplings to first generation quarks, a necessary condition for obtaining large $A_{FB}^{t\bar{t}}$. Thus, they can mediate large contributions to $2 \to 2$ quark scattering, potentially spoiling the good agreement between measurements and SM theory predictions for dijets. Tevatron and LHC bounds on their couplings to light quarks are collected in Table V. They are derived using partonic cross sections evaluated at LO in α_s, with the renormalization and PDF factorization scales identified with the transverse momenta of the two outgoing partons. Rapidity related experimental cuts on the two leading jets (the dijet measurements are inclusive) are emulated by imposing these cuts on the outgoing partons. Clearly, a parton level treatment introduces considerable uncertainties. Nevertheless, our bounds should still be indicative of the constraints one would obtain with more precise inclusive Monte Carlo simulations, carried out at NLO and including showering and full detector response.

In Tables V and VI we quote upper bounds on the couplings η and η_1 (or f_q) of the light quarks to the scalar and vector fields, respectively, for a range of masses. There are four sets of bounds, obtained from searches for dijet resonances in the dijet invariant mass (M_{jj}) spectra at CDF [129] and LHC [130–133], and from dijet angular distribution measurements at DØ [134] and CMS [135]. The CDF dijet resonance search [129] (corresponding to a luminosity of 1.3 fb^{-1}) imposes a rapidity cut of $|y| < 1$ on the two leading jets. For the LHC dijet resonance searches we use the CMS data [130] (2.9 pb^{-1}) for 500 GeV scalar or vector masses, the ATLAS data [131] (36 pb^{-1}) for 700 GeV masses, and the more recent ATLAS [132] (0.81 fb^{-1}) and CMS [133] (1 fb^{-1}) data for heavier masses. These studies impose a rapidity cut of $|y| < 2.5$ (2.8 in [132]) on the two leading jets, with a rapidity separation for these jets satisfying $|\Delta y| < 1.3$ (1.2 in [132]). Rapidity cuts are imposed in order to eliminate a large fraction of the dominantly t-channel, hence forward, QCD dijet background at large p_T; s-channel NP effects will be more isotropic. As already mentioned, we implement these cuts on the two outgoing partons.

The dijet angular distribution measurements quote normalized differential cross sections $1/\sigma_{\mathrm{dijet}}\, d\sigma/d\chi$,

S_V^3 Mass	TeV M_{jj}	LHC M_{jj}	TeV χ	LHC χ	S_{VI} Mass	TeV M_{jj}	LHC M_{jj}	TeV χ	LHC χ
300	1.0	-	1.2	1.1	300	0.3	-	0.4	0.5
500	1.2	n.b.	0.5	0.9	500	0.3	2.2	0.2	0.5
700	2.0	0.7	0.7	0.6	700	0.6	0.2	0.2	0.2
900	2.5	0.3	0.6	0.5	900	0.7	0.1	0.2	0.2
1100	2.8	0.4	0.5	0.6	1100	1.4	0.1	0.2	0.1
1300	4.0	0.5	1.3	0.6	1300	1.6	0.1	0.7	0.1
1500	6.0	0.6	1.6	0.3	1500	1.8	0.1	0.8	0.1
1700	n.b.	0.6	1.8	0.5	1700	2.0	0.1	0.8	0.1
1900	n.b.	0.6	2.0	0.4	1900	2.6	0.1	0.9	0.1
2100	n.b.	0.7	2.1	0.6	2100	3.0	0.1	1.0	0.1

TABLE V: Approximate upper bounds on the couplings of the scalars S_V, S_{VI} to light quarks due to the measured dijet invariant mass spectra (labeled M_{jj}) and angular distributions (labeled χ) at the tevatron and LHC, as explained in the text. The masses correspond to the scalar field flavors S_V^3 and $S_{VI}^{11=22=12}$. If no bound is determined we denote this with "n.b.".

where the angular variable is $\chi \equiv (1+|\cos\theta|)/(1-|\cos\theta|)$ and θ is the scattering angle for the $2 \to 2$ parton scattering process in the parton CM frame. The differential cross sections are integrated over dijet mass intervals of a few hundred GeV in size, and results are presented in bins of χ for $0 < \chi < 16$. The normalization, $\sigma_{\rm dijet}$, is the measured cross section integrated over the dijet mass interval and over $0 < \chi < 16$. Whereas the χ distributions for the QCD dijet background are relatively flat (due to t-channel dominance), more central NP effects, e.g., from s-channel resonances, will peak at low χ. The DØ angular measurements [134] (0.7 fb^{-1}) include a cut on $y_{\rm boost} \equiv 0.5\,|y_1 + y_2| < 1$, where $y_{1,2}$ are the rapidities of the two leading jets. The CMS angular measurements [135] (36 pb^{-1}) employ a similar cut of $y_{\rm boost} < 1.11$. Again, we implement these cuts on the two outgoing partons.

In general, the dijet invariant mass spectrum of a NP model can exhibit both an s-channel peak in the vicinity of the mass of the mediating field, and a monotonic rise relative to the SM prediction at larger M_{jj}. At the Tevatron, our scalar examples would possess the latter feature, due to u-channel effects, but an s-channel peak would be less prominent, particularly for model S_V. Therefore, for these models the bounds on the light quark couplings quoted in the Tevatron "M_{jj}" columns of Table V are obtained by requiring that the ratios of the predicted to SM $d\sigma/dM_{jj}$ spectra (with both evaluated at LO) lie within the PDF uncertainty band in Fig. 1b of the CDF study [129]. In particular, we do not make use of the bump hunter bounds on the new particle production cross sections. The widths of the intermediate scalar fields are identified with the two-body decay widths to quarks neglecting phase space, $\Gamma = \eta^2\, m_s/(2\,\pi)$ for

	$\mathrm{II_o}$				$\mathrm{VI_o}$				$\mathrm{VI_s}$			
Mass	TeV M_{jj}	LHC M_{jj}	TeV χ	LHC χ	TeV M_{jj}	LHC M_{jj}	TeV χ	LHC χ	TeV M_{jj}	LHC M_{jj}	TeV χ	LHC χ
300	0.4	-	0.9	1.7	0.6	-	1.4	2.2	0.6	-	1.7	1.4
500	0.4	0.8	0.3	1.3	0.4	0.9	0.4	1.5	0.5	1.0	0.5	1.4
700	0.4	0.8	0.3	0.9	0.4	1.0	0.5	1.0	0.5	1.1	0.6	1.2
900	0.3	0.3	0.2	0.7	0.5	0.3	0.3	0.9	0.6	0.3	0.4	1.0
1100	0.4	0.3	0.4	0.8	1.1	0.4	0.6	1.0	1.3	0.5	0.8	1.2
1300	0.7	0.5	1.1	0.9	1.0	0.6	1.6	1.2	1.2	0.6	1.6	1.2
1500	2.7	0.5	2.6	0.9	4.8	0.6	4.3	1.1	3.4	0.7	3.1	1.2
1700	4.0	0.5	3.5	1.2	6.4	0.7	5.7	1.6	4.8	0.7	4.1	1.6
1900	5.3	0.7	4.4	1.0	7.7	0.9	6.5	1.3	6.1	0.8	4.8	1.4
2100	6.5	0.8	5.2	1.4	8.8	1.0	7.2	1.8	7.8	0.8	5.6	1.8

TABLE VI: Approximate upper bounds on the couplings f_q of the vectors $\mathrm{II_o}$, $\mathrm{VI_o}$ and VI_s to light quarks, due to the measured dijet invariant mass spectra (labeled M_{jj}) and angular distributions (labeled χ) at the Tevatron and LHC, as explained in the text.

$\mathrm{S_V}$ and $\mathrm{S_{VI}}$. The vector examples can produce prominent s-channel peaks at the Tevatron. We therefore obtain the Tevatron M_{jj} bounds quoted in Table VI from the CDF bump hunter 95% CL upper limits on the product of a Z' production cross section $\times$ its branching ratio to dijets (Br) $\times$ acceptance (A), setting $\mathrm{Br} \times \mathrm{A} = 1$ (see Table I of [129]). For vector masses in excess of the last measured invariant mass bin, $M_{jj} \in [1225, 1350]$ GeV, we require that the ratios of the predicted to SM dijet cross sections in this bin lie below the 95% CL upper bound, obtained from the systematic and PDF uncertainty errors added in quadrature (the corresponding ratios in the lower bins would be much smaller than such bounds, given the widths of the vector fields). The intermediate vector two body decay widths to quarks are $\eta^2\, m_V/(16\,\pi)$ for IIo and VIs, and $\eta^2\, m_V/(96\,\pi)$ for VIo. To obtain bounds on the scalar and vector couplings from the ATLAS and CMS dijet resonance searches we again use bump hunter 95% CL upper limits on new particle production cross sections, setting $\mathrm{Br} \times \mathrm{A} = 1$. Specifically, for the CMS studies [130, 133] we make use of the bounds provided for qq final states (see Table 1 of [130] for a 500 GeV resonance mass, and Table 1 of [133]); for the ATLAS studies in [132] we use the upper limits in Table 3, and in [131] we use the bound in Figure 3 (for a 700 GeV resonance mass).

To set the bounds on the light quark couplings from the dijet angular distribution measurements, we conservatively require that in each bin of χ and in each M_{jj} interval, the addition of NP does not result in a shift of $1/\sigma_{\mathrm{dijet}}\, d\sigma/d\chi$ that is larger than the 1σ error. In the case of the DØ measurement [134], the errors are statistics dominated (see the "EPAPS" document cited therein), and we can neglect the systematic and

SM theory errors. For the CMS study [135] we add the theory and experimental errors in quadrature. In all of our examples, the largest deviations occur at small χ, and they tend to concentrate in the invariant mass intervals closest to the new particle masses, as would be expected for s-channel resonances. We can see from a comparison of all the bounds in Tables V and VI that the LHC bounds have superseded the Tevatron bounds for new scalar or vector masses ≥ 1 TeV, and that they are particularly restrictive for model $\mathrm{S_{VI}}$.

It is important to note that the constraints determined above are on the couplings of the $\mathrm{H_F}$ symmetric couplings of the new fields to light quarks. Only in the $y_t \to 0$ limit, when the full $\mathrm{G_F}$ symmetry is restored, are these couplings the same as the couplings involving heavy quarks. Thus, these bounds cannot be directly translated into limits on the allowed $A_{FB}^{t\bar{t}}$, in general. Rather, these bounds dictate to what degree $\mathrm{G_F} \to \mathrm{H_F}$ flavor breaking is required, in order to have couplings that are suitable for explaining the $A_{FB}^{t\bar{t}}$ anomaly while being consistent with dijet constraints. Considering the benchmark scalar examples in Fig. 3, flavor symmetry breaking is probably not required in model $\mathrm{S_V}$, while moderate breaking is required in model $\mathrm{S_{VI}}$. In the case of vector models $\mathrm{VI_{s,o}}$, we can see that in examples in which simultaneous agreement with all of the top data is obtained with the help of the $\mathrm{G_F} \to \mathrm{H_F}$ symmetry breaking hierarchy $f_q f_t << f_{qt}$, see Fig. 9 some flavor symmetry breaking would probably also be required in order accommodate the dijet bounds ($f_q < f_{qt}$); however, in models in which agreement with the top data is achieved with the help of enhanced vector decay widths, see Fig. 2, little or no flavor symmetry breaking appears to be required by the dijet bounds.

We close this Section with a brief discussion of collider constraints on scalar model $\mathrm{S_I}$. In particular, we consider the recent DØ bounds [116] on anomalous dijet production in Wjj final states, prompted by a potential signal at CDF [117], and constraints from UA2 dijet measurements [118]. The scalar doublet fields S_{ij}, $i,j = \{1,2\}$ couple to light quarks with equal $\mathrm{H_F}$ symmetric couplings η_{ij}, see Eq. 18, which would lead to dijet peaks in Wjj final states via associated $W + S_{ij}$ production. DØ has presented 95% CL upper bounds on the cross section for such processes, ranging from 2.57 pb to 1.28 pb for dijet resonance masses of 110 - 170 GeV, i.e., in the preferred range for enhancing $A_{FB}^{t\bar{t}}$ in model $\mathrm{S_I}$. We apply these bounds to the sum over cross sections for the four scalar doublet fields (charged and neutral components). The resulting 95% CL upper bounds on the couplings η_{ij} are ≈ 0.2 for these masses. Finally, we find that the UA2 dijet measurements do not provide meaningful constraints on these couplings once finite width effects for the S_{ij} and interference with the SM are taken into account.

D. Residual Constraints from FCNCs

The fact that there is a global flavor symmetry $\mathrm{H_F}$ in the models we consider helps to avoid low energy constraints from Flavor Changing Neutral Currents (FCNCs) even though the NP has weak scale masses. In this section, as always when considering flavor bounds, we adopt a strict interpretation of the MFV hypothesis and assume that $\mathrm{G_F}$ is only broken by the SM Yukawas. The detailed analysis of FCNC constraints from $B_{d,s}$, D and K mixing is given in Appendix C while here we only collect the main results.

We discuss the models in the two categories, universal and Yukawa suppressed, that we have introduced. (In the notation of Ref. [13] these are the models that receive only contributions from class-1 or class-2 operators). The universal models give roughly the same contributions to B_d and B_s mixing amplitudes, when normalized to the SM. For vector or scalar masses about 1 TeV, the coupling constants have to be less than about 0.1. The models of the universal type are vector models $\mathrm{III_{s,o}}, \mathrm{IV_{s,o}}, \mathrm{VIII_{s,o}}, \mathrm{IX_{s,o}}$ and scalar model $\mathrm{S_{XIV}}$.

The Yukawa suppressed models give contributions to the mixing amplitudes that are CKM suppressed (with the same CKM structure as the leading short distance contributions in the SM). They are, in addition, Yukawa suppressed. The suppression can start at linear or quadratic order in light quark Yukawas. The FCNC bounds are satisfied for η couplings of $\mathcal{O}(1)$ for vector or scalar masses above ~ 1 TeV for linear Yukawa suppressed models. For quadratically Yukawa suppressed models the FCNC constraints are even weaker and are already satisfied for masses above ~ 300 GeV.

Finally, meaningful constraints can be obtained for certain quark couplings in model $\mathrm{S_I}$ from the $B \to K\pi$ branching ratios [37, 115]. For example, if the LH quarks in the $\mathrm{S_I}$ Lagrangian of Eq. (18) are defined in the up quark mass eigenstate basis, the couplings of the charged scalars in the quark mass eigenstate bases would include the terms

$$\eta_{k\,1}\, S^-_{k\,1}\, (V^\dagger_{\mathrm{CKM}})_{j\,k}\, \bar{d}'_{j\,L}\, u'_R \;\; + \;\; h.c.\,, \tag{28}$$

where $j, k = \{1, 2, 3\}$. In the $\mathrm{G_F}$ symmetric limit, the contributions to $B \to K\pi$, $\pi\pi$ from tree-level exchanges of the scalars S^-_{k1} would exactly cancel. However, in the limit of large $\mathrm{G_F} \to \mathrm{H_F}$ symmetry breaking (as would be required in order to maintain consistency with the Wjj bounds while accounting for enhanced $A^{t\bar{t}}_{FB}$) the couplings would be constrained. The tightest bounds come from $B \to K^+\pi^-$. Borrowing from the analysis of [37], we find $\eta_{k\,1} < 0.23\,(m_S/125\ \mathrm{GeV})$, when considering the exchange of S^-_{31} and S^-_{21} separately. Thus, tree-level exchange of the scalar doublet fields S_{3i} could not account for $A^{t\bar{t}}_{FB}$ in this case. However, if the couplings of the LH quarks in Eq. (18) are defined in the LH down quark mass eigenstate basis, the scalars $S^-_{3\,i}$ would only couple to b_L in the $\mathrm{H_F}$ symmetric limit, as in Eq. 22, and

there would be no obstruction to $A_{FB}^{t\bar{t}}$ enhancement from $B \to K\pi$.

V. LHC SIGNALS

We next turn to signals at the LHC from a flavor symmetric sector. The NP fields couple to light quark bilinears so that generically deviations in the phenomenology of dijet observables at LHC and the Tevatron are expected. No statistically significant deviation in these observables has been measured to date, thus placing bounds on the couplings of NP fields to light quark bilinears. For a set of sample models we derived the bounds in Section IV C showing that $\mathcal{O}(1)$ couplings of these fields to quark bilinears are generally still allowed. Deviations from the QCD prediction can arise from an s-channel resonance effect, a t-channel driven rise in the dijet invariant mass spectra at large M_{jj}, or a combination of both signatures.

A prototypical signal of colored $\mathrm{G_F}$ symmetric fields is pair production, $g\,g \to V\,V$ and $g\,g \to S\,S$. This flavor diagonal scattering comes about due to the kinetic terms of the new scalar and vector fields, and the rate is driven by a coupling fixed by gauge invariance. The $gg \to SS$ production cross section in the $\mathrm{G_F}$ symmetric limit as a function of scalar meson mass is shown in Fig. 13. As this signal requires the pair production of the NP states, there is a significant fall in the cross section with the mass of the scalars. A simple approximation to the fall in the pair production cross section as a function of m_S is given by $\sigma_{\rm eff} \sim (1, 16, 20)\ \mathrm{pb} \times \exp(-m_s/95\,\mathrm{GeV})$ for the color representations $(\mathbf{3}, \mathbf{6}, \mathbf{8})$. This approximates the full result within the PDF uncertainty band over the mass region $0.15 - 1.5\,\mathrm{TeV}$. We expect the behavior of the $g\,g \to V\,V$ cross sections to be of a similar order of magnitude. Note that the non renormalizable nature of the effective vector field will lead to corrections to the cross section that grow with $\sqrt{s}/m_V$. These effects, however, are accompanied with the fall in the cross section with $\sqrt{s}$ due to PDF suppression.

Dedicated four quark jet studies where one searches for pairs of equal mass resonances with no missing energy can place strong bounds on models of this form in principle. The cross section for 4-jets at the 7 TeV LHC with all four jets having at least p_T of 300 GeV (500 GeV) is $1.6 \cdot 10^{-3}$ pb ($1.6 \cdot 10^{-4}$ pb), obtained using `ALPGEN`. Compared to the pair production cross section the QCD background is thus of moderate size. The condition that the four jets reconstruct resonances of approximately equal mass can aid in reducing the QCD four jet background. We leave a detailed study of the discovery prospects for a future study.

There are a number of other LHC signal features that are common to $\mathrm{G_F}$ symmetric models. When a signal requires flavor violation, such as the production of same sign tops, the rate is suppressed by the required CKM suppression and Yukawas to generate the tops from the initial state - as in the SM. The t-channel models aiming to explain the $A_{FB}^{t\bar{t}}$ anomaly without such a flavor symmetry can be strongly

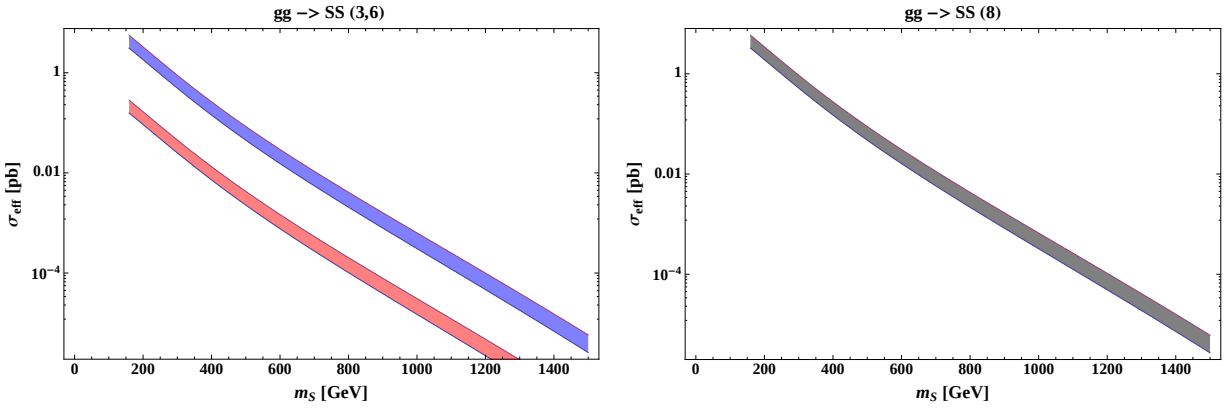

FIG. 13: Production cross sections of $g\,g \to S\,S$ for color triplets (red left), sextets (blue left) and octet (grey right) scalar field S. We show $\sigma_{eff} = \sigma/\dim[F]$ for a single flavor. We use MSTW208 pdfs and the PDF error bands shown are defined by taking $\mu = [2(2m_S), (2m_S)/2]$. Details of the calculation are in the Appendix.

constrained by bounds on same sign top signal at LHC [136]. The $\mathrm{G_F}$ symmetric models we have studied are essentially unbounded by this measurement.

Other signatures that are linked to explanations of the $A_{FB}^{t\bar{t}}$ anomaly do offer the prospect of constraining these models, such as a resonance decaying to $t + j$. This can be seen in $t\bar{t} + j$ production, and is a generic feature of t-channel models that can give enhanced $A_{FB}^{t\bar{t}}$ not just $\mathrm{G_F}$ symmetric models. Prospects for early LHC discovery were explored in Ref. [38, 44]. It is also feasible that for t-channel dominated models, the enhanced very forward $t\bar{t}$ cross section may be observable at LHCb [137]. We have shown that generically the new physics effect on the $t\,\bar{t}$ invariant mass spectra in the models we have considered are measurable in the near future. The cuts can be optimized at LHC to increase the prospects of measuring an excess of $t\,\bar{t}$ events due to new physics of this form while suppressing the SM background - see [138] for a recent study.

VI. CONCLUSIONS

In this paper, we have explored the collider physics of new physics sectors symmetric under the flavor group $\mathrm{G_F} = \mathrm{U(3)_{U_R}} \times \mathrm{U(3)_{D_R}} \times \mathrm{U(3)_{Q_L}}$ and its subgroup $\mathrm{H_F} = \mathrm{U(2)_{U_R}} \times \mathrm{U(2)_{D_R}} \times \mathrm{U(2)_{Q_L}} \times \mathrm{U(1)_3}$. These are the flavor symmetry groups of the SM quark sector in the absence of all yukawa couplings, and in the limit that only the top and bottom yukawa couplings are kept, respectively. Flavor symmetric fields cataloged in Tables I and II can have EW scale masses and $\mathcal{O}(1)$ couplings to quark bi-linears. This is because the representations of these fields under the SM gauge group and the flavor group are motivated to address a generic experimental conflict – the flavor problem of NP. Moreover, the flavor symmetries eliminate NP contributions to single top and same sign top production, which otherwise would be tightly

constrained. For fields that transform under $\mathrm{G_F}$ and have $\mathcal{O}(1)$ couplings to light quarks we find that a lower bound on their masses of roughly $150\,\mathrm{GeV}$ can be obtained from the absence of anomalous multi-jet events at LEP2. More detailed studies of EWPD, however, have the potential to improve these constraints.

Upper bounds on the couplings of $\mathrm{G_F}$ symmetric fields to light quarks can be set through studies of dijet resonance searches and angular distributions at the Tevatron and LHC. Based on the partonic LO study of dijet production we have determined these bounds in a number of sample models. Our results indicate that the LHC data sets are starting to constrain the allowed couplings to be $\lesssim 0.1$ in some of these models, in particular if they lead to resonant uu quark pair production as in models with color sextet scalars (e.g., model $\mathrm{S_{VI}}$ in Table II).

FCNC bounds on flavor symmetric models depend on how G_F is broken. In the $\mathrm{H_F}$ symmetric limit there are no NP contributions to meson mixing. We have analyzed NP contributions to meson mixing assuming MFV breaking of the $\mathrm{H_F}$ symmetry. The contributions to meson mixing are of second order in the product of MFV flavor breaking coefficients and vector or scalar couplings to quarks. We find that for models that contribute to B_d and B_s mixing with the same product of CKM elements as the SM box diagrams (and no additional light quark yukawa coupling factors) these coefficients have to be $\lesssim 0.1$ for vector or scalar masses of 1 TeV (these are vector models $\mathrm{III_{s,o}}, \mathrm{IV_{s,o}}, \mathrm{VIII_{s,o}}, \mathrm{IX_{s,o}}$ and the scalar model $\mathrm{S_{XIV}}$). The bounds on couplings for the remaining models are much looser.

The fields we have introduced and studied are of particular interest in the LHC discovery era. As an application we have examined the potential impact of such field content on two current experimental anomalies, the top quark forward-backward asymmetry, $A_{FB}^{t\bar{t}}$, and the $B_{s,d}$ dimuon charge asymmetry. Many of the flavor symmetric models can yield large $A_{FB}^{t\bar{t}}$, while maintaining agreement with the total top pair production cross section. However, simultaneous agreement with the $m_{t\bar{t}}$ differential cross section is more difficult to achieve. Generically, scalar models have difficulties accommodating all of the top quark data. The scalar models can either give u-channel contributions to $t\bar{t}$ production (models $\mathrm{S_V} - \mathrm{S_{XIV}}$) or t-channel contributions (models $\mathrm{S_I} - \mathrm{S_{IV}}$). The u-channel models exhibit significant tension with the differential spectrum. Of the t-channel models we have checked that model $\mathrm{S_I}$ shows good agreement with the differential spectrum, for masses of order 100 GeV. While it has difficulty reproducing the CDF $m_{t\bar{t}}$ dependent A_{FB} at the one sigma level, it should be noted that the recent DØ $A_{FB}^{t\bar{t}}$ measurement appears to exhibit a smaller $m_{t\bar{t}}$ dependence.

Vector models can contribute to $t\bar{t}$ production in the u-channel, s-channel, t-channel, or the s-channel and t-channel simultaneously. Phenomenologically preferred t-channel dominance can be a feature of the flavor structure (models $\mathrm{VII_{s,o}}$), or can be attained either through some flavor breaking or additional decay channels to broaden the s-channel decay widths. This leads to good agreement with all the top quark data,

with a preference for lighter vector meson masses (see models $\mathrm{VI_{s,o}}$ in Fig. 9, or Fig. 2 and Ref. [35], and models $\mathrm{VII_{s,o}}$ in Fig. 8). Note that flavor breaking or broadening of the widths (via non-$q\bar{q}$ final states) also insures consistency with resonance searches in the dijet data.

When studying the potential of new physics explanations of the $A_{FB}^{t\bar{t}}$ anomaly we have determined model independent acceptance corrections. These are appropriate for comparing against Tevatron data that can be applied to any model to good approximation at the partonic level- these results are given in Section III A 1.

Assuming MFV for $\mathrm{H_F}$ symmetry breaking, we have systematically examined the effects of scalar and vector fields on the dimuon charge asymmetry anomaly. Flavor symmetric models that can easily give relatively larger contributions to B_s mixing than to B_d mixing are preferred. Several flavor symmetric models can accommodate this pattern with tree level exchanges: vector models $\mathrm{I_{s,o}}, \mathrm{V_{s,o}}$ and scalar models $\mathrm{S_{IV}}, \mathrm{S_{VIII}}$, with $\mathcal{O}(1)$ MFV flavor breaking coefficients and NP masses of no more than a few 100 GeV, and models $\mathrm{X_{\bar{3},6}}$, $\mathrm{S_{III}}$, for masses around 1 TeV. None of these, however, can also explain the large $A_{FB}^{t\bar{t}}$, while simultaneously obeying all constraints. The dimuon charge asymmetry anomaly can also be explained by the experimentally less favored possibility - equal contributions to B_s and B_d mixing amplitudes (once normalized to the SM contributions). There are a number of models that can contribute to $t\bar{t}$ production as well as $B_{s,d}$ meson mixing. Of these, vector models $\mathrm{VII_{s,o}}$ and scalar model $\mathrm{S_I}$ are preferred, leading to both very small deviations in the differential $t\bar{t}$ spectrum and enhancement of $A_{FB}^{t\bar{t}}$. The contributions to $B_{s,d}$ arise at 1-loop and can be of the right size.

The models we have introduced and motivated can be discovered at the LHC through a number of processes: $t\bar{t} + j$ with $t + j$ forming a vector or scalar resonance peak; deviations in the $m_{t\bar{t}}$ differential cross section; pair production via $gg \to SS, VV$, where two resonance peaks are reconstructed in four jet final state; and deviations in dijet observables.

In conclusion, flavor symmetric fields by virtue of their flavor safe properties can have masses near the electroweak scale. They are therefore candidates for discovery at the LHC, as the lowest lying states of more complete models, which may or may not be directly linked to electroweak symmetry breaking. Flavor symmetric sectors have a rich, predictive, and mostly unexplored phenomenology. It is interesting to note that the list of fields that are $\mathrm{G_F}$ symmetric and can directly couple to quark bilinears is relatively short. Systematically exploring the phenomenology of flavor symmetric sectors is therefore feasible.

Acknowledgments

The work of B.G. was supported in part by the U.S. Department of Energy under contract DE-FG03-97ER40546. A. K. is supported by DOE grant FG02-84-ER40153. AK thanks the Weizmann Institute Phenomenology group for their hospitality while this work was being carried out. MT thanks Mark Wise, Maxim Pospelov and Jonathan Arnold for past collaboration related to some of the material discussed in this paper and the Triumf theory group for hospitality while this paper was being finalized. We thank K. Blum, O. Gedalia, Y. Hochberg, J. Kamenik, I.-W. Kim, S. J. Lee, Z. Ligeti, Y. Nir, G.Perez, J. Shu, and Y. Soreq for discussions regarding NP models in $t\bar{t}$ production. We use this opportunity to congratulate Jernej Kamenik on the birth of his first son Tian.

Appendix A: Flavor Symmetric Lagrangians

In this appendix we collect the Lagrangians of the vector fields in nontrivial $\mathrm{G_F}$ representations. The form of the scalar Lagrangians is given in [3] and we use that notation in the main part of the paper and in the Appendix for ease of comparison (for concreteness we also show explicit form of the relevant scalar Lagrangians at the end of this Appendix). For parameterizing the breaking of $\mathrm{G_F}$ we use the language of MFV, where the breaking is due to SM Yukawas only. For the unitary transformations that diagonalize the quark mass matrices we use the following notation

$$\begin{aligned} \mathcal{U}(u,R)^\dagger\, Y_U\, \mathcal{U}(u,L) &= \sqrt{2}\mathcal{M}_u/v \equiv Y_U^{\rm diag} \simeq \mathrm{diag}(0,0,y_t), \\ \mathcal{U}(d,R)^\dagger\, Y_D\, \mathcal{U}(d,L) &= \sqrt{2}\mathcal{M}_d/v \equiv Y_D^{\rm diag} \simeq \mathrm{diag}(0,0,y_b). \end{aligned} \tag{A1}$$

These relate the flavor (q_i) and mass eigenstates (q_i')

$$\begin{aligned} u_L =& \mathcal{U}(u,L) u'_L, \quad u_R = \mathcal{U}(u,R) u'_R, \\ d_L =& \mathcal{U}(d,L) d'_L, \quad d_R = \mathcal{U}(d,R) d'_R. \end{aligned}$$

In (A1) $\mathcal{M}_u$ and $\mathcal{M}_d$ are the diagonal up-type and down-type quark mass matrices and $v \simeq 246$ GeV is the SM Higgs vev. The Cabbibo-Kobayashi-Maskawa (CKM) matrix $V_{\rm CKM}$ is then given by

$$V_{\rm CKM} = \mathcal{U}(u,L)^\dagger\, \mathcal{U}(d,L). \tag{A2}$$

Two basis choices that we will frequently use are the "up" and "down" quark mass bases. In the "up" quark basis $Y_U^\dagger Y_U \to (Y_U^{\rm diag})^2, Y_D^\dagger Y_D \to V_{\rm CKM}(Y_D^{\rm diag})^2 V_{\rm CKM}^\dagger$, so that down-quarks are rotated from the mass eigenstates to keep interactions with the W bosons diagonal. Similarly in the down quark mass basis, the up quarks are rotated by $V_{\rm CKM}^\dagger$, so that $Y_U^\dagger Y_U \to V_{\rm CKM}^\dagger (Y_U^{\rm diag})^2 V_{\rm CKM}, Y_D^\dagger Y_D \to (Y_D^{\rm diag})^2$.

1. Vector fields $\mathrm{I} - \mathrm{IV}$

The vector fields $\mathrm{I_{s,o}} - \mathrm{IV_{s,o}}$ are flavor singlets, but can be either singlets or in adjoint representations of color and/or weak $SU(2)_L$. The interaction Lagrangian with quarks then has the same forms as the interactions with corresponding gauge fields would have. For instance, for $\mathrm{I_{s,o}}$, it is

$$\mathcal{L}_I = \eta \bar{d}_R \not{V} d_R, \tag{A3}$$

where $V_\mu = V_\mu^A T^A$ for $\mathrm{I_o}$ fields, with T^A the Gell-Mann matrices normalized to $\mathrm{Tr}(T^A T^B) = \delta^{AB}/2$. The interaction Lagrangians for $\mathrm{II_{s,o}}, \mathrm{III_{s,o}}$ are obtained from the above through replacements, $d_R \to u_R$ and $d_R \to Q_L$, respectively. In the interaction Lagrangians $\mathrm{IV_{s,o}}$ the short-hand notation for the sum of vector field multiplets is $V_\mu = V_\mu^a \sigma^a/2$ for $\mathrm{IV_s}$ model and $V_\mu = V_\mu^{A,a} T^A \sigma^a/2$ for $\mathrm{IV_o}$ model, with σ^a the Pauli matrices.

2. Fields $\mathrm{V_{s,o}}$

These fields are color singlets (octets) and $\mathrm{SU(3)_D}$ octets. The interaction and mass terms in the Lagrangian are similar to the case of the $\mathrm{SU(3)_U}$ octet fields $\mathrm{VI_{s,o}}$ given in Eqs. (3)-(7) and Eqs. (A4)-(A6), but with the obvious $u_R \to d_R$ and $y_t \to y_b$, $Y_U \to Y_D$ replacements. In the SM, $y_b \sim 0.02$ so that all the vectors in the multiplet are degenerate to a good approximation. The degeneracy can be lifted in theories with more than one Higgs where y_b can be $O(1)$, as occurs for example in the large $\tan\beta$ limit of the MSSM.

3. Fields $\mathrm{VI_{s,o}}$

These real fields are $\mathbf{1}, \mathbf{8}$ under color and $\mathbf{8}$ under flavor. We denote them by V_μ^B and $V_\mu^{A,B}$, with color (flavor) labels $A(B) = 1, \ldots, 8$. The quark-vector interaction Lagrangian and the mass terms were already given in Section II using the short-hand notation $V_\mu^s = T^B V_\mu^B, V_\mu^o = \mathcal{T}^A T^B V_\mu^{A,B}$. Here we write out the terms keeping all the indices explicit. The $\mathrm{G_F}$ symmetric quark-vector interactions (4) are

$$\mathcal{L}_{\mathrm{VI_s}} = \eta_1^s\ (\bar{u}_R)^{\alpha,i}\ (T^B)_i^j \not{V}^B (u_R)_{\alpha,j}, \qquad \mathcal{L}_{\mathrm{VI_o}} = \eta_1^o\, (\bar{u}_R)^{\alpha,i}\, (\mathcal{T}^A)_\alpha^\beta\, (T^B)_i^j \not{V}^{A,B} (u_R)_{\beta,j}, \tag{A4}$$

where $\alpha, \beta, \gamma...$ $(i, j, k...)$ are color (flavor) indices. The couplings $\eta_1^{s,o}$ are real because the interaction terms are hermitian. The $\mathrm{G_F} \to \mathrm{H_F}$ breaking interaction terms due to $Y_U\, Y_U^\dagger$ insertions (5) have the following explicit form in the mass eigenstate basis (keeping only the terms proportional to y_t)

$$\Delta\mathcal{L}_{\mathrm{VI_o}} = y_t^2 \left[(\eta_2^o)^\star (\bar{u}'_R)^\alpha \not{\tilde{V}}_\mu^{A,B}\, (\mathcal{T}^A)_\alpha^\beta\, (T^B)_3^i (u'_R)_{\beta,i} + h.c.\right] - \frac{y_t^4\, \eta_3^o}{2\sqrt{3}} (\bar{u}'_R)^{\alpha,i}\, \not{\tilde{V}}_\mu^{A,8}\, (\mathcal{T}^A)_\alpha^\beta (u'_R)_\beta, \tag{A5}$$

$$\Delta\mathcal{L}_{\mathrm{VI_s}} = y_t^2 \left[(\eta_2^s)^\star\, (\bar{u}'_R)^\alpha \not{\tilde{V}}_\mu^B\, (T^B)_3^i (u'_R)_{\alpha,i} + h.c.\right] - \frac{y_t^4\, \eta_3^s}{\sqrt{3}} (\bar{u}'_R)^{\alpha,i}\, \not{\tilde{V}}_\mu^8\, (T^8)_3^3 (u'_R)_\alpha. \tag{A6}$$

4. Fields $\mathrm{VII_{s,o}}$

These fields are in the $(\bar{3}, 3, 1)$ representation of flavor. As for fields V, VI we use the short-hand notation

$$V_\mu^s = T^B V_\mu^B, \qquad V_\mu^o = \mathcal{T}^A T^B V_\mu^{A,B}, \tag{A7}$$

with $\mathcal{T}^A$ the color Gell-Mann matrices. The flavor matrices T^B now also include an identity matrix, so that for $B = 1, \ldots, 8$, T^B are the Gell-Mann matrices, and $T^9 = \mathbb{1}/\sqrt{6}$. Note that $V_\mu^\dagger \neq V_\mu$, because the V_μ fields are in the $(\bar{3}, 3, 1)$ representation of $\mathrm{G_F}$. The transformation to the mass eigenstate basis is

$$V_\mu^a = \mathcal{U}(d, R) \tilde{V}_\mu^a\, \mathcal{U}(u, R)^\dagger, \qquad a = o, s, \tag{A8}$$

explicitly showing that $V_\mu^{o,s}$ are not hermitian (note also that V_μ^B, $V_\mu^{A,B}$ carry nonzero hyper-charge). The tree level quark coupling Lagrangian terms are (no summation over $a = o, s$)

$$\mathcal{L}_{\rm VII_a} = \eta_1^a \bar{d}_R \not{V}_\mu^a u_R + h.c., \tag{A9}$$

with $\eta_1^{o,s}$ complex in general. Explicitly the two terms are

$$\mathcal{L}_{\rm VII_o} = \eta_1^o \, (V_\mu^{A,B} T^B)_j^i \, (\bar{d}_R)^{\alpha,j} \, \gamma^\mu \, (\mathcal{T}^A)_\alpha^\beta \, (u_R)_{\beta,i}, + \text{h.c.}, \tag{A10}$$

$$\mathcal{L}_{\rm VII_s} = \eta_1^s \, (V_\mu^B T^B)_j^i \, (\bar{d}_R)^{\alpha,j} \, \gamma^\mu \, (u_R)_{\alpha,i} + \text{h.c.}. \tag{A11}$$

The flavor breaking introduces corrections to these interaction terms from insertions of the $Y_U \, Y_U^\dagger$ and $Y_D \, Y_D^\dagger$. Keeping only the terms proportional to y_t^2 for $\mathrm{G_F} \to \mathrm{H_F}$, the leading contribution is given by $\eta_2^a \bar{d}_R \not{V}_\mu^a Y_U Y_U^\dagger u_R$, which gives in the mass eigenstate basis the following interactions

$$\Delta\mathcal{L}_{\rm VII_o} = y_t^2 \left[\eta_2 (\bar{d'}_R)^{\alpha,i} \, \gamma^\mu \, (\mathcal{T}^A)_\alpha^\beta \, (t'_R)_\beta, \right] \, (\tilde{V}_\mu^{A,B} T^B)_i^3 + h.c., \tag{A12}$$

$$\Delta\mathcal{L}_{\rm VII_s} = y_t^2 \, \left[\eta_2 (\bar{d'}_R)^{\alpha,i} \, \gamma^\mu \, (t'_R)_\alpha \right] \, (\tilde{V}_\mu^B T^B)_i^3 + h.c. \tag{A13}$$

The mass terms are

$$\mathcal{L}_{\rm VII_a} = 2(1+\delta_{a,o}) \left\{ m_{V_a}^2 \, \mathrm{Tr} \left[\tilde{V}_\mu^a \, \tilde{V}^{\mu a \dagger} \right] + \lambda \, (H^\dagger \, H) \, \mathrm{Tr} \left[\tilde{V}_\mu^a \, \tilde{V}^{\mu a \dagger} \right] \right\}, \qquad a = o, s, \tag{A14}$$

while the top quark Yukawa splits the mass spectrum through corrections to the mass Lagrangian of the form $2(1+\delta_{a,o}) \, \zeta_1 Tr[\tilde{V}_\mu^a Y_U Y_U^\dagger \, \tilde{V}^{\mu a \dagger}]$. The mass of the field V_μ^8 gets split from the rest by the term $2(1 + \delta_{a,o}) \, \zeta_2 Tr[\tilde{V}_\mu^a Y_U Y_U^\dagger \, \tilde{V}^{\mu a \dagger} Y_D Y_D^\dagger]$. These splittings result in the following mass spectrum

$$m_1^2 = m_2^2 = m_3^2 = m_V^2 \left(1 + \frac{\lambda}{2} \frac{v^2}{m_V^2} \right), \tag{A15}$$

$$m_4^2 = m_5^2 = m_6^2 = m_7^2 = m_V^2 \left(1 + \frac{\lambda}{2} \frac{v^2}{m_V^2} + \frac{\zeta_1}{2} \, y_t^2 \right), \tag{A16}$$

$$m_8^2 = m_V^2 \left(1 + \frac{\lambda}{2} \frac{v^2}{m_V^2} + \frac{2\zeta_1}{3} y_t^2 + \frac{2\zeta_2}{3} \, y_b^2 \, y_t^2 \right), \tag{A17}$$

$$m_9^2 = m_V^2 \left(1 + \frac{\lambda}{2} \frac{v^2}{m_V^2} + \frac{\zeta_1}{3} y_t^2 + \frac{\zeta_2}{3} \, y_b^2 \, y_t^2 \right), \tag{A18}$$

where we neglect terms suppressed by off-diagonal CKM elements or first two generation Yukawas.

5. Fields $\mathrm{VIII_{s,o}}$

The scalar matrix of fields $V_\mu^s = T^B V_\mu^B$, and the octet matrix of fields $V_\mu^o = \mathcal{T}^A T^B V_\mu^{A,B}$, now transform as a bi-fundamental of $\mathrm{U(3)_Q}$, i.e. $V_\mu^{o,s} \to V_Q V_\mu^{o,s} V_Q^\dagger$ for a transformation that takes the left-handed

quark fields to $Q_L \to V_Q Q_L$ (suppressing the flavor indices). Note that the fields $V_\mu^{o,s}$ are hermitian, $V_\mu^{o,s\dagger} = V_\mu^{o,s}$. The interaction with quarks is then given by

$$\mathcal{L}_{\mathrm{VIII_a}} \;=\; \eta_1^a \bar{Q}_L \not{V}_\mu^a Q_L, \tag{A19}$$

or writing out the color and flavor indices explicitly

$$\mathcal{L}_{\mathrm{VIII_o}} \;=\; \eta_1^o \, V_\mu^{A,B} \, (\bar{Q}_L)^{\alpha,i} \, \gamma^\mu \, (\mathcal{T}^A)^\beta_\alpha \, (T^B)^j_i (Q_L)_{\beta,j}, \tag{A20}$$

$$\mathcal{L}_{\mathrm{VIII_s}} \;=\; \eta_1^s \, V_\mu^B \, (\bar{Q}_L)^{\alpha,i} \, \gamma^\mu \, (T^B)^j_i (Q_L)_{\alpha,j}. \tag{A21}$$

The flavor symmetric mass Lagrangian for the vectors is

$$\mathcal{L}^{\mathrm{mass}}_{\mathrm{VIII_{o,s}}} = (1+\delta_{a,o}) \left\{ m_V^2 \, \mathrm{Tr}\left[\tilde{V}_\mu \, \tilde{V}^\mu\right] + \lambda \, (H^\dagger \, H) \, \mathrm{Tr}\left[\tilde{V}_\mu \, \tilde{V}^\mu\right] \right\}, \tag{A22}$$

where the color and flavor indices are suppressed. The masses are split by the presence of the SM Yukawas breaking the flavor group. In contrast to cases V and VII here both insertions of $Y_U^\dagger \, Y_U$ and $Y_D^\dagger \, Y_D$ are possible. The flavor breaking terms are

$$\Delta\mathcal{L}^{\mathrm{mass}}_{\mathrm{VIII_{o,s}}}/m_V^2 = \zeta_1 \mathrm{Tr}\left[\tilde{V}_\mu \, Y_U^\dagger \, Y_U \tilde{V}^\mu\right] + \zeta_1' \mathrm{Tr}\left[\tilde{V}_\mu \, Y_D^\dagger \, Y_D \tilde{V}^\mu\right] + \zeta_2 \mathrm{Tr}\left[Y_U^\dagger \, Y_U \tilde{V}_\mu \, Y_U^\dagger \, Y_U \tilde{V}^\mu\right] + \cdots \tag{A23}$$

with ζ_i all real (complex couplings are possible at higher orders in Yukawa insertions). In general, the masses for V_μ are not diagonalized by the $\mathcal{U}(u,L)$ or $\mathcal{U}(d,L)$ unitary transformation, but by a unitary transformation that differs by $\sim V_{\mathrm{CKM}}$ from the two. For simplicity, we work in the limit where the contributions from y_b are much smaller than from y_t. In this limit the vector field mass matrix is diagonalized using $\mathcal{U}(u,L)$, giving a spectrum

$$m_1^2 = m_2^2 = m_3^2 \;=\; m_V^2 \left(1 + \frac{\lambda}{2}\frac{v^2}{m_V^2}\right), \tag{A24}$$

$$m_4^2 = m_5^2 = m_6^2 = m_7^2 \;=\; m_V^2 \left(1 + \frac{\lambda}{2}\frac{v^2}{m_V^2} + \frac{\zeta_1}{2}\, y_t^2\right), \tag{A25}$$

$$m_8^2 \;=\; m_V^2 \left(1 + \frac{\lambda}{2}\frac{v^2}{m_V^2} + \frac{\zeta_1}{3} y_t^2 + \frac{\zeta_2}{3} y_t^4\right). \tag{A26}$$

The mass degeneracy is lifted at y_b^2 order from a contribution of the form $y_b^2 (V_{\mathrm{CKM}})_{i3} (V_{\mathrm{CKM}}^\dagger)_{j3}$ (*i.e.,* from the term proportional to ζ_1' in (A23)).

We are now ready to write down the flavor breaking couplings between the vector and the quark fields. These are given by

$$\begin{aligned}\Delta\mathcal{L}_{\mathrm{VIII_a}} = &\left[\eta_2^a \bar{Q}_L Y_U^\dagger Y_U \not{V}_\mu^a Q_L + h.c.\right] + \left[\eta_3^a \bar{Q}_L Y_D^\dagger Y_D \not{V}_\mu^a Q_L + h.c.\right] \\ &+ \left[\eta_4^a \bar{Q}_L Y_U^\dagger Y_U \not{V}_\mu^a Y_D^\dagger Y_D Q_L + h.c.\right] + \cdots,\end{aligned} \tag{A27}$$

where we only display one of the possible terms with four insertions of Yukawa matrices. Note that $\eta_{2,3,4}$ can all be complex. We first display the couplings to the up-quarks in the "up" basis

$$\begin{aligned}\Delta\mathcal{L}_{\rm VIII_o} &= y_t^2\eta_2^o\left[(\bar{t}'_L)^\alpha(\mathcal{T}^A)^\beta_\alpha(T^B)^i_3\,\tilde{\not{V}}^{A,B}_\mu(u'_L)_{i\beta}\right]\\ &+ y_b^2\eta_3^o(V_{\rm CKM})^3_i\,(V^*_{\rm CKM})^j_3\left[(\bar{u}'_L)^{i\alpha}(\mathcal{T}^A)^\beta_\alpha(T^B)^k_j\not{V}^{A,B}_\mu(u'_L)_{k\beta}\right]\\ &+ y_t^2y_b^2\eta_4^o\,(V_{\rm CKM})^3_i(V^*_{\rm CKM})^j_3\left[(\bar{t}'_L)^\alpha(\mathcal{T}^A)^\beta_\alpha\,(T^B)^i_3\tilde{\not{V}}^{A,B}_\mu(u'_L)_{j\beta}\right].\end{aligned}\tag{A28}$$

The couplings to the bottom quarks we display in the "down" basis

$$\begin{aligned}\Delta\mathcal{L}_{\rm VIII_o} &= y_t^2\eta_2^o(V^*_{\rm CKM})^3_i\,(V_{\rm CKM})^j_3\left[(\bar{d}'_L)^{i\alpha}(\mathcal{T}^A)^\beta_\alpha(T^B)^k_j\not{V}^{A,B}_\mu(d'_L)_{k\beta}\right]\\ &+ y_b^2\eta_3^o\left[(\bar{b}'_L)^\alpha(\mathcal{T}^A)^\beta_\alpha(T^B)^i_3\,\not{V}^{A,B}_\mu(d'_L)_{i\beta}\right]\\ &+ y_t^2y_b^2\eta_4^o\,(V^*_{\rm CKM})^3_i(V_{\rm CKM})^j_3\left[(\bar{d}'_L)^{i\alpha}(\mathcal{T}^A)^\beta_\alpha\,(T^B)^3_j\not{V}^{A,B}_\mu(b'_L)_\beta\right].\end{aligned}\tag{A29}$$

For each of these two cases, the vector fields have to be put in the "up" or "down" basis respectively. In the limit where we neglect y_b insertions, the "up" basis coincides with the mass basis for the vector fields, while the vector fields are not mass diagonal in the "down" basis. The couplings for the singlet case are obtained from the above expressions by replacing $(\mathcal{T}^A)^\beta_\alpha \to \delta^\beta_\alpha$.

6. Fields $\mathrm{IX}_{\rm s,o}$

The discussion for this case is very similar to the previous one. The fields are given by $V^{B,i}_\mu$ for the color singlet and $V^{A,B,i}_\mu$ for the color octet case, where $i = 1, 2, 3$ is the weak $\mathrm{SU}(2)_{\rm L}$ index. All basis independent expressions apply also in this case, if the matrices of fields are defined as $V^s_\mu = T^B\sigma^iV^{B,i}_\mu/2$, and the octet matrix of fields $V^o_\mu = \mathcal{T}^AT^B\sigma^iV^{A,B,i}_\mu/4$, where σ^i are the Pauli matrices. Phenomenologically the most important difference is that there are now charged currents.

7. Fields $\mathrm{X}_{\bar{3},6}$

These fields are weak doublets and belong to the bi-fundamental representation of the flavor group $(1, 3, 3)$. They are either anti-triplets of color, in which case we have the fields $(V_\mu)^{r\gamma}_{i,j}$, or they are sextets of color, in which case the fields are $(V_\mu)^r_{i,j,\alpha,\beta} = (V_\mu)^r_{i,j,\beta,\alpha}$. Here r is the weak $\mathrm{SU}(2)_{\rm L}$ index, α, β are the flavor indices, while i and j are the indices of the $(1, 3, 1)$ and $(1, 1, 3)$ representations respectively. In Section II we have written the Lagrangian in short-hand notation, while here we show the terms keeping the indices explicit. The tree level quark coupling Lagrangian terms are (suppressing the $\mathrm{SU}(2)_{\rm L}$ indices)

$$\mathcal{L}_{X_{\bar{3}}} \;=\; \eta_1\,\epsilon_{\alpha\beta\gamma}\,(V_\mu)^\gamma_{i,j}\,(\bar{d}_R)^{\alpha i}\,\gamma^\mu\,(Q^c_L)^{\beta j} + h.c.,\tag{A30}$$

$$\mathcal{L}_{X_6} \;=\; \eta_1\,(V_\mu)_{i,j,\alpha,\beta}\,(\bar{d}_R)^{\alpha i}\,\gamma^\mu\,(Q^c_L)^{\beta j} + h.c.,\tag{A31}$$

which in the mass eigenstate basis are

$$\mathcal{L}_{X_{\bar{3}}} \;=\; \eta_1\,\epsilon_{\alpha\beta\gamma}\,(\tilde{V}^1_\mu)^\gamma_{i,j}\,(\bar{d'}_R)^{\alpha i}\,\gamma^\mu\,(u'^c_L)^{\beta j} + \eta_1\,\epsilon_{\alpha\beta\gamma}\,(V_{\rm CKM})^k_j\,(\tilde{V}^2_\mu)^\gamma_{i,k}\,(\bar{d'}_R)^{\alpha i}\,\gamma^\mu\,(d'^c_L)^{\beta j} + h.c \quad \text{(A32)}$$

$$\mathcal{L}_{X_6} \;=\; \eta_1\,(V^1_\mu)_{i,j,\alpha,\beta}\,(\bar{d'}_R)^{\alpha i}\,\gamma^\mu\,(u'^c_L)^{\beta j} + \eta_1\,(V_{\rm CKM})^k_j\,(\tilde{V}^2_\mu)_{i,k,\alpha,\beta}\,(\bar{d'}_R)^{\alpha i}\,\gamma^\mu\,(d'^c_L)^{\beta j} + h.c.. \quad \text{(A33)}$$

with $(\tilde{V}^1_\mu)$ and $(\tilde{V}^2_\mu)$ the charge and neutral vector fields, respectively.

8. Fields $\mathrm{XI}_{\bar{3},6}$

The analysis is very similar to case X. The couplings to quarks, vector fields mass spectra and splittings can be obtained from the discussion on case X with the replacements $d_R \leftrightarrow u_R$, $Y_D \leftrightarrow Y_U$. For instance, the quark coupling Lagrangian terms are (suppressing the $\mathrm{SU(2)_L}$ index)

$$\mathcal{L}_{\mathrm{XI}_{\bar{3}}} \;=\; \eta_1\,\epsilon_{\alpha\beta\gamma}\,(V_\mu)^\gamma_{i,j}\,(\bar{u}_R)^{\alpha i}\,\gamma^\mu\,(Q^c_L)^{\beta j} + h.c., \quad \text{(A34)}$$

$$\mathcal{L}_{\mathrm{XI}_6} \;=\; \eta_1\,(V_\mu)_{i,j,\alpha,\beta}\,(\bar{u}_R)^{\alpha i}\,\gamma^\mu\,(Q^c_L)^{\beta j} + h.c.. \quad \text{(A35)}$$

9. Scalar Fields I, V, VI, IX, X

For convenience, the interaction Lagrangians for the scalar models under discussion, in the $\mathrm{G_F}$ symmetric limit, are provided below:

$$\mathcal{L}_{\rm I} = \eta\,(\,S^0_{ij}\bar{u}_{i\,L}u_{j\,R} + S^-_{ij}\bar{d}_{i\,L}u_{j\,R}) + h.c.\,, \quad \text{(A36)}$$

$$\mathcal{L}_{\rm V} = \eta\,\epsilon^{\alpha\beta\gamma}\epsilon_{ijk}\,S^i_\alpha\,u^j_{R\beta}\,u^k_{R\gamma} \;+\; h.c.\,, \qquad \mathcal{L}_{\rm VI} = \eta\,S^{a,b}(\hat{T}^a)_{ij}(\hat{\mathcal{T}}^b)^{\alpha\beta}\,u^i_{R\alpha}\,u^j_{R\beta} \;+\; h.c., \quad \text{(A37)}$$

$$\mathcal{L}_{\rm IX} = \eta\,\epsilon^{\alpha\beta\gamma}S^\alpha_{ij}d^i_{R\beta}\,u^j_{R\gamma} \;+\; h.c.\,, \qquad \mathcal{L}_{\rm X} = \eta\,S^a_{ij}(\hat{T}^a)^{\alpha\beta}\,d^i_{R\alpha}\,u^j_{R\beta} \;+\; h.c., \quad \text{(A38)}$$

where the η are dimensionless flavor universal couplings, Latin (Greek) indices label flavor (color), and Lorentz spinor indices are suppressed. The generators $\hat{T}^a$ and $\hat{\mathcal{T}}^b$ of the symmetric sextet flavor and color representations are the symmetric 3×3 matrices, normalized such that $\mathrm{Tr}(\hat{T}^a\hat{T}^b) = 2\delta^{ab}$ and $a, b = 1, \cdots, 6$. The scalar fields appearing in $\mathcal{L}_{\rm I,V,VI,IX,X}$ are canonically normalized. In $\mathcal{L}_{\rm I}$ we show explicitly the Yukawa couplings of the charged and neutral components of the scalar doublets. The relevant NP cross section formulae for top quark pair production can be found in Appendix B. The decay widths of the scalars are $\kappa\,\eta^2\,m_S/16\pi$, where $\kappa = 1,\ 4,\ 2,\ 1,\ 1$ in models $\mathrm{S_V}$, $\mathrm{S_{VI}}$, $\mathrm{S_{IX}}$, $\mathrm{S_X}$, $\mathrm{S_I}$, respectively (assuming all quark decay channels are open and ignoring phase space effects).

Appendix B: Details on $2 \to 2, 3$ scattering calculations and phenomenology

In this Appendix we give some details of the calculations for $t\bar{t}$ and light quark $q\bar{q}$ production in the scalar and vector MFV models. The comparisons with experimental data at the Tevatron and LHC were done in Sections III and IV C.

a. $2 \to 2$ *scattering in the scalar models*

The relevant interaction Lagrangians for the scalar models are given in Eqs. (A37) – (A36). The general formula for the spin averaged matrix element squared for $q\bar{q} \to t\bar{t}$, including interference with the SM, for the exchange of a color triplet or sextet in the u-channel is [18]

$$\sum_{ij} |\mathcal{M}|^2 = 64 \sum_{ij} \left[\frac{g_s^2\, \eta^2\, C_0}{s} \left(\frac{(s\, m_t^2 + u_t^2)(u - m_s^2)}{(u - m_s^2)^2 + \Gamma^2\, m_s^2} \right) + \frac{4\, \eta^4\, C_2\, u_t^2}{(u - m_s^2)^2 + \Gamma^2\, m_s^2} \right] , \tag{B1}$$

where $v_t \equiv v - m_t^2$ for $v = \{s, t, u\}$. For the exchange of a color singlet or octet in the t-channel one has to make the replacement $u \to t$ above. The color factors for an exchange of a $(\mathbf{1}, \bar{\mathbf{3}}, \mathbf{6}, \mathbf{8})$ of $\mathrm{SU}(3)_\mathrm{c}$ are given by $C_0 = (4, 1, -1, -2/3)$ and $C_2 = (9, 3/4, 3/2, 2)$.

The differential partonic $2 \to 2$ cross section averaged over initial spins and colors and summed over final states is given by

$$\frac{d\,\hat{\sigma}}{d\,z} = \frac{\beta}{32\,\pi\,s} \overline{\sum_{ij}} |\mathcal{M}_{ij}|^2. \tag{B2}$$

where $\overline{\sum_{ij}} |\mathcal{M}_{ij}|^2 = \frac{1}{4}\,\frac{1}{9} \sum_{ij} |\mathcal{M}_{ij}|^2$. Here $\beta = \sqrt{1 - 4m^2/s}$ is the velocity of the final state quark (with mass m) in the initial state partonic rest frame while $z = \cos\theta$ and θ is the scattering angle in the partonic CM frame. The sum in Eq. (B2) is over all contributing matrix elements. The initial states are weighted with the appropriate PDFs to obtain the hadronic cross section. When evaluating the dijet constraints we use MSTW2008 PDF sets [94]. The renormalization scale is set to the p_T of the jets, $\mu = M_{jj}\,\sqrt{1 - z^2}/2$, where $z = \cos\theta$ is the partonic scattering angle from the beam line and M_{jj} is the invariant mass of the dijets.

In the case of light quark pair production, in models $\mathrm{S_V}$ and $\mathrm{S_{VI}}$ there are u-channel exchange contributions to $u\,\bar{u} \to c\,\bar{c}, c\,\bar{c} \to u\,\bar{u}$, and in $\mathrm{S_{VI}}$ there are additional u-channel exchange contributions to $u\,\bar{u} \to u\,\bar{u},\ c\,\bar{c} \to c\,\bar{c}$. The corresponding matrix elements squared can be obtained from Eq. (B1), taking care to include factors of 2 and 4, respectively, in the first and second terms for the latter subprocesses. s-channel exchange in models S_V and $\mathrm{S_{VI}}$ contribute to $u\,c \to u\,c + \mathrm{c.c.}$, and in $\mathrm{S_{VI}}$ there are additional contributions to $u\,u \to u\,u + \mathrm{c.c.},\ \ cc \to cc + \mathrm{c.c.}$. The corresponding cross sections can be obtained via crossing symmetry from the above, and including t channel SM contributions, also see [36].

Following [139], experimental cuts on the rapidity y and the rapidity separation Δy of the two leading jets in dijet production are implemented at the partonic level in the $2 \to 2$ subprocesses via

$$\frac{d\sigma}{dM_{jj}} = \sigma_N \frac{M_{jj}}{s} \int_{-y_B^0}^{y_B^0} d\,y_B \int_{-z_0}^{z_0} d\,z \sum_{ij} f_i(\tau\, e^{y_B})\, f_j(\tau\, e^{-y_B}) \frac{d\,\hat{\sigma}}{d\,z} \tag{B3}$$

where $\sigma_N = 0.3894 \cdot 10^9 \mathrm{pb}$, s is the hadronic center of mass energy, $\tau = \sqrt{M_{jj}^2/s}$, $f_{i,j}$ are the MSTW parton densities, and Y_B is the boost rapidity of the subprocess frame. The rapidity cuts $|y_{1,2}| < Y_{\max}$ correspond to the integration limits

$$y_B^0 = \mathrm{Min}[Y_{\max}, -\log[M_{jj}^2/s]/2] \tag{B4}$$

and a cut $\Delta y < (\Delta y)^{\max}$ enters the angular integration limits as

$$z^0 = \mathrm{Min}[z^{\max}, \tanh(Y_{\max} - |y_B|)]. \tag{B5}$$

where $z^{\max} = (\mathrm{Exp}[(\Delta y)^{\max}] - 1)/(\mathrm{Exp}[(\Delta y)^{\max}] + 1)$.

b. Vector models $2 \to 2$ production

The vector models can be divided into two sets: the cases I-IX that couple only right-handed or left-handed quarks, and the models X and XI, where the right-handed quarks are coupled to left-handed (charge conjugated) quarks. To obtain a general equation for the $q\bar{q} \to t\bar{t}$ cross section for the first subset of models I-IX, we consider a generic Lagrangian (with trivial changes in notation if vectors couple to right-handed quarks)

$$\mathcal{L} = f_q \bar{q}_L \not{V} q_L + f_t \bar{t}_L \not{V} t_L + [f_{qt} \bar{q}_L \not{V} t_L + h.c.], \tag{B6}$$

where we have suppressed flavor, weak and color indices. This gives for the weighted average of the amplitude squared for the $q\bar{q} \to t\bar{t}$ scattering

$$\begin{aligned}\overline{\sum}|\mathcal{M}|^2 = {} & \mathcal{C}_1 \frac{|f_q f_t|^2}{36} \frac{s^2(1+\beta_\theta)^2}{s_V^2 + \Gamma_V^2 m_V^2} + \mathcal{C}_3 \frac{|f_{qt}|^4}{36} \frac{s^2}{t_V^2 + \Gamma_V^2 m_V^2} \left((1+\beta_\theta)^2 + \frac{m_t^4}{4m_V^4} \left[(1-\beta_\theta)^2 + 16 \frac{m_V^2}{s} \right] \right) \\ & + \mathcal{C}_2 \frac{|f_{qt}|^2}{18} \frac{f_q f_t (s_V t_V + \Gamma_V^2 m_V^2)}{(s_V^2 + \Gamma_V^2 m_V^2)(t_V^2 + \Gamma_V^2 m_V^2)} s^2 \left((1+\beta_\theta)^2 + 2 \frac{m_t^4}{s m_V^2} \right)\end{aligned} \tag{B7}$$

while the interference with the LO SM one gluon exchange gives

$$\begin{aligned}\overline{\sum} 2\mathrm{Re}(\mathcal{M}\mathcal{M}_{SM}^*) = {} & \frac{8\pi\alpha_S}{9} \mathcal{C}_4 |f_{qt}|^2 \frac{t_V}{t_V^2 + \Gamma_V^2 m_V^2} s \left(\frac{m_t^2}{s} + \frac{1}{4}(1+\beta_\theta)^2 + \frac{m_t^2}{2m_V^2} \left[\frac{m_t^2}{s} + \frac{1}{4}(1-\beta_\theta)^2 \right] \right) \\ & + \frac{8\pi\alpha_S}{9} \mathcal{C}_5 \frac{f_q f_t s_V}{s_V^2 + \Gamma_V^2 m_V^2} s \left[\frac{m_t^2}{s} + \frac{1}{4}(1+\beta_\theta)^2 \right].\end{aligned} \tag{B8}$$

Case	Couples to q	f_q	f_t	f_{qt}	$\mathcal{C}_1^s$	$\mathcal{C}_2^s$	$\mathcal{C}_3^s$	$\mathcal{C}_4^s$	$\mathcal{C}_5^s$	$\mathcal{C}_1^o$	$\mathcal{C}_2^o$	$\mathcal{C}_3^o$	$\mathcal{C}_4^o$	$\mathcal{C}_5^o$
$\mathrm{I_{s,o}}$	d,s,b	η_1	0	0	9	0	0	0	0	2	0	0	0	2
$\mathrm{II_{s,o}}$	u,c	η_1	$\eta_1+y_t^2\eta_2$	0	9	0	0	0	0	2	0	0	0	2
$\mathrm{III_{s,o}}$	u,d,s,c,b	η_1	$\eta_1+y_t^2\eta_2$	0	9	0	0	0	0	2	0	0	0	2
$\mathrm{IV_{s,o}}$	u,c	η_1	$\eta_1+y_t^2\eta_2$	0	9	-6	36	8	0	2	$\frac{4}{3}$	8	$-\frac{4}{3}$	2
	d,s,b	η_1	$\eta_1+y_t^2\eta_2$	$\eta_1\delta_{q,b}$	9	-6	36	8	0	2	$\frac{4}{3}$	8	$-\frac{4}{3}$	-2
$\mathrm{V_{s,o}}$	d,s,b	η_1	0	0	$\frac{1}{4}$	$-\frac{1}{4}$	$\frac{9}{4}$	2	0	$\frac{1}{18}$	$\frac{1}{18}$	$\frac{1}{2}$	$-\frac{1}{3}$	$-\frac{1}{3}$
$\mathrm{VI_{s,o}}$	u,c	η_1	$\eta_1+2y_t^2Re(\eta_2)$	$\eta_1+y_t^2\eta_2$	$\frac{1}{4}$	$-\frac{1}{4}$	$\frac{9}{4}$	2	0	$\frac{1}{18}$	$\frac{1}{18}$	$\frac{1}{2}$	$-\frac{1}{3}$	$-\frac{1}{3}$
$\mathrm{VII_{s,o}}$	d,s,b	0	0	$\eta_1+y_t^2\eta_2$	0	0	$\frac{9}{4}$	2	0	0	0	$\frac{1}{2}$	$-\frac{1}{3}$	0
$\mathrm{VIII_{s,o}}$	u,d,s,c,b	$\eta_1+y_t^2 2Re(\eta_2)\delta_{q,b}$	$\eta_1+y_t^2 2Re(\eta_2)$	$\eta_1+y_t^2\eta_2$	$\frac{1}{4}$	$\frac{-1}{4}$	$\frac{9}{4}$	2	0	$\frac{1}{18}$	$\frac{1}{18}$	$\frac{1}{2}$	$-\frac{1}{3}$	$-\frac{1}{3}$
$\mathrm{IX_{s,o}}$	u,c	$\eta_1+y_t^2 2Re(\eta_2)\delta_{q,b}$	$\eta_1+y_t^2 2Re(\eta_2)$	$\eta_1+y_t^2\eta_2$	$\frac{1}{4}$	$-\frac{1}{4}$	$\frac{9}{4}$	2	0	$\frac{1}{18}$	$\frac{1}{18}$	$\frac{1}{2}$	$-\frac{1}{3}$	$-\frac{1}{3}$
	d,s	$\eta_1+y_t^2 2Re(\eta_2)\delta_{q,b}$	$\eta_1+y_t^2 2Re(\eta_2)$	$\eta_1+y_t^2\eta_2$	$\frac{1}{4}$	$\frac{1}{2}$	9	4	0	$\frac{1}{18}$	$-\frac{1}{9}$	2	$-\frac{2}{3}$	$\frac{1}{3}$
	b	$\eta_1+y_t^2 2Re(\eta_2)\delta_{q,b}$	$\eta_1+y_t^2 2Re(\eta_2)$	$\eta_1+y_t^2\eta_2$	1	-$\frac{2}{3}$	4	$\frac{8}{3}$	0	$\frac{2}{9}$	$\frac{4}{27}$	$\frac{8}{9}$	$-\frac{4}{9}$	$-\frac{2}{3}$

TABLE VII: The contributions to $t\bar{t}$ cross section from MFV vector resonances. The coefficients $\mathcal{C}_i$ are to be used in Eqs. (B7), (B8), where we have kept for simplicity only leading flavor breaking in the couplings of quarks to the vector, while neglecting the flavor breaking in the vector propagators (and in models IV, IX, X, XI also neglecting the electroweak symmetry breaking contributions to vector masses).

Here $s_V = s - m_V^2$, and similarly $t_V = t - m_V^2, u_V = u - m_V^2$. Explicitly one has

$$t = m_t^2 - \frac{1}{2}s(1-\beta_\theta), \qquad u = m_t^2 - \frac{1}{2}s(1+\beta_\theta), \tag{B9}$$

with $\beta_\theta = \beta\cos\theta$, while $\beta = \sqrt{1-4m_t^2/s}$ is the top velocity in the $t\bar{t}$ rest frame. We have used the same notational conventions as in the scalar case above. This formula should be summed over all possible initial quark states q, which depends on the particular MFV vector field considered.

The expressions for the contributions to the $t\bar{t}$ cross section for the second subset, cases X and XI, are very similar to the above. The important difference is that both left-handed and right-handed quarks couple to the vectors at the same time. The general form of the interaction Lagrangian in this case is

$$\mathcal{L} = \bar{t}\gamma^\mu(f_L P_L + f_R P_R)V_\mu\, q^c + h.c., \tag{B10}$$

which gives for the weighted average of the amplitude squared contribution to $q\bar{q} \to t\bar{t}$ scattering

$$\begin{aligned}\overline{\sum}|\mathcal{M}|^2 = \mathcal{C}_1'(|f_L|^4+|f_R|^4)\frac{12s^2}{36u_V^2}\left[\frac{m_t^4}{4m_V^4}\left((1+\beta_\theta)^2+16\frac{m_V^2}{s}\right)+(1-\beta_\theta)^2\right]+\\ +\mathcal{C}_2'2|f_L|^2|f_R|^2\frac{12s^2}{36u_V^2}\left[\frac{m_t^4}{4m_V^4}\left((1+\beta_\theta)^2+16\frac{m_V^2}{s}\right)+4\left(1-2\frac{m_t^2}{s}\right)^2\right].\end{aligned} \tag{B11}$$

The interference with the SM one gluon exchange is

$$\overline{\sum} 2Re(\mathcal{M}\mathcal{M}^*_{SM}) = \frac{-1}{9}\pi\alpha_S \mathcal{C}_3'(|f_L|^2+|f_R|^2)\frac{s}{u_V}\left[(1-\beta_\theta)^2 + 8\frac{m_t^2}{s} + \frac{m_t^2}{m_V^2}(1+\beta_\theta)^2 + 4\frac{m_t^4}{m_V^2 s}\right]. \tag{B12}$$

For the coefficients in these equations we have $\mathcal{C}_1' = \mathcal{C}_2' = 1(1/2)$, $\mathcal{C}_3' = 2(1)$ for $\bar{\mathbf{3}}(\mathbf{6})$ cases, while $f_L = \eta_1 + y_t^2\eta_2$, $f_R = 0$ for model X and $f_L = \eta_1 + y_t^2\eta_2$, $f_R = \eta_1$ for model XI.

For light quark pair production we use the generic form of the interaction Lagrangian (B6), but replace the top quarks with light quarks. We denote by f_q the flavor diagonal coupling of vectors to quarks (these will contribute in the s-channel). The flavor off-diagonal couplings for terms contributing in the t-channel are denoted as $f_{q\,q'}$. In the numerical analysis we set $f_q = f_{qq'}$, which follows from $\mathrm{H_F}$ symmetry.

We examine dijet constraints on three sample models, $\mathrm{II_o}$, VI_s and $\mathrm{VI_o}$. The spin and color averaged amplitudes for $u\bar{u} \to c\bar{c}$ or $c\bar{c} \to u\bar{u}$ processes are

$$\overline{\sum}|\mathcal{M}|^2 = \frac{|f_u f_c|^2}{9}\frac{\mathcal{C}_1 u^2}{s_V^2+\Gamma_V^2 m_V^2} + \frac{2|f_{uc}|^2}{9}\frac{\mathcal{C}_2 f_u f_c(s_V t_V + \Gamma_V^2 m_V^2)}{(s_V^2+\Gamma_V^2 m_V^2)(t_V^2+\Gamma_V^2 m_V^2)}\,u^2 + \frac{|f_{uc}|^4}{9}\frac{\mathcal{C}_3 u^2}{t_V^2+\Gamma_V^2 m_V^2} \tag{B13}$$

and

$$\overline{\sum} 2\mathrm{Re}(\mathcal{M}\mathcal{M}^*_{SM}) = \frac{8\pi\alpha_S}{9}\left(\mathcal{C}_4|f_{uc}|^2\frac{t_V}{t_V^2+\Gamma_V^2 m_V^2} + \mathcal{C}_5\frac{f_u f_c s_V}{s_V^2+\Gamma_V^2 m_V^2}\right)\frac{u^2}{s}, \tag{B14}$$

where $t = -s(1-\cos\theta)/2,\ u = -s(1+\cos\theta)/2$. The C_i's are

$$\mathcal{C}_1 = \frac{1}{18},\quad \mathcal{C}_2 = \frac{1}{18},\quad \mathcal{C}_3 = \frac{1}{2},\quad \mathcal{C}_4 = -\frac{1}{3},\quad \mathcal{C}_5 = -\frac{1}{3} \tag{B15}$$

for model $\mathrm{VI_o}$,

$$\mathcal{C}_1 = \frac{1}{4},\quad \mathcal{C}_2 = -\frac{1}{4},\quad \mathcal{C}_3 = \frac{9}{4},\quad \mathcal{C}_4 = 2,\quad \mathcal{C}_5 = 0\,, \tag{B16}$$

for model $\mathrm{VI_s}$, and

$$\mathcal{C}_1 = 2,\quad \mathcal{C}_2 = 0,\quad \mathcal{C}_3 = 0,\quad \mathcal{C}_4 = 0,\quad \mathcal{C}_5 = 2 \tag{B17}$$

for model $\mathrm{II_o}$.

For the processes $u\bar{u} \to u\bar{u}$ or $c\bar{c} \to c\bar{c}$ the spin and color averaged amplitudes squared are

$$\overline{\sum}|\mathcal{M}|^2 = \frac{f_q^4}{9}u^2\left(\frac{\mathcal{C}_1}{s_V^2+\Gamma_V^2 m_V^2} + 2\,\mathcal{C}_2\,\frac{s_V t_V + \Gamma_V^2 m_V^2}{(s_V^2+\Gamma_V^2 m_V^2)(t_V^2+\Gamma_V^2 m_V^2)} + \frac{\mathcal{C}_3}{t_V^2+\Gamma_V^2 m_V^2}\right) \tag{B18}$$

We have to add new terms to the interference between the NP and SM, because now there is also a t-channel contribution in the SM. The modified equation is

$$\overline{\sum} 2\mathrm{Re}(\mathcal{M}\mathcal{M}^*_{SM}) = \frac{8\pi\alpha_S}{9}\,u^2\,f_q^2\left[\frac{t_V}{t_V^2+\Gamma_V^2 m_V^2}\left(\frac{C_4^s}{s}+\frac{C_4^t}{t}\right) + \frac{s_V}{s_V^2+\Gamma_V^2 m_V^2}\left(\frac{C_5^s}{s}+\frac{C_5^t}{t}\right)\right] \tag{B19}$$

The $\mathcal{C}_i$'s are

$$\mathcal{C}_1 = \frac{2}{9}, \quad \mathcal{C}_2 = -\frac{2}{27}, \quad \mathcal{C}_3 = \frac{2}{9}, \quad \mathcal{C}_4^s = -\frac{2}{9}, \quad \mathcal{C}_4^t = \frac{2}{3}, \quad \mathcal{C}_5^s = \frac{2}{3}, \quad \mathcal{C}_5^t = -\frac{2}{9} \tag{B20}$$

in model $\mathrm{VI_o}$,

$$\mathcal{C}_1 = 1, \quad \mathcal{C}_2 = \frac{1}{3}, \quad \mathcal{C}_3 = 1, \quad \mathcal{C}_4^s = \frac{4}{3}, \quad \mathcal{C}_4^t = 0, \quad \mathcal{C}_5^s = 0, \quad \mathcal{C}_5^t = \frac{4}{3} \tag{B21}$$

in model $\mathrm{VI_s}$, and

$$\mathcal{C}_1 = 2, \quad \mathcal{C}_2 = -\frac{2}{3}, \quad \mathcal{C}_3 = 2, \quad \mathcal{C}_4^s = -\frac{2}{3}, \quad \mathcal{C}_4^t = 2, \quad \mathcal{C}_5^s = 2, \quad \mathcal{C}_5^t = -\frac{2}{3} \tag{B22}$$

for model $\mathrm{II_o}$

Using crossing symmetry, the processes $u\bar{c} \to u\bar{c} + \text{c.c.}$ are obtained from Eqs. (B13), (B14) via the substitutions $s \to t,\ t \to s,\ u \to u$; the processes $uc \to uc + \text{c.c.}$ are obtained from Eqs. (B13), (B14) via the substitutions $s \to t,\ t \to u,\ u \to s$; and the processes $uu \to uu + \text{c.c.}$, $cc \to cc + \text{c.c.}$ are obtained from Eqs. (B18), (B19) via the substitutions $s \to t,\ t \to u,\ u \to s$.

c. LEP $e^+\,e^- \to f\,\bar{f}V$ production

Consider a vector Lagrangian of the form $\mathcal{L} = \eta\, V^\mu\, \bar{\psi}_R\, \gamma_\mu\, \psi_R$. Then the amplitude squared for the production of a color singlet vector V through $e^+\,e^- \to \gamma^\star \to V\bar{f}\,f$ is given by

$$\begin{aligned}\overline{|\mathcal{M}|^2} = -\frac{8e^4Q^2N_c|\eta|^2}{s_1^2 s_2^2}\Bigg[&\frac{1}{s^2}\left(2m_v^2(s_1s_2 - s_1t_1 - s_2t_2)^2\right) \\ &- \frac{1}{s}\Bigg(2s_1s_2m_v^4 - 2(s_1+s_2)(s_1t_1+s_2t_2)m_v^2 + s_1s_2\big({s_1}^2 - 2t_2s_1 + {s_2}^2 - 2s_2t_1 + 2({t_1}^2+{t_2}^2)\big)\Bigg) \\ &+ m_v^2(s_1-s_2)^2 + 2s_1s_2(s_1+s_2-t_1-t_2) - 2ss_1s_2\Bigg].\end{aligned} \tag{B23}$$

Here we have used the three body final state Mandelstam variables using the notation of [141], with the momenta assignments $e^-(p_a), e^+(p_b), \bar{f}(p_1), V(p_2), f(p_3)$ and e is the electromagnetic coupling constant while Q is the charge of a particular quark. The corresponding production cross section at LEP is given by

$$\sigma(e^+\,e^- \to \gamma^\star \to V\bar{f}\,f) = \frac{1}{2^{10}\pi^4 s^2}\int \frac{ds_1\,ds_2\,dt_1\,dt_2\,\overline{|\mathcal{M}|}^2\,\theta\left[-\mathcal{G}\right]}{\sqrt{-\mathcal{G}}}, \tag{B24}$$

where the physical region that determines the integration range satisfies the condition that the Gram determinant $\mathcal{G} \leq 0$. The Gram determinant for the $2 \to 3$ production is explicitly given by

$$\begin{aligned}\mathcal{G} \;=\; &\frac{1}{16}\left[m_v^4 s^2 - 2m_v^2 s(s\,t_1 + s\,t_2 + s_1(s_2-t_1) - s_2t_2 + 2t_1t_2)\right. \\ &\left.+2s_1(s(s_2(t_1+t_2)+t_1(t_2-t_1)) + s_2t_2(t_1-s_2)) + (s(t_1-t_2)+s_2t_2)^2 + s_1^2(s_2-t_1)^2\right].\end{aligned} \tag{B25}$$

d. LHC $gg \to SS$ production

For a field in a flavor representation F, and color representation R, the cross section for $g\,g \to S\,S$ is

$$\frac{d\sigma}{dt} = \frac{\dim(F)\,\pi\,\alpha_s^2}{8^2\,s^2}\left[C_1\,F_1 + C_2\,F_2 + C_3\,F_3 + C_4\,F_4\right]. \tag{B26}$$

Here the functions F_i are

$$\begin{aligned}
F_1 &= 2 + \frac{s-2\,m_s^2}{t-m_s^2} + \frac{s-2\,m_s^2}{u-m_s^2},\\
F_2 &= \frac{(u-t)^2}{2\,s^2} + \left[\frac{(m_s^2-u)(4m_s^2-s) + (t-u)(s-2m_s^2)/2}{s(t-m_s^2)} + u \leftrightarrow t\right],\\
F_3 &= 4\,m_s^4\left(\frac{1}{(t-m_s^2)^2} + \frac{1}{(u-m_s^2)^2}\right),\\
F_4 &= \frac{2(s-2m_s^2)^2}{(u-m_s^2)(t-m_s^2)}.
\end{aligned} \tag{B27}$$

The color factors, for the $R = (\mathbf{3}, \mathbf{6}, \mathbf{8})$ representations ($G = \mathbf{8}$) are

$$\begin{aligned}
C_1 &= C(R)\dim(G)(2C_2(R) - C_2(G)/2) = (14/3, 310/3, 108),\\
C_2 &= C(R)C_2(G)\dim(G) = (12, 60, 72),\\
C_3 &= [C_2(R)]^2\dim(R) = (16/3, 200/3, 72),\\
C_4 &= C(R)\dim(G)(C_2(R) - C_2(G)/2) = (-2/3, 110/3, 36).
\end{aligned} \tag{B28}$$

Appendix C: Low Energy Constraints

The main motivation for studying flavor symmetric extensions of the SM is to have an effective way of suppressing FCNCs allowing new states of fairly low mass. In this appendix we give a brief account of the constraints on our models from low energy data. We focus on processes that can be very restrictive, $K - \bar{K}$, $B_{s,d} - \bar{B}_{s,d}$ and $D - \bar{D}$ mixing.

The effective weak Hamiltonian describing the $B_s - \bar{B}_s$ mixing in the SM is

$$\mathcal{H}_{\rm eff}^{\rm SM} = \eta_W \eta_{RG} \frac{\left(V_{ts}^* V_{tb}\right)^2}{\Lambda_{SM}^2} \left(\bar{s}_L \gamma^\mu b_L\right)^2, \tag{C1}$$

where

$$\Lambda_{SM} = \frac{2\pi}{G_F m_W \sqrt{S_0(x_t)}} = 4.39\ \text{TeV}. \tag{C2}$$

This is larger than m_W by an order of magnitude because SM contribution arises at one loop level from box diagrams with t and W exchanges. The factor η_W encodes the QCD corrections to the matching at the hard

scale $\mu_W \sim m_W$, while η_{RG} is the correction due to the running from μ_W to μ_b. In NDR at NLO they are $\eta_W = 0.970$, $\eta_{RG} = 0.860$ (using $\alpha_S(m_z) = 0.1184$, $\mu_W = m_W$, $\mu_b = m_b = 4.2$ GeV and $\bar{m}_t = 164$ GeV for which $S_0(x_t) = 2.33$). The SM weak hamiltonians for the $B_d - \bar{B}_D$, $K - \bar{K}$ and $D - \bar{D}$ mixing follow from (C1) with the obvious replacements in quark flavors. In addition K and D mixing amplitudes receive large nonlocal contributions in the SM.

NP contributions can modify the effective weak Hamiltonian to $\mathcal{H}_{\rm eff}^{\rm SM} + \Delta\mathcal{H}_{\rm eff}^{\rm NP}$. To make the comparison with the experiment easier we normalize the NP contributions to the SM predictions. For $B_{s,d}$ mixing we thus define

$$h_{s,d} e^{i2\sigma_{s,d}} \equiv \frac{\langle B_{s,d}|\Delta\mathcal{H}_{\rm eff}^{\rm NP}|\bar{B}_{s,d}\rangle}{\langle B_{s,d}|\mathcal{H}_{\rm eff}^{SM}|\bar{B}_{s,d}\rangle}. \tag{C3}$$

Note that $\sigma_{s,d}$ measures the deviation of NP weak phase from the SM one (for B_s mixing the SM weak phase is very small, $O(1^\circ)$, while for B_d mixing it is $2\beta \sim 45^\circ$). Since the (real part) of $\langle K^0|\mathcal{H}_{\rm eff}^{SM}|\bar{K}^0\rangle$ receives potentially large long distance contributions from $\Delta S = 1$ operators, we normalize the NP matrix elements to the measured mass difference

$$h_K e^{i2\sigma_K} \equiv \frac{M_{12}^{NP}}{\Delta m_K} = \frac{1}{\Delta m_K} \cdot \frac{\langle K^0|\Delta\mathcal{H}_{\rm eff}^{\rm NP}|\bar{K}^0\rangle}{2m_K}. \tag{C4}$$

Similarly there are potentially large long distance effects in $D - \bar{D}$ mixing amplitude, so that we define in the same way

$$h_D e^{i2\sigma_D} \equiv \frac{M_{12}^{NP}}{\Delta m_D} = \frac{1}{\Delta m_D} \cdot \frac{\langle D^0|\Delta\mathcal{H}_{\rm eff}^{\rm NP}|\bar{D}^0\rangle}{2m_D}. \tag{C5}$$

Note that σ_K and σ_D measure the *total* weak phase of the NP contributions to the mixing, not just the deviation from the SM one. No NP in the mixing corresponds to $h_s = h_d = k_K = h_D = 0$.

From the agreement of measured and predicted values of ϵ_K we obtain the bound at 95% C.L.

$$|h_K \sin(2\sigma_K)| \lesssim 1.3 \times 10^{-3}. \tag{C6}$$

Conservatively we use the the prediction $|\epsilon_K| = (2.01^{+0.59}_{-0.66}) \cdot 10^{-3}$ from [122], which is in good agreement with the measured value $|\epsilon_K| = (2.229 \pm 0.010) \cdot 10^{-3}$ (for a different treatment of lattice inputs see [140]). The bound on $h_K \cos 2\sigma_K$ is more uncertain because of potentially large long distance contributions. Assuming conservatively that Δm_K is saturated by NP gives $|h_K \cos 2\sigma_K| \lesssim 0.5$. The CP violation in $D - \bar{D}$ mixing is well constrained and so $|h_D \sin(2\sigma_D)| \lesssim 0.3$, at 95 % C.L. [142] (the NP contribution to ϕ_{12}^D is $2\sigma_D$, while the SM CP violating contribution is negligible). Conservatively assuming that NP saturates the mass difference Δm_D we obtain $h_D \lesssim 0.5$.

The NP contributions to the effective weak Hamiltonian in (C1), $\Delta\mathcal{H}_{\rm eff}^{\rm NP}$, are described by local operators

$$\Delta\mathcal{H}_{\rm eff}^{\rm NP} = \sum_i C_i Q_i + \sum_i \tilde{C}_i \tilde{Q}_i \tag{C7}$$

where the sum runs over the full set of dimension 6 local operators. For B_s mixing these are [143]

$$Q_1 = (\bar{s}_L\gamma_\mu b_L)(\bar{s}_L\gamma_\mu b_L), \qquad Q_{2,4} = (\bar{s}_R b_L)(\bar{s}_{R,L} b_{L,R}), \qquad Q_{3,5} = (\bar{s}_R^\alpha b_L^\beta)(\bar{s}_{R,L}^\beta b_{L,R}^\alpha), \tag{C8}$$

Above $P_{L,R} = (1 \pm \gamma_5)/2$, while color indices are not displayed, if the summation is within brackets. The operators $\tilde{Q}_i$ are obtained from Eq. (C8) by making a $P_R \leftrightarrow P_L$ replacement. Note that Q_1 is the operator in the SM effective weak Hamiltonian Eq. (C1).

The SM and NP weak hamiltonians for the B_d, K and D mixing follow from (C1) and (C8) with the obvious replacements in quark flavors. In addition K and D mixing amplitudes receive large nonlocal contributions in the SM. We evaluate the matrix elements for the operators Q_i in the same way as described in Eqs. (8)-(10) of [143], including the numerical values, except for the updated values of $f_{B_d} = 205 \pm 12$ MeV, $f_{B_s} = 250 \pm 12$ MeV [144] and the quark masses, for which we use the PDG 2010 values $\beta = (21.8 \pm 0.9)^\circ$ and $\gamma = (67 \pm 4)^\circ$ [145]. The matrix elements for $\tilde{Q}_i$ are the same as for Q_i since QCD interactions are parity conserving.

1. Models I-IX

The models I-IX give contributions to the effective Hamiltonian for B_s mixing that at scale $\mu = m_b$ take the form

$$\Delta\mathcal{H}_{\rm eff}^{{\rm NP},B_s} = \frac{\kappa_s}{M_V^2}(y_t^2 V_{tb}V_{ts}^*)^2 \eta' \eta_{RG} \left[\bar{b}_L\gamma^\mu s_L \; \bar{b}_L\gamma_\mu s_L\right], \tag{C9}$$

or of its parity image: replacing $\bar{b}_R\gamma^\mu s_R \; \bar{b}_R\gamma_\mu s_R$ for $\bar{b}_L\gamma^\mu s_L \; \bar{b}_L\gamma_\mu s_L$. Parity symmetry of the strong interactions implies that these operators have identical matrix elements between one particle states. The value of model dependent constant κ_s is listed in Table VIII, while M_V stands for the average mass of the MFV-vector exchanged. The factor η' is a QCD correction that arises from running from the scale of the new physics, M_V, to the electroweak scale, M_W. In calculating bounds we set $\eta' = 1$ incurring an error of order $[\alpha_S(M_W)/4\pi]\ln(M_V/M_W) \approx 0.01\ln(M_V/M_W)$.

The contributions to B_d, D and K mixing we define analogously (for simplicity of notation setting $\eta'\eta_{RG} = 1$),

$$\Delta\mathcal{H}_{\rm eff}^{{\rm NP},B_d} = \frac{\kappa_d}{M_V^2}(y_t^2 V_{tb}V_{td}^*)^2(\bar{d}_L\gamma^\mu b_L)^2, \qquad \Delta\mathcal{H}_{\rm eff}^{{\rm NP},K} = \frac{\kappa_K}{M_V^2}(y_t^2 V_{ts}V_{td}^*)^2(\bar{d}_L\gamma^\mu s_L)^2, \tag{C10}$$

$$\Delta\mathcal{H}_{\rm eff}^{{\rm NP},D} = \frac{\kappa_D}{M_V^2}(y_b^2 V_{ub}^* V_{cb})^2(\bar{c}_L\gamma^\mu u_L)^2. \tag{C11}$$

Case	$\Delta\mathcal{L}$		
	$\kappa_{s,d}/C_{s,o}$	$\kappa_K/C_{s,o}$	$\kappa_D/C_{s,o}$
$\mathrm{I}_{\mathrm{s,o}}$	$\eta_1\,\bar{d}_R(\not{V}Y_D\Delta_U Y_D^\dagger)d_R+\left[\eta_2\,\bar{d}_R(\not{V}Y_D\Delta_U\Delta_D Y_D^\dagger)d_R+h.c.\right]$		
	$y_{s,d}^2y_b^2(\eta_1+\eta_2y_b^2)^2$	$y_d^2y_s^2(\eta_1+\eta_2y_b^2)^2$	0
$\mathrm{II}_{\mathrm{s,o}}$	$\eta_1\,\bar{u}_R(\not{V}Y_U\Delta_D Y_U^\dagger)u_R+\left[\eta_2\,\bar{u}_R(\not{V}Y_U\Delta_U\Delta_D Y_U^\dagger)u_R+h.c.\right]$		
	0	0	$y_u^2y_c^2(\eta_1+\eta_2y_c^2)^2$
$\mathrm{III}_{\mathrm{s,o}}$	$\eta_1\bar{Q}_L(\not{V}\Delta_U)Q_L+\eta_1'\bar{Q}_L(\not{V}\Delta_D)Q_L+\left[\eta_2\bar{Q}_L(\not{V}\Delta_U\Delta_D)Q_L+h.c.\right]$		
	$\left(\eta_1+\eta_2y_b^2\right)^2$	η_1^2	$\eta_1'^2$
$\mathrm{IV}_{\mathrm{s,o}}$	$\eta_0\bar{Q}_L\not{V}Q_L+\eta_1\bar{Q}_L(\not{V}\Delta_U)Q_L+\eta_1'\bar{Q}_L(\not{V}\Delta_D)Q_L+\left[\eta_2\bar{Q}_L(\not{V}\Delta_U\Delta_D)Q_L+h.c.\right]$		
	$\left(\eta_1+\eta_2y_b^2\right)^2+\Delta_{CC}$	$\eta_1^2+\Delta_{CC}$	$\eta_1'^2+\Delta_{CC}$
$\mathrm{V}_{\mathrm{s,o}}$	$\eta_1\bar{d}_R\not{V}d_R+\left[\eta_2\bar{d}_R\not{V}\left(Y_D\Delta_U Y_D^\dagger\right)d_R+h.c.\right]+\eta_3\bar{d}_R\left(Y_D\Delta_U Y_D^\dagger\right)\not{V}\left(Y_D\Delta_U Y_D^\dagger\right)d_R$		
	$y_{s,d}^2y_b^2\left[\frac{\eta_2^2}{4r_3^2}+\frac{(\eta_2-2\eta_2^*)^2}{12r_8^2}+\frac{\eta_1\eta_3}{r_{6,4}^2}\right]$	$y_d^2y_s^2\left[\frac{(\eta_2-\eta_2^*)^2}{4r_3^2}+\frac{(\eta_2+\eta_2^*)^2}{12r_8^2}+\frac{\eta_1\eta_3}{r_1^2}\right]$	0
$\mathrm{VI}_{\mathrm{s,o}}$	$\eta_1\bar{u}_R\not{V}u_R+\left[\eta_2\bar{u}_R\not{V}\left(Y_U\Delta_D Y_U^\dagger\right)u_R+h.c.\right]+\eta_3\bar{u}_R\left(Y_U\Delta_D Y_U^\dagger\right)\not{V}\left(Y_U\Delta_D Y_U^\dagger\right)u_R$		
	0	0	$y_u^2y_c^2\left[\frac{(\eta_2^*-\eta_2)^2}{4r_3^2}+\frac{(\eta_2+\eta_2^*)^2}{12r_8^2}+\frac{\eta_1\eta_3}{r_1^2}\right]$
$\mathrm{VII}_{\mathrm{s,o}}$	$\eta_1\,\bar{d}_R\not{V}u_R+\eta_2\,\bar{d}_R(Y_D\Delta_U Y_D^\dagger)\not{V}u_R+\mathrm{h.c.}$		
	Δ_{CC}	Δ_{CC}	Δ_{CC}
$\mathrm{VIII}_{\mathrm{s,o}}$	$\eta_1\bar{Q}_L\not{V}Q_L+[\eta_2\bar{Q}_L\Delta_U\not{V}Q_L+\eta_2'\bar{Q}_L\Delta_D\not{V}Q_L+h.c.]+\eta_3\bar{Q}_L\Delta_U\not{V}\Delta_UQ_L+\eta_3'\bar{Q}_L\Delta_D\not{V}\Delta_DQ_L$		
	$\frac{\eta_2^{*2}}{4r_3^2}+\frac{(\eta_2^*-2\eta_2)^2}{12r_8^2}+\frac{\eta_1\eta_3}{r_{6,4}^2}$	$\frac{(\eta_2^*-\eta_2)^2}{4r_3^2}+\frac{(\eta_2+\eta_2^*)^2}{12r_8^2}+\frac{\eta_1\eta_3}{r_1^2}$	$\frac{(\eta_2'-\eta_2'^*)^2}{4r_3^2}+\frac{(\eta_2'+\eta_2'^*)^2}{12r_8^2}+\frac{\eta_1\eta_3'}{r_1^2}$
$\mathrm{IX}_{\mathrm{s,o}}$	$\eta_1\bar{Q}_L\not{V}Q_L+[\eta_2\bar{Q}_L\Delta_U\not{V}Q_L+\eta_2'\bar{Q}_L\Delta_D\not{V}Q_L+h.c.]+\cdots$		
	$\frac{\eta_2^{*2}}{4r_3^2}+\frac{(\eta_2^*-2\eta_2)^2}{12r_8^2}+\Delta_{CC}$	$\frac{(\eta_2^*-\eta_2)^2}{4r_3^2}+\frac{(\eta_2+\eta_2^*)^2}{12r_8^2}+\Delta_{CC}$	$\frac{(\eta_2'-\eta_2'^*)^2}{4r_3^2}+\frac{(\eta_2'+\eta_2'^*)^2}{12r_8^2}+\Delta_{CC}$

TABLE VIII: The part of interaction Lagrangian $\Delta\mathcal{L}$ relevant for meson mixing amplitudes and coefficients κ_i in (C9)-(C11) for each of the models I-IX. We use the abbreviations $\Delta_U=Y_U^\dagger Y_U$, $\Delta_D=Y_D^\dagger Y_D$ and $r_i=m_{V_i}/m_V$ for the ratios of vector meson masses in the flavor multiplet to the average vector meson mass m_V, while Δ_{CC} stands for a 1-loop contribution, a box diagram, from exchange of charged MFV-vectors; see text. The factors of $C_s=1(C_o=\frac{1}{3})$ must be included for color singlet (octet) vectors. Due to lack of space we display for model IX results only for leading complex parameters (the undisplayed leading real terms are the same as for model VIII).

The coefficients $\kappa_{s,d,K,D}$ are collected in Table VIII. In models V, VIII and IX several vector fields mediate mixing and we indicate their separate contributions. This requires we distinguish among their masses , with M_V then denoting their average mass in the defining formulae (C9)-(C11) for κ_i.

Numerically, for $B_{d,s}$ mixing contributions we have

$$h_{d,s}e^{2i\sigma_{d,s}} = \kappa_{d,s}y_t^4\frac{\eta'}{\eta_W}\frac{\Lambda_{SM}^2}{M_V^2} \approx 20\times\kappa_{d,s}y_t^4\left(\frac{1\text{ TeV}}{M_V}\right)^2. \tag{C12}$$

The contribution to the K mixing is

$$h_K e^{i2\sigma_K} = \kappa_K y_t^4 (V_{ts}V_{td}^*)^2\frac{m_K}{3\Delta m_K}\frac{f_K^2\hat{B}_K}{m_V^2} \approx 0.1\times\kappa_K e^{i2\beta}y_t^4\left(\frac{1\text{ TeV}}{M_V}\right)^2, \tag{C13}$$

and for the D mixing

$$h_D e^{i2\sigma_D} = \kappa_D y_b^4 (V_{ub}^*V_{cb})^2\frac{m_D}{3\Delta m_D}\frac{f_D^2 B_1^D}{m_V^2} \approx (0.3\cdot 10^{-2})\times\kappa_D e^{i2\gamma}y_b^4\left(\frac{1\text{ TeV}}{M_V}\right)^2. \tag{C14}$$

In the numerics above we use $f_K = 156$ MeV, $\hat{B}_K = 0.79$ [143], $B_1^D = 0.865$ [143], the averages of CKM elements from CKMfitter ICHEP2010 update [145]. The standard CKM unitarity triangle angles have the values $\beta = (21.8\pm 0.9)^\circ$ and $\gamma = (67.2\pm 3.9)^\circ$. We have also included the effect of running from electroweak scale to m_D for $D-\bar{D}$ mixing, however, this is numerically unimportant and results in a percent level shift in h_D.

The flavor constraints thus require that (for $M_V = 1$ TeV) the κ_i coefficients for the particular model are below $\kappa_d \lesssim 0.02$, $\kappa_K \lesssim 10^{-2}$ (unless the phase of κ_K is finely tuned not to give a contribution to ϵ_K), and $\kappa_D \lesssim 20$. In order to explain the hint for nonzero phase of B_s mixing, on the other hand, requires $h_s \sim 0.02$ or $h_s \sim 0.1$ for the two solutions, with appropriate weak phases.

We make the following observations regarding models I-IX:

- We can group the models into two categories. The first category form "universal" models, where the contributions to the mixing amplitudes are due to class-1 operators in the notation of [13]. For universal models we have

  $$\kappa_s = \kappa_d \simeq \kappa_K \sim \kappa_D, \tag{C15}$$

  where the last approximate equalities are valid, if all the couplings η_i are of the same size. In addition in $y_b \to 0$ limit $\kappa_{s,d} = \kappa_K$.

- The second category form the "Yukawa suppressed" models, where the contributions to the mixing come from operators with additional Yukawa suppression (the so-called class-2 operators in the notation of [13]). These are the models $\text{II}_{\text{s,o}}$, $\text{VI}_{\text{s,o}}$, that contribute only to $D-\bar{D}$ mixing and the models $\text{I}_{\text{s,o}}$, $\text{V}_{\text{s,o}}$, for which

  $$\kappa_d : \kappa_s : \kappa_K = y_d^2 : y_s^2 : \frac{y_s^2 y_d^2}{y_b^2}, \tag{C16}$$

  (the relation to κ_K is only approximate for model V).

- Universal models can require small values for $\eta_i \sim 0.1 \cdot (M_V/1\ \mathrm{TeV})$ in order to avoid $K - \bar{K}$ and $B_d - \bar{B}_d$ mixing constraints. This is an order of magnitude smaller then the flavor-conserving couplings typically required to obtain large $A_{FB}^{t\bar{t}}$. This by itself is not a problem as the flavor violating couplings could be loop suppressed.

- Yukawa suppressed models have no problems satisfying FCNC bounds. The typical sizes of contributions to h_i are

$$h_s e^{i2\sigma_s} \simeq 0.09 \times y_t^4 \frac{\kappa_s}{y_s^2} \left(\frac{y_s}{0.02}\right)^2 \left(\frac{0.3\ \mathrm{TeV}}{m_V}\right)^2, \tag{C17}$$

$$h_d e^{i2\sigma_d} \simeq (2 \cdot 10^{-4}) \times y_t^4 \frac{\kappa_d}{y_d^2} \left(\frac{y_d}{10^{-3}}\right)^2 \left(\frac{0.3\ \mathrm{TeV}}{m_V}\right)^2, \tag{C18}$$

$$h_K e^{i2\sigma_K} \simeq (5 \cdot 10^{-10}) \times y_t^4 \frac{\kappa_K}{y_d^2 y_s^2} \left(\frac{y_d}{10^{-3}}\right)^2 \left(\frac{y_s}{0.02}\right)^2 \left(\frac{0.3\ \mathrm{TeV}}{m_V}\right)^2, \tag{C19}$$

$$h_D e^{i2\sigma_D} \simeq (8 \cdot 10^{-16}) \times y_b^4 \frac{\kappa_D}{y_u^2 y_c^2} \left(\frac{y_u}{10^{-5}}\right)^2 \left(\frac{y_c}{5 \cdot 10^{-3}}\right)^2 \left(\frac{0.3\ \mathrm{TeV}}{m_V}\right)^2, \tag{C20}$$

  where we have normalized $y_{s,d}$ to values typical for large $\tan\beta$ ($y_b \sim 1$). The contributions to B_d, K and D mixing are completely negligible for these models.

- Yukawa suppressed models $\mathrm{I_{s,o}}$, $\mathrm{V_{s,o}}$ can potentially explain B_s mixing anomaly, if $y_b \sim \mathcal{O}(1)$ and $\eta_i \sim \mathcal{O}(1)$, while vectors need to have electroweak scale masses of no more than a few 100 GeV. For this a flavor diagonal weak phase is needed [92]. A flavor diagonal weak phase arises if the coefficients η_i are complex. For models I-VI the coefficients can be real only for terms that are higher order in Yukawas and therefore non-hermitian: $\eta_{0,1,3}$ and η_1' are all real, while η_2 can be complex. In models $\mathrm{VII_{s,o}}$ all η_i can be complex. In models V, VIII and IX the contributions to the mixing carry a weak phase only if the vector mesons are not degenerate.

Finally, in models IV, VII and IX we include a contribution Δ_{CC} from charged vectors that produce mixing through a 1-loop box diagram, much like in the standard model. For example, for model $\mathrm{IV_s}$ we find for the contribution to B_s, B_d and K mixing

$$\Delta_{\mathrm{CC}} = \frac{1}{128\pi^2} \frac{\eta_0^4}{y_t^4} S_0(x_{tV})\,, \tag{C21}$$

where $x_{tV} = (m_t/M_V)^2$ and [146]

$$S_0(x) = x\left[\frac{1}{4} + \frac{9}{4}\frac{1}{1-x} - \frac{3}{2}\frac{1}{(1-x)^2}\right] - \frac{3}{2}\left(\frac{x}{1-x}\right)^3 \ln(x)\,. \tag{C22}$$

For model $\mathrm{VII_s}$ the B_s mixing contribution is

$$\Delta_{\mathrm{CC}} = \frac{1}{64\pi^2}(y_b y_s)^2 S_0(x_{tV}) \left[|\eta_1\eta_2|^2 + \mathrm{Re}(\eta_1^*\eta_2)^2\right]\,, \tag{C23}$$

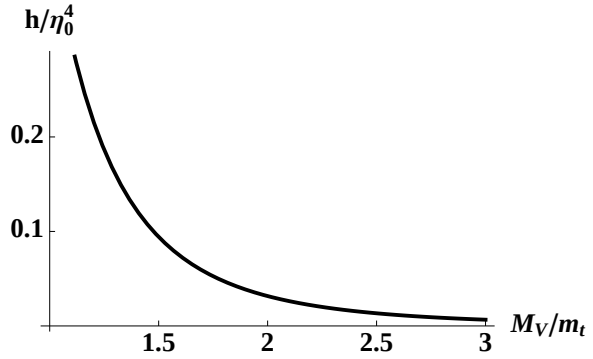

FIG. 14: Correction h, in units of η_0^4, to BB mixing in Model $\mathrm{IV_s}$ from double exchange of charged currents as a function of vector mass in units of top mass.

while the B_d and K mixing contributions are obtained through the replacements $y_s \to y_d$ and $y_b \to y_d$, respectively. Above, we have assumed degenerate MFV-vectors for simplicity. For $\mathrm{IV_o}$ and $\mathrm{VII_o}$ insert an additional factor of $11/6$ in these formulae. Fig. 14 shows the correction $h = h_s = h_d$ in model $\mathrm{IV_s}$ resulting only from Δ_{CC}, as a function of the top to charged vector mass ratio m_t/M_V. The figure is for $\eta_0 = 1$, but can easily be rescaled as indicated. The bound $h < 0.2$ gives $M_V > 200$ GeV (using $m_t = 164$ GeV) for $\eta_0 = 1$, increasing to $M_V > 420$ GeV for $\eta_0 = 2$. In estimating this effect we have assumed the box diagram for these vectors is precisely as for the case of W's in the SM, because the GIM mechanism renders the diagram finite even in unitary gauge.

In the $D - \bar{D}$ case, in contrast to the $B - \bar{B}$ case, the long distance contribution is believed to dominate the double charge current exchange amplitude. Since this is not computable, we settle for estimating Δ_{CC} by comparing the perturbative box diagram to the corresponding one in the SM. Since all internal quarks are light the computation simplifies: for example, in model $\mathrm{IV_s}$ the ratio is

$$\frac{\mathrm{NP_{Box}}}{\mathrm{SM_{Box}}} = \left(\frac{\eta_0}{g_2}\right)^4 \left(\frac{M_W}{M_V}\right)^4 \approx \left(\frac{190\eta_0}{M_V(\mathrm{GeV})}\right)^4 , \tag{C24}$$

so that, for example, the new physics is a factor of 10 suppressed relative the SM for $M_V/\eta_0 \gtrsim 340$ GeV.

2. Models X and XI

The vector models give a contribution to the effective Hamiltonian for B_s mixing that at the scale $\mu \sim m_V$ takes the form

$$\Delta\mathcal{H}_{\mathrm{eff}}^{\mathrm{NP},B_s} = \frac{2\kappa_s}{M_V^2}(y_t^2 V_{tb}V_{ts}^*)^2\,(Q_4 - Q_5)\,, \tag{C25}$$

where the operators $Q_{4,5}$ are given in (C8). The contributions to B_d, K and D mixing are defined in the same way, with appropriate replacement of the CKM factors and quark fields, as in (C10), (C11). The above

Case	$\Delta\mathcal{L}$		
	$\kappa_{s,d}$	κ_K	κ_D
$X_{\bar{3},6}$	$\eta_1 \bar{d}_R \not{V} Q_L^c + \eta_2 \bar{d}_R \not{V} \Delta_U^* Q_L^c + \eta_3 \bar{d}_R (Y_D \Delta_U Y_D^\dagger) \not{V} Q_L^c + \eta_4 \bar{d}_R (Y_D \Delta_U Y_D^\dagger) \not{V} \Delta_U^* Q_L^c + h.c.$		
	$y_{s,d}\, y_b \left[\frac{\eta_1 \eta_4^*}{r_{ii}^2} + \frac{\tilde{\eta}_1^* \eta_4}{r_{33}^2} + \frac{\eta_2 \tilde{\eta}_3^*}{r_{i3}} + \frac{\tilde{\eta}_2^* \eta_3}{r_{3i}} \right]$	$y_s\, y_d \left[\frac{\eta_1 \eta_4^* + 2\Re \eta_2 \eta_3^*}{r_{ii}^2} + \frac{\tilde{\eta}_1^* \eta_4}{r_{33}^2} \right]$	0
$XI_{\bar{3},6}$	$\eta_1 \bar{u}_R \not{V} Q_L^c + \eta_2 \bar{u}_R \not{V} \Delta_D^* Q_L^c + \eta_3 \bar{u}_R (Y_U \Delta_D Y_U^\dagger) \not{V} Q_L^c + \eta_4 \bar{u}_R (Y_U \Delta_D Y_U^\dagger) \not{V} \Delta_D^* Q_L^c + h.c.$		
	0	0	$y_u\, y_c \left[\frac{\eta_1^* \eta_4 + 2\Re \eta_2 \eta_3^*}{r_{ii}^2} + \frac{\tilde{\eta}_1' \eta_4^*}{r_{33}^2} \right]$

TABLE IX: The same as Table VIII, but for models X and XI. We further defined $\tilde{\eta}_1 = \eta_1 + \eta_2 y_t^2 + \eta_3 y_t^2 y_b^2 + \eta_4 y_t^4 y_b^2$, $\tilde{\eta}_2 = \eta_2 + \eta_4 y_t^2$, $\tilde{\eta}_3 = \eta_3 + \eta_4 y_t^2$, and $\tilde{\eta}_1' = \eta_1 + \eta_2 y_b^2 + \eta_3 y_b^2 y_t^2 + \eta_4 y_b^4 y_t^2$. The results are written in the limit of degenerate vectors mediating transitions between the first two generations. Above the index i stands for $i = 1, 2$.

expression is for color triplets, $X_{\bar{3}}, XI_{\bar{3}}$. The result for color sextets, X_6, XI_6, is obtained with a replacement $(Q_4 - Q_5) \to -(Q_4 + Q_5)/2$. The factors κ_i are collected in Table IX.

To obtain the low energy predictions, we include the RG running using the equations and numerical values for the matrix elements given in [143]. As before, we use the updated values of CKM elements from CKMFitter, ICHEP2010 update [145]. We obtain

$$h_s e^{i2\sigma_s} \simeq 1.7(-2.1) \times y_t^4 \frac{\kappa_s}{y_s} \left(\frac{y_s}{0.02} \right) \left(\frac{1\ \text{TeV}}{m_V} \right)^2, \tag{C26}$$

$$h_d e^{i2\sigma_d} \simeq 0.09(-0.11) \times y_t^4 \frac{\kappa_d}{y_d} \left(\frac{y_d}{10^{-3}} \right) \left(\frac{1\ \text{TeV}}{m_V} \right)^2, \tag{C27}$$

$$h_K e^{i2\sigma_K} \simeq 5(-4) \cdot 10^{-3} \times e^{i2\beta} y_t^4 \frac{\kappa_K}{y_d y_s} \left(\frac{y_s}{0.02} \right) \left(\frac{y_d}{10^{-3}} \right) \left(\frac{1\ \text{TeV}}{m_V} \right)^2, \tag{C28}$$

$$h_D e^{i2\sigma_D} \simeq 1.4(-1.5) \cdot 10^{-8} \times e^{i2\gamma} y_b^4 \frac{\kappa_D}{y_u y_c} \left(\frac{y_u}{10^{-5}} \right) \left(\frac{y_c}{5 \cdot 10^{-3}} \right) \left(\frac{1\ \text{TeV}}{m_V} \right)^2, \tag{C29}$$

where the first values are for color triplet models and in the brackets for the color sextet models.

We make the following observations:

- Models X and XI are of the "Yukawa suppressed" category, but the class-2 operators that they give rise to are linear in y_s, y_d suppression, which is quite atypical. Commonly the suppression in class-2 operators is quadratic in light Yukawas. The ratios of κ_i for models X are

$$\kappa_d : \kappa_s : \kappa_K = y_d : y_s : \frac{y_s y_d}{y_b}, \tag{C30}$$

  where the ratio with κ_K is only approximate.

- Models $X_{\bar{3},6}$ offer the possibility to explain $A_{FB}^{t\bar{t}}$ and B_s mixing anomaly at the same time, if flavor violating couplings η_i are a factor few smaller than the corresponding couplings in the flavor conserving part of the Lagrangian.

3. Models S_{I-IV}

The models S_{I-IV} give contributions to B_s mixing of the form

$$\Delta\mathcal{H}_{\rm eff}^{{\rm NP},B_s} = -\frac{\kappa_s}{M_S^2}(y_t^2 V_{tb}V_{ts}^*)^2 Q_4, \tag{C31}$$

where the operators $Q_{4,5}$ are given in (C8). The contributions to B_d, K and D mixing are defined in the same way, with appropriate replacement of the CKM factors and quark fields, as in (C10), (C11). The above expression is for models S_I and S_{III}, while for models S_{II} and S_{IV} the result is obtained with a replacement $Q_4 \to -Q_4/6 + Q_5/2$. The factors κ_i are collected in Table X. Numerically these models are very similar to the MFV models X and XI,

$$-h_s e^{i2\sigma_s} \simeq 1.5(0.05) \times y_t^4 \frac{\kappa_s}{y_s}\left(\frac{y_s}{0.02}\right)\left(\frac{1\ {\rm TeV}}{m_S}\right)^2, \tag{C32}$$

$$-h_d e^{i2\sigma_d} \simeq 7(0.3)\cdot 10^{-2} \times y_t^4 \frac{\kappa_d}{y_d}\left(\frac{y_d}{10^{-3}}\right)\left(\frac{1\ {\rm TeV}}{m_S}\right)^2, \tag{C33}$$

$$-h_K e^{i2\sigma_K} \simeq 3.6(-0.1)\cdot 10^{-3} \times e^{i2\beta} y_t^4 \frac{\kappa_K}{y_d y_s}\left(\frac{y_s}{0.02}\right)\left(\frac{y_d}{10^{-3}}\right)\left(\frac{1\ {\rm TeV}}{m_S}\right)^2, \tag{C34}$$

$$-h_D e^{i2\sigma_D} \simeq 1.1(0.01)\cdot 10^{-8} \times e^{i2\gamma} y_b^4 \frac{\kappa_D}{y_u y_c}\left(\frac{y_u}{10^{-5}}\right)\left(\frac{y_c}{5\cdot 10^{-3}}\right)\left(\frac{1\ {\rm TeV}}{m_S}\right)^2, \tag{C35}$$

where the values in the brackets are for the models S_{II} and S_{IV}, for which numerical cancellation between the matrix elements of the two operators occurs.

4. Models S_{V-XIV}

Of the remaining models only models $S_{VI,VIII,XIV}$ lead to tree level FCNCs. The models $S_{V,VII,IX,XI}$ and S_{XIII} do not lead to tree level FCNCs because of its color triplet structure (and thus antisymmetric contraction of indices). The models S_X and S_{XII} lead to charge currents and thus give FCNCs at loop level only.

We next focus on the models that lead to FCNCs at tree level. They give contributions to B_s mixing of the form

$$\Delta\mathcal{H}_{\rm eff}^{{\rm NP},B_s} = -\frac{4\kappa_s}{M_S^2}(y_t^2 V_{tb}V_{ts}^*)^2 \tilde{Q}_1, \tag{C36}$$

Case	$\Delta\mathcal{L}$		
	$\kappa_{s,d}$	κ_K	κ_D
I, II	$\eta_0\bar{u}_R S Q_L + \eta_1\bar{u}_R S\Delta_D Q_L + \eta_2\bar{u}_R(Y_U\Delta_D Y_U^\dagger)SQ_L + \eta_3\bar{u}_R(Y_U\Delta_D Y_U^\dagger)S\Delta_D Q_L + h.c.$		
	0	0	$y_u y_c\big[2\frac{\Re(\eta_0\eta_3^*+\eta_1\eta_2^*)}{r_{ii}^2} + \frac{\lvert y_t\eta_3\rvert^2}{r_{33}^2}\big]$
III, IV	$\eta_0\bar{d}_R S Q_L + \eta_1\bar{d}_R S\Delta_U Q_L + \eta_2\bar{d}_R(Y_D\Delta_U Y_D^\dagger)SQ_L + \eta_3\bar{d}_R(Y_D\Delta_U Y_D^\dagger)S\Delta_U Q_L + h.c.$		
	$y_{d,s}y_b\big[\frac{\eta_1\eta_2^*}{r_{ii}^2} + \frac{\tilde{\eta}_0\eta_3^*}{r_{i3}^2} + \frac{\eta_3\eta_0^*}{r_{3i}^2} + \frac{\tilde{\eta}_2\tilde{\eta}_1^*}{r_{33}^2}\big]$	$y_d y_s\big[2\frac{\Re(\eta_0\eta_3^*+\eta_1\eta_2^*)}{r_{ii}^2} + \frac{\lvert y_b\eta_3\rvert^2}{r_{33}^2}\big]$	0

TABLE X: The same as Table VIII, but for models $\mathrm{S}_{\mathrm{I-IV}}$. We also use the abbreviations $\tilde{\eta}_0 = \eta_0 + \eta_1 y_t^2$, $\tilde{\eta}_1 = \eta_1 + \eta_3 y_b^2 y_t^2$, $\tilde{\eta}_2 = \eta_2 + \eta_3 y_t^2$. The results are written in the limit of degenerate scalars mediating transitions between the first two generations. Above the index i stands for $i = 1, 2$. In all the models there is also a 1-loop contribution Δ_{CC} (not displayed).

where the operator $\tilde{Q}_1$ is replaced by Q_1 for model $\mathrm{S}_{\mathrm{XIV}}$. The contributions to B_d, K and D mixing are defined in the same way, with appropriate replacement of the CKM factors and quark fields, as in (C10), (C11). The factors κ_i are collected in Table XI. Numerically the analysis is exactly the same as for MFV vector models $\mathrm{S}_{\mathrm{I-X}}$. The Yukawa suppressed (class-2 operator) models are S_{VI} and $\mathrm{S}_{\mathrm{VIII}}$, while $\mathrm{S}_{\mathrm{XIV}}$ is an example of the universal model (class-1 operator model).

5. Models $\mathrm{S}_{\mathrm{H,8}}$

The models $\mathrm{S}_{\mathrm{H,8}}$ give contributions to B_s mixing of the form

$$\Delta\mathcal{H}_{\mathrm{eff}}^{\mathrm{NP},B_s} = \kappa_s\left(\frac{1}{m_{S_1}^2} - \frac{1}{m_{S_2}^2}\right)(y_t^2 V_{tb}V_{ts}^*)^2(\tilde{C}_2\tilde{Q}_2 + \tilde{C}_3\tilde{Q}_3), \tag{C37}$$

where the operators $\tilde{Q}_{2,3}$ are given in (C8), $m_{S_{1,2}}$ are the masses of CP even and odd neutral scalars, and $\tilde{C}_2 = 1/2(1/4)$, $\tilde{C}_3 = 0(-1/12)$ for models S_{H} (S_8). The contributions to B_d, K and D mixing are defined in the same way, with appropriate replacement of the CKM factors and quark fields, as in (C10), (C11). Numerically (taking $m_{S_2} \gg m_{S_1}$ limit for simplicity),

$$h_{s,d}e^{i2\sigma_{s,d}} \simeq -15(5)\times y_t^4\kappa_{s,d}\left(\frac{1\ \mathrm{TeV}}{m_{S_1}}\right)^2, \tag{C38}$$

$$h_K e^{i2\sigma_K} \simeq 1.1(-0.3)\cdot 10^{-2}\times e^{i2\beta}y_t^4\frac{\kappa_K}{y_s^2}\left(\frac{y_s}{0.02}\right)^2\left(\frac{1\ \mathrm{TeV}}{m_{S_1}}\right)^2, \tag{C39}$$

$$h_D e^{i2\sigma_D} \simeq -1.1(0.3)\cdot 10^{-6}\times e^{i2\gamma}y_b^4\frac{\kappa_D}{y_c^2}\left(\frac{y_c}{5\cdot 10^{-3}}\right)^2\left(\frac{1\ \mathrm{TeV}}{m_{S_1}}\right)^2, \tag{C40}$$

Case	$\Delta\mathcal{L}$		
	$\kappa_{s,d}$	κ_K	κ_D
VI	$\eta_0\bar{u}^c_R S u_R + \eta_1\bar{u}^c_R S(Y_U\Delta_D Y_U^\dagger)u_R + \eta_1'\bar{u}^c_R(Y_U\Delta_D Y_U^\dagger)^T S u_R + \eta_2\bar{u}^c_R(Y_U\Delta_D Y_U^\dagger)^T S(Y_U\Delta_D Y_U^\dagger)u_R + h.c.$		
	0	0	$2\Re(\eta_1\eta_1'^* + \eta_0\eta_2'^*)y_u^2 y_c^2$
VIII	$\eta_0\bar{d}^c_R S d_R + \eta_1\bar{d}^c_R S(Y_D\Delta_U Y_D^\dagger)d_R + \eta_1'\bar{d}^c_R(Y_D\Delta_U Y_D^\dagger)^T S d_R + \eta_2\bar{d}^c_R(Y_D\Delta_U Y_D^\dagger)^T S(Y_D\Delta_U Y_D^\dagger)d_R + h.c.$		
	$y_{d,s}^2 y_b^2\big[\frac{2\Re\eta_1\eta_1'^*}{r_{i3}^2} + \frac{\eta_0\eta_2^*}{r_{ii}^2} + \frac{\eta_2\eta_0^*}{r_{33}^2}\big]$	$y_d^2 y_s^2 2\Re(\eta_1\eta_1'^* + \eta_0\eta_2^*)$	0
XIV	$\eta_0\bar{Q}^c_L S Q_L + \eta_1\bar{Q}^c_L S\Delta_U Q_L + \eta_1'\bar{Q}^c_L\Delta_U^T S Q_L + \eta_2\bar{Q}^c_L\Delta_U^T S\Delta_U Q_L + h.c.$		
	$\big[\frac{2\Re\eta_1\eta_1'^*}{r_{i3}^2} + \frac{\eta_0\eta_2^*}{r_{ii}^2} + \frac{\eta_2\eta_0^*}{r_{33}^2}\big]$	$2\Re(\eta_1\eta_1'^* + \eta_0\eta_2^*)$	$2\Re(\tilde{\eta}_1\tilde{\eta}_1'^* + \eta_0\tilde{\eta}_2^*)$

TABLE XI: The same as Table VIII, but for models $\mathrm{S}_{\mathrm{V-XIV}}$. Only models that lead to tree level FCNCs are shown. The results are written in the limit of degenerate scalars mediating transitions between the first two generations. Above the index i stands for $i = 1, 2$. For model $\mathrm{S}_{\mathrm{XIV}}$ the terms that contribute to $D - \bar{D}$ mixing have not been written out explicitly in $\Delta\mathcal{L}$. They can be obtained with $\Delta_U \to \Delta_D$ and have coupling $\tilde{\eta}_i$.

Case	$\Delta\mathcal{L}$		
	$\kappa_{s,d}$	κ_K	κ_D
H, 8	$\eta_0\bar{d}_R Y_D S Q_L + \eta_0'\bar{u}_R Y_U S Q_L + \eta_1\bar{d}_R(Y_D\Delta_U)S Q_L + \eta_1'\bar{u}_R(Y_U\Delta_D)S Q_L + h.c.$		
	$y_b^2\eta_1^2 + \Delta_{CC}$	$y_s^2\eta_1^2 + \Delta_{CC}$	$y_c^2\eta_1'^2 + \Delta_{CC}$

TABLE XII: The same as Table VIII, but for models $\mathrm{S}_{\mathrm{H,8}}$. The 1-loop contributions Δ_{CC} arise from charge currents.

where the values in the brackets are for model S_8.

[1] S. L. Glashow and S. Weinberg, Phys. Rev. D **15**, 1958 (1977).

[2] K. Agashe, M. Papucci, G. Perez and D. Pirjol, arXiv:hep-ph/0509117.

[3] J. M. Arnold, M. Pospelov, M. Trott and M. B. Wise, JHEP **1001**, 073 (2010) [arXiv:0911.2225 [hep-ph]].

[4] Y. Grossman, Y. Nir, J. Thaler, T. Volansky and J. Zupan, Phys. Rev. D **76**, 096006 (2007) [arXiv:0706.1845 [hep-ph]].

[5] J. M. Arnold, B. Fornal and M. Trott, JHEP **1008**, 059 (2010) [arXiv:1005.2185 [hep-ph]].

[6] T. Aaltonen *et al.* [The CDF Collaboration], arXiv:1101.0034 [hep-ex].

[7] V. M. Abazov *et al.* [D0 Collaboration], [arXiv:1107.4995 [hep-ex]].

[8] CDF Collaboration, CDF note 10398, http://www-cdf.fnal.gov/physics/new/top/2011/DilAfb/

[9] V. M. Abazov *et al.* [D0 Collaboration], arXiv:1005.2757.

[10] M. R. J. Williams *et al.* [on behalf of D0 Collaboration], [arXiv: 1106.6308 [hep-ex]].

[11] R. S. Chivukula and H. Georgi, Phys. Lett. B **188** (1987) 99.

[12] G. D'Ambrosio et al., Nucl. Phys. B **645** (2002) 155 [arXiv:hep-ph/0207036].

[13] A. L. Kagan, G. Perez, T. Volansky and J. Zupan, arXiv:0903.1794 [hep-ph].

[14] A. V. Manohar and M. B. Wise, Phys. Rev. D **74**, 035009 (2006) [arXiv:hep-ph/0606172].

[15] Q. H. Cao, D. McKeen, J. L. Rosner, G. Shaughnessy and C. E. M. Wagner, Phys. Rev. D **81**, 114004 (2010) [arXiv:1003.3461 [hep-ph]].

[16] K. Blum, C. Delaunay, O. Gedalia, Y. Hochberg, S. J. Lee, Y. Nir, G. Perez, Y. Soreq, [arXiv:1102.3133 [hep-ph]].

[17] G. M. Tavares, M. Schmaltz, [arXiv:1107.0978 [hep-ph]].

[18] J. Shu, T. M. P. Tait and K. Wang, Phys. Rev. D **81**, 034012 (2010) [arXiv:0911.3237].

[19] T. Feldmann and T. Mannel, Phys. Rev. Lett. **100** (2008) 171601 [arXiv:0801.1802 [hep-ph]].

[20] T. Feldmann, M. Jung and T. Mannel, arXiv:0906.1523 [hep-ph].

[21] R. Barbieri, G. Isidori, J. Jones-Perez, P. Lodone and D. M. Straub, arXiv:1105.2296 [hep-ph].

[22] S. Jung, H. Murayama, A. Pierce and J. D. Wells, Phys. Rev. D **81**, 015004 (2010) [arXiv:0907.4112].

[23] K. Cheung, W. Y. Keung and T. C. Yuan, Phys. Lett. B **682**, 287 (2009) [arXiv:0908.2589].

[24] S. Jung, A. Pierce and J. D. Wells, arXiv:1108.1802 [hep-ph].

[25] P. Ferrario, G. Rodrigo, Phys. Rev. **D80**, 051701 (2009). [arXiv:0906.5541 [hep-ph]].

[26] P. H. Frampton, J. Shu and K. Wang, Phys. Lett. B **683**, 294 (2010) [arXiv:0911.2955 [hep-ph]].

[27] A. Arhrib, R. Benbrik and C. H. Chen, Phys. Rev. D **82**, 034034 (2010) [arXiv:0911.4875].

[28] I. Dorsner, S. Fajfer, J. F. Kamenik and N. Kosnik, Phys. Rev. D **81**, 055009 (2010) [arXiv:0912.0972 [hep-ph]].

[29] J. F. Kamenik, J. Shu and J. Zupan, arXiv:1107.5257 [hep-ph].

[30] S. Jung, A. Pierce and J. D. Wells, arXiv:1103.4835 [hep-ph].

[31] J. Shelton and K. M. Zurek, Phys. Rev. D **83** (2011) 091701 [arXiv:1101.5392 [hep-ph]].

[32] A. E. Nelson, T. Okui and T. S. Roy, arXiv:1104.2030 [hep-ph].

[33] K. S. Babu, M. Frank and S. K. Rai, Phys. Rev. Lett. **107**, 061802 (2011) [arXiv:1104.4782 [hep-ph]].

[34] J. Shu, K. Wang and G. Zhu, arXiv:1104.0083 [hep-ph].

[35] B. Grinstein, A. L. Kagan, M. Trott and J. Zupan, Phys. Rev. Lett. **107** (2011) 012002 [arXiv:1102.3374 [hep-ph]].

[36] Z. Ligeti, M. Schmaltz and G. M. Tavares, arXiv:1103.2757 [hep-ph].

[37] K. Blum, Y. Hochberg and Y. Nir, arXiv:1107.4350 [hep-ph].

[38] M. I. Gresham, I. W. Kim and K. M. Zurek, arXiv:1102.0018 [hep-ph].

[39] K. Cheung and T. C. Yuan, Phys. Rev. D **83**, 074006 (2011) [arXiv:1101.1445 [hep-ph]].

[40] V. Barger, W. Y. Keung and C. T. Yu, Phys. Rev. D **81**, 113009 (2010) [arXiv:1002.1048 [hep-ph]].

[41] V. Barger, W. Y. Keung and C. T. Yu, Phys. Lett. B **698**, 243 (2011) [arXiv:1102.0279 [hep-ph]].

[42] E. L. Berger, Q. H. Cao, C. R. Chen, C. S. Li and H. Zhang, Phys. Rev. Lett. **106**, 201801 (2011) [arXiv:1101.5625].

[43] B. Bhattacherjee, S. S. Biswal and D. Ghosh, Phys. Rev. D **83**, 091501 (2011) [arXiv:1102.0545 [hep-ph]].

[44] M. I. Gresham, I. W. Kim and K. M. Zurek, arXiv:1107.4364 [hep-ph].

[45] C. Degrande, J. -M. Gerard, C. Grojean, F. Maltoni, G. Servant, JHEP **1103**, 125 (2011). [arXiv:1010.6304 [hep-ph]].

[46] J. A. Aguilar-Saavedra, M. Perez-Victoria, JHEP **1105**, 034 (2011). [arXiv:1103.2765 [hep-ph]].

[47] K. -m. Cheung, Phys. Rev. **D53**, 3604-3615 (1996). [hep-ph/9511260].

[48] O. Antipin, G. Valencia, Phys. Rev. **D79**, 013013 (2009). [arXiv:0807.1295 [hep-ph]].

[49] S. K. Gupta, A. S. Mete, G. Valencia, Phys. Rev. **D80**, 034013 (2009). [arXiv:0905.1074 [hep-ph]].

[50] Z. Hioki, K. Ohkuma, Eur. Phys. J. **C65**, 127-135 (2010). [arXiv:0910.3049 [hep-ph]].

[51] D. Choudhury, P. Saha, [arXiv:0911.5016 [hep-ph]].

[52] Z. Hioki, K. Ohkuma, Eur. Phys. J. **C71**, 1535 (2011). [arXiv:1011.2655 [hep-ph]].

[53] Z. HIOKI, K. OHKUMA, Phys. Rev. **D83**, 114045 (2011). [arXiv:1104.1221 [hep-ph]].

[54] D. -W. Jung, P. Ko, J. S. Lee, S. -h. Nam, Phys. Lett. **B691**, 238-242 (2010). [arXiv:0912.1105 [hep-ph]].

[55] C. Zhang, S. Willenbrock, Phys. Rev. **D83**, 034006 (2011). [arXiv:1008.3869 [hep-ph]].

[56] C. Delaunay, O. Gedalia, Y. Hochberg, G. Perez, Y. Soreq, JHEP **1108**, 031 (2011). [arXiv:1103.2297 [hep-ph]].

[57] J. Cao, Z. Heng, L. Wu, J. M. Yang, Phys. Rev. **D81**, 014016 (2010). [arXiv:0912.1447 [hep-ph]].

[58] B. Xiao, Y. -k. Wang, S. -h. Zhu, Phys. Rev. **D82**, 034026 (2010). [arXiv:1006.2510 [hep-ph]].

[59] J. Cao, L. Wang, L. Wu, J. M. Yang, [arXiv:1101.4456 [hep-ph]].

[60] K. M. Patel, P. Sharma, JHEP **1104**, 085 (2011). [arXiv:1102.4736 [hep-ph]].

[61] E. R. Barreto, Y. A. Coutinho, J. Sa Borges, Phys. Rev. **D83**, 054006 (2011). [arXiv:1103.1266 [hep-ph]].

[62] N. Craig, C. Kilic, M. J. Strassler, [arXiv:1103.2127 [hep-ph]].

[63] M. R. Buckley, D. Hooper, J. Kopp, E. Neil, Phys. Rev. **D83**, 115013 (2011). [arXiv:1103.6035 [hep-ph]].

[64] S. Jung, A. Pierce, J. D. Wells, [arXiv:1104.3139 [hep-ph]].

[65] P. J. Fox, J. Liu, D. Tucker-Smith, N. Weiner, [arXiv:1104.4127 [hep-ph]].

[66] Y. Cui, Z. Han, M. D. Schwartz, JHEP **1107**, 127 (2011). [arXiv:1106.3086 [hep-ph]].

[67] M. Duraisamy, A. Rashed, A. Datta, [arXiv:1106.5982 [hep-ph]].

[68] J. A. Aguilar-Saavedra, M. Perez-Victoria, [arXiv:1107.0841 [hep-ph]].

[69] I. Dorsner, S. Fajfer, J. F. Kamenik, N. Kosnik, Phys. Rev. **D82**, 094015 (2010). [arXiv:1007.2604 [hep-ph]].

[70] C. Delaunay, O. Gedalia, S. J. Lee, G. Perez, E. Ponton, [arXiv:1101.2902 [hep-ph]].

[71] G. Isidori, J. F. Kamenik, Phys. Lett. **B700**, 145-149 (2011). [arXiv:1103.0016 [hep-ph]].

[72] R. S. Chivukula, E. H. Simmons, C. -P. Yuan, Phys. Rev. **D82**, 094009 (2010). [arXiv:1007.0260 [hep-ph]].

[73] Y. Bai, J. L. Hewett, J. Kaplan, T. G. Rizzo, JHEP **1103**, 003 (2011). [arXiv:1101.5203 [hep-ph]].

[74] B. Xiao, Y. -k. Wang, S. -h. Zhu, [arXiv:1011.0152 [hep-ph]].

[75] P. Ferrario, G. Rodrigo, JHEP **1002**, 051 (2010). [arXiv:0912.0687 [hep-ph]].

[76] M. V. Martynov, A. D. Smirnov, Mod. Phys. Lett. **A25**, 2637-2643 (2010). [arXiv:1006.4246 [hep-ph]].

[77] M. Bauer, F. Goertz, U. Haisch, T. Pfoh, S. Westhoff, JHEP **1011**, 039 (2010). [arXiv:1008.0742 [hep-ph]].

[78] C. -H. Chen, G. Cvetic, C. S. Kim, Phys. Lett. **B694**, 393-397 (2011). [arXiv:1009.4165 [hep-ph]].

[79] G. Burdman, L. de Lima, R. D. Matheus, Phys. Rev. **D83**, 035012 (2011). [arXiv:1011.6380 [hep-ph]].

[80] D. Choudhury, R. M. Godbole, S. D. Rindani, P. Saha, Phys. Rev. **D84**, 014023 (2011). [arXiv:1012.4750 [hep-ph]].

[81] J. Cao, L. Wu, J. M. Yang, Phys. Rev. **D83**, 034024 (2011). [arXiv:1011.5564 [hep-ph]].

[82] R. Foot, Phys. Rev. **D83**, 114013 (2011). [arXiv:1103.1940 [hep-ph]].

[83] U. Haisch and S. Westhoff, arXiv:1106.0529 [hep-ph].

[84] B. A. Dobrescu, P. J. Fox and A. Martin, Phys. Rev. Lett. **105**, 041801 (2010) [arXiv:1005.4238 [hep-ph]].

[85] A. J. Buras, M. V. Carlucci, S. Gori and G. Isidori, JHEP **1010**, 009 (2010) [arXiv:1005.5310 [hep-ph]].

[86] M. Jung, A. Pich and P. Tuzon, JHEP **1011**, 003 (2010) [arXiv:1006.0470 [hep-ph]].

[87] C. H. Chen, C. Q. Geng and W. Wang, JHEP **1011**, 089 (2010) [arXiv:1006.5216 [hep-ph]].

[88] K. Blum, Y. Hochberg and Y. Nir, JHEP **1009**, 035 (2010) [arXiv:1007.1872 [hep-ph]].

[89] A. J. Buras, K. Gemmler and G. Isidori, Nucl. Phys. B **843**, 107 (2011) [arXiv:1007.1993 [hep-ph]].

[90] A. J. Buras, G. Isidori and P. Paradisi, Phys. Lett. B **694**, 402 (2011) [arXiv:1007.5291 [hep-ph]].

[91] M. Trott and M. B. Wise, JHEP **1011**, 157 (2010) [arXiv:1009.2813 [hep-ph]].

[92] Z. Ligeti, M. Papucci, G. Perez and J. Zupan, Phys. Rev. Lett. **105**, 131601 (2010) [arXiv:1006.0432 []].

[93] V. Ahrens, A. Ferroglia, M. Neubert, B. D. Pecjak and L. L. Yang, arXiv:1106.6051 [hep-ph].

[94] A. D. Martin, W. J. Stirling, R. S. Thorne and G. Watt, Eur. Phys. J. C **63**, 189 (2009) [arXiv:0901.0002].

[95] W. Hollik and D. Pagani, arXiv:1107.2606 [hep-ph].

[96] N. Kidonakis, [arXiv:1105.5167 [hep-ph]].

[97] O. Antunano, J. H. Kuhn and G. Rodrigo, Phys. Rev. D **77**, 014003 (2008) [arXiv:0709.1652 [hep-ph]].

[98] M. T. Bowen, S. D. Ellis and D. Rainwater, Phys. Rev. D **73**, 014008 (2006) [arXiv:hep-ph/0509267].

[99] J. H. Kuhn and G. Rodrigo, Phys. Rev. D **59**, 054017 (1999) [arXiv:hep-ph/9807420].

[100] S. Moch and P. Uwer, Nucl. Phys. Proc. Suppl. **183**, 75 (2008) [arXiv:0807.2794 [hep-ph]].

[101] M. Czakon, A. Mitov, G. F. Sterman, Phys. Rev. **D80**, 074017 (2009). [arXiv:0907.1790 [hep-ph]].

[102] M. Beneke, M. Czakon, P. Falgari, A. Mitov, C. Schwinn, Phys. Lett. **B690**, 483-490 (2010). [arXiv:0911.5166 [hep-ph]].

[103] N. Kidonakis, Phys. Rev. **D82**, 114030 (2010). [arXiv:1009.4935 [hep-ph]].

[104] N. Kidonakis and R. Vogt, Phys. Rev. D **78** (2008) 074005 [arXiv:0805.3844 [hep-ph]].

[105] M. Cacciari, S. Frixione, M. L. Mangano, P. Nason and G. Ridolfi, JHEP **0809** (2008) 127 [arXiv:0804.2800 [hep-ph]].

[106] V. Ahrens, A. Ferroglia, M. Neubert, B. D. Pecjak, L. L. Yang, [arXiv:1103.0550 [hep-ph]].

[107] N. Kidonakis, [arXiv:1105.3481 [hep-ph]].

[108] T. Aaltonen *et al.* [CDF Collaboration], Phys. Rev. Lett. **102** (2009) 222003 [arXiv:0903.2850 [hep-ex]].

[109] V. Ahrens, A. Ferroglia, M. Neubert, B. D. Pecjak and L. L. Yang, JHEP **1009** (2010) 097 [arXiv:1003.5827].

[110] M. I. Gresham, I. W. Kim and K. M. Zurek, arXiv:1103.3501 [hep-ph].

[111] J. Alwall, P. Demin, S. de Visscher, R. Frederix, M. Herquet, F. Maltoni, T. Plehn, D. L. Rainwater *et al.*, JHEP **0709**, 028 (2007). [arXiv:0706.2334 [hep-ph]].

[112] T. Sjostrand, S. Mrenna, P. Z. Skands, JHEP **0605**, 026 (2006). [hep-ph/0603175].

[113] T. Aaltonen *et al.* [CDF Collaboration], Phys. Rev. Lett. **101** (2008) 202001 [arXiv:0806.2472 [hep-ex]].

[114] J. A. Aguilar-Saavedra and M. Perez-Victoria, arXiv:1105.4606 [hep-ph].

[115] G. Zhu, arXiv:1104.3227 [hep-ph].

[116] V. M. Abazov [D0 Collaboration], Phys. Rev. Lett. **107**, 011804 (2011) [arXiv:1106.1921 [hep-ex]].

[117] T. Aaltonen *et al.* [CDF Collaboration], Phys. Rev. Lett. **106**, 171801 (2011). [arXiv:1104.0699 [hep-ex]].

[118] J. Alitti et al. [UA2 Collaboration], Nucl. Phys. B 400, 3 (1993).

[119] ATLAS Collaboration, ATLAS-CONF-2011-087, http://cdsweb.cern.ch/record/1356196/files/ATLAS-CONF-2011-087.pdf

[120] CMS Collaboration, CMS-PAS-TOP-10-007, http://cdsweb.cern.ch/record/1335720?ln=en

[121] M. Mulders, talk on behalf of the CMS Collaboration presented at EPS High Energy Phsyics Conference 2011, July 21-27 Grenoble, France.

[122] A. Lenz *et al.*, Phys. Rev. D **83** (2011) 036004 [arXiv:1008.1593 [hep-ph]].

[123] CDF Collaboration, CDF Note 10206

[124] D0 Collaboration, D0 Note 6098-CONF

[125] C. P. Burgess, M. Trott and S. Zuberi, JHEP **0909**, 082 (2009) [arXiv:0907.2696 [hep-ph]].

[126] M. S. Carena et al. Phys. Rev. D **70**, 093009 (2004) [arXiv:hep-ph/0408098].

[127] R. Barbieri, A. Strumia, [hep-ph/0007265].

[128] G. F. Giudice, B. Gripaios and R. Sundrum, arXiv:1105.3161 [hep-ph].

[129] T. Aaltonen *et al.* [CDF Collaboration], Phys. Rev. D **79**, 112002 (2009) [arXiv:0812.4036 [hep-ex]].

[130] V. Khachatryan *et al.* [CMS Collaboration], Phys. Rev. Lett. **105**, 211801 (2010) [arXiv:1010.0203 [hep-ex]].

[131] G. Aad *et al.* [ATLAS Collaboration], New J. Phys. **13**, 053044 (2011) [arXiv:1103.3864 [hep-ex]].

[132] ATLAS Collaboration, ATLAS conference note ATLAS-CONF-2011-095.

[133] CMS Collaboration, CMS-EXO-11-015, arXiv:1107.4771 [hep-ex].

[134] V. M. Abazov *et al.* [D0 Collaboration], Phys. Rev. Lett. **103**, 191803 (2009) [arXiv:0906.4819 [hep-ex]] . "EAPS Document with data: E-PRLTAO-103-025946"

[135] V. Khachatryan *et al.* [CMS Collaboration], arXiv:1102.2020 [hep-ex].

[136] S. Chatrchyan *et al.* [CMS Collaboration], arXiv:1106.2142 [hep-ex].

[137] A. L. Kagan, J. F. Kamenik, G. Perez and S. Stone, arXiv:1103.3747 [hep-ph].

[138] J. F. Arguin, M. Freytsis and Z. Ligeti, arXiv:1107.4090 [hep-ph].

[139] K. D. Lane and M. V. Ramana, Phys. Rev. D **44**, 2678 (1991).

[140] E. Lunghi and A. Soni, Phys. Lett. B **697** (2011) 323 [arXiv:1010.6069 [hep-ph]].

[141] E. Byckling, K. Kajantie, Particle Kinematics, John Wiley & Sons Ltd (January 1, 1973)

[142] A. L. Kagan and M. D. Sokoloff, Phys. Rev. D **80** (2009) 076008 [arXiv:0907.3917 [hep-ph]].

[143] M. Bona *et al.* [UTfit Collaboration], JHEP **0803** (2008) 049 [arXiv:0707.0636 [hep-ph]].

[144] J. Laiho, E. Lunghi and R. S. Van de Water, Phys. Rev. D **81** (2010) 034503 [arXiv:0910.2928 [hep-ph]]; and 2011 updates at `http://krone.physik.unizh.ch/~lunghi/webpage/LatAves/index.html`

[145] J. Charles *et al.* [CKMfitter Group], Eur. Phys. J. C **41** (2005) 1 [arXiv:hep-ph/0406184], we are using the ICHEP2010 update from `http://ckmfitter.in2p3.fr`.

[146] T. Inami, C. S. Lim, Prog. Theor. Phys. **65**, 297 (1981).

[147] H. Zhang, E. L. Berger, Q. H. Cao, C. R. Chen and G. Shaughnessy, Phys. Lett. B **696**, 68 (2011) [arXiv:1009.5379 [hep-ph]].